

Nonlinear Continuum Mechanics and Modeling the Elasticity of Soft Biological Tissues with a Focus on Artery Walls

Ray W. Ogden

Abstract This chapter provides a detailed summary of the background from the nonlinear theory of continuum mechanics that is required in the modeling of the elastic properties of soft biological tissues. In particular, it highlights methods for including the fibrous structure of such tissues within the constitutive description of the material properties at the macroscopic level. Of particular relevance in this connection are the so-called preferred directions associated with fibers and the structure tensors and associated deformation invariants that are needed for taking these fibers and their dispersed directions into consideration. These are incorporated into the material models and the effect of fiber structure on the material response is then illustrated with several basic examples. Generalizations of structure tensors are also used for including within the theory the important residual stresses that are evident in unloaded tissues such as arteries and the myocardium, and the influence of residual stresses on the material response is illustrated by considering the extension and inflation of a thick-walled circular cylindrical tube.

1 Introduction

This chapter is based on lectures given at the Summer School on ‘Biomechanics: Trends in Modeling and Simulation’ in Graz, Austria, in September 2014, but includes additional material that was not presented in the lectures. Effective modeling of the mechanics of soft biological tissues, such as the layered walls of arteries, the myocardium and skin, requires a sophisticated application of the nonlinear theory of continuum mechanics. Within the structure of these tissues a key component is the protein collagen, which endows the material with anisotropic properties because of its significant stiffness relative to the surrounding material within which it is embedded. We refer to the surrounding (less stiff) material as the *matrix*, which, depending on the tissue under consideration, includes elastin fibers, proteoglycans, and smooth

R.W. Ogden (✉)
University of Glasgow, Glasgow, UK
e-mail: raymond.ogden@glasgow.ac.uk

© Springer International Publishing Switzerland 2017
G.A. Holzapfel and R.W. Ogden (eds.), *Biomechanics: Trends in Modeling
and Simulation*, Studies in Mechanobiology, Tissue Engineering
and Biomaterials 20, DOI 10.1007/978-3-319-41475-1_3

83

muscle cells, for example. Tissues have a naturally fibrous structure, which has a strong influence on their mechanical response. Thus, from the mechanical perspective, it is important to be able to understand the influence of the fiber structure on the overall mechanical response of the composite materials of which the fibers are constituents, and nonlinear continuum mechanics provides the vehicle for analyzing this response.

Consider, for example, a length of artery, which may be idealized as a circular cylindrical tube, as illustrated in Fig. 1. Typically, in the simplest terms, an artery contains two families of collagen fibers that are helically arranged and symmetrically disposed relative to its axis, with the fiber directions locally lying within the tangent plane, i.e., they have no radial component. Suppose that each family makes an angle φ with the circumferential direction. Of course, the picture is much more complex than we have indicated here—for example, there is dispersion of the fiber directions within each family, there is in general a small radial component of each fiber direction and the arrangement is different within each layer of an artery wall. These matters will concern us later in the chapter, but for our initial illustration we consider the simple situation depicted in Fig. 1.

This enables us to provide a simple illustration of the influence of fiber orientation on the mechanical response of an artery. This is the content of Fig. 2, which shows how the pressure in a circular cylindrical tube depends on its radial expansion (as measured by the circumferential stretch—the ratio of inner deformed radius to undeformed radius) for different fiber orientations in the absence of axial extension. The curves shown, which exhibit highly nonlinear behavior, are characteristic of those for arteries found in the literature and are based on a model of these characteristics (see, for example, Holzapfel et al. 2000). The response becomes stiffer as the fiber directions become closer to circumferential than axial, which reflects the high stiffness of collagen fibers. The shapes are also very similar to those obtained in uniaxial tests on, for example, strip samples of different artery wall layers (see, for example, Holzapfel et al. 2005). There is a soft ‘toe’ region where the wavy collagen fibers provide little

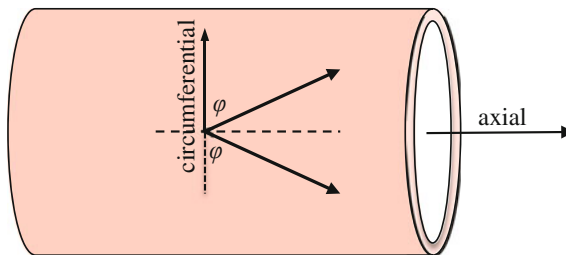


Fig. 1 Depiction of an undeformed artery as a thin-walled circular cylindrical tube with two symmetrically and helically arranged families of (collagen) fibers locally lying in the tangent plane and with directions making angles φ with the circumferential direction. The two symmetrically arranged *arrows* indicate the directions of the tangents to the fibers at a general point

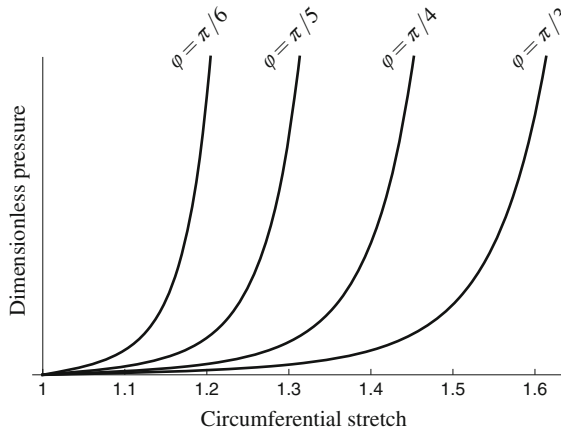


Fig. 2 Representative curves of (dimensionless) pressure versus circumferential stretch on inflation of an artery without axial extension for several values of the angle φ shown in Fig. 1. The curves highlight both the nonlinearity of the material response and the significant effect of fiber orientation. The response is much stiffer for fibers oriented more toward the circumferential direction than the axial direction

if any resistance to tension, which is borne by the soft matrix, followed by rapid stiffening as they reach their natural lengths.

We are concerned here with the elastic response of arteries, but the framework of the nonlinear theory of elasticity underpins the basic elastic response of all soft fibrous materials and is a starting point for more general continuum theories. Our aim is to describe the elastic behavior of these materials by the construction of constitutive laws, informed by data from experimental tests. The fiber directions within a tissue endow the material locally with so-called *preferred directions*, as a result of which the mechanical response of the material is anisotropic.

From the point of view of modeling the elastic properties of tissues the complications associated with the fibrous structure are well known and have been the subject of many publications, and for an extensive list of references we refer to Holzapfel et al. (2000), Gasser et al. (2006) and Holzapfel and Ogden (2010), for example. Another issue, which increases the complication, is the existence of residual stresses in unloaded tissue exemplified by the residual stress in artery walls, as evidenced by the so-called opening angle test (Vaishnav and Vossoughi 1983; Chuong and Fung 1986). In this, a short ring of excised artery (and therefore unloaded radially and axially) when cut radially springs open significantly into a sector, thereby demonstrating the existence of residual stress in the intact state. A two-dimensional idealized version of this experimental test, in which a circular ring of artery springs open into the sector of a circular ring, is illustrated in Fig. 3.

Thus, both residual stresses and the tissue structure need to be accounted for in the development of constitutive laws for soft biological tissues, and this is the concern of this chapter as we develop nonlinearly elastic constitutive laws for these materials,

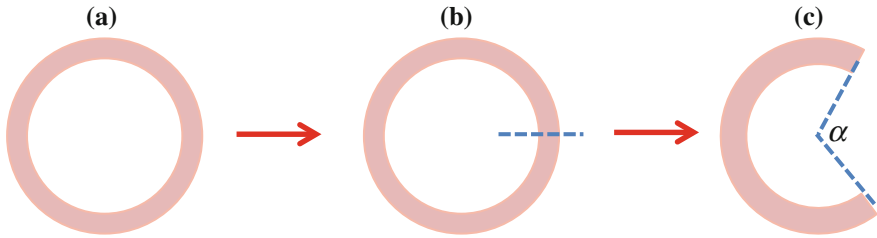


Fig. 3 A ring of artery (a) is cut radially (b) and deforms into a sector of a circular ring (c) with the opening angle α , thus demonstrating that in the unloaded configuration (a) there exist (radial and circumferential) residual stresses relief of which results in configuration (c)

with a focus on their passive and time-independent response. For general background on the mechanics of tissues we refer to the classical text of Fung (1993) and for detailed discussion of the mechanical properties of arteries and, more generally cardiovascular solid mechanics, the works of Humphrey (1995, 2002) should be consulted. For developments in the continuum description of arterial wall mechanics we refer to Holzapfel et al. (2000, 2015), Gasser et al. (2006), and Holzapfel and Ogden (2010) and references therein, while for the myocardium we cite Holzapfel and Ogden (2009a). See also the collections of papers in the edited volumes by Holzapfel and Ogden (2003, 2006, 2009b).

In Sect. 2, we provide a description of the kinematics of deformation, introduce a number of stress tensors and derive the equations governing equilibrium, while in Sect. 3 we focus on general aspects of the constitutive law of an elastic material based on a strain-energy function and the associated stress tensors. More comprehensive treatments of the nonlinear theory of elasticity can be found in, for example, standard texts such as Ogden (1997, 2003a), and Holzapfel (2000) and the collection of articles in Fu and Ogden (2001). Particular attention is paid here to the role of structure tensors and invariants associated with preferred directions in the development of the strain-energy function for different material symmetries. The notion of a structure tensor is also used to include residual stress in the constitutive law of an elastic material.

In Sect. 4 the theory for fiber-reinforced materials, with two fiber families (and without residual stress), is then applied in a basic application to homogeneous deformations, in particular to the problem of pure homogeneous strain of a thin sheet of material, a setup that is often used in experiments for helping to characterize the mechanical properties of fibrous materials. The general results are illustrated for a special choice of constitutive law which has a role, in various modified forms, throughout the chapter.

This is followed, in Sect. 5, by an application of the theory to a key boundary-value problem involving a nonhomogeneous deformation relevant to the behavior of arteries, namely that of the extension and inflation of a thick-walled elastic tube reinforced symmetrically with two families of fibers. The corresponding thin-walled approximation is derived and used for illustration of the pressure and axial load response of a tube. The difference between the response with and without fibers and

the effect of different fiber orientations is highlighted by applying the material model from Sect. 4. The effect of residual stress is then illustrated by a further application to the problem of extension and inflation of a thick-walled elastic tube in Sect. 5.3, and a particular form of the residual stress is chosen along with simple constitutive laws, enabling explicit expressions to be obtained for the pressure and axial load applied to achieve a prescribed axial extension and inflation of the tube. For purposes of numerical calculation and graphical illustration, a range of particular values of the parameters of the problem is selected, leading to comparative plots of the pressure and axial load for a residually stressed tube, with and without fiber reinforcement.

The model strain-energy function fits data for the overall response of an artery, and it also fits well the data for the medial layer, but it does less well for the intimal and adventitial layers. One possible explanation for this is that rather than being perfectly aligned the fibers are dispersed in their orientations, and this is more evident in the adventitia than in the media, for example. Therefore, to take account of fiber dispersion the model was modified by Gasser et al. (2006). In Sect. 6 is described the model based on fiber dispersion, which is accounted for via a so-called *generalized structure tensor* and associated generalized invariants. In particular, for three dimensions a rotationally symmetric dispersion is considered which involves just a single dispersion parameter as a measure of the degree of dispersion. A two-dimensional counterpart of this is also examined.

For the rotationally symmetric model a π -periodic von Mises distribution is used to quantify the dispersion, and with the same general structure the model strain-energy function from the previous sections is modified to accommodate the dispersion. This extended model is applied to the extension–inflation problem to illustrate the significant difference that inclusion of dispersion makes. Then, using the model and data relating to the adventitia of a human iliac artery, the problem of the nonhomogeneous uniaxial extension of strips from the circumferential and axial directions is examined using a finite element calculation, further highlighting the significant influence of dispersion.

However, it has been found in the recent extensive series of experiments of Schriefl et al. (2012) on separate intimal, medial, and adventitial layers of human thoracic and abdominal aortas and common iliac arteries that the fiber dispersion does not possess rotational symmetry in three dimensions. The dispersion was found to be essentially symmetric in the circumferential/axial plane (in-plane) but has a small radial component (out-of-plane). To accommodate these new data the rotationally symmetric model of Gasser et al. (2006) has therefore been adapted in Holzapfel et al. (2015) by developing new generalized structure tensors and generalized invariants. This work is described in Sect. 6.4. In particular, this modification uses a bivariate von Mises distribution to characterize the in-plane and out-of-plane dispersions involving two dispersion parameters, one in-plane and one out-of-plane, as distinct from the single dispersion parameter associated with a rotationally symmetric dispersion.

Within the same general structure as for the previous models, the strain-energy function has been modified merely by updating the definitions of the generalized invariants. Based on a set of data obtained from histology and imaging, values of the dispersion parameters and mean fiber orientations were exemplified in Schriefl

et al. (2012), and, with these values, the corresponding material parameters were determined in Holzapfel et al. (2015) by fitting data from uniaxial tension tests on circumferential and axial specimens of an adventitial layer of a human non-atherosclerotic abdominal aorta. Following Holzapfel et al. (2015) this complete set of parameters is used finally in a finite element simulation of a nonhomogeneous uniaxial extension test on this adventitial layer. Some concluding remarks form the content of Sect. 7.

In Holzapfel et al. (2015) we have provided a brief review of dispersion models, which are based on two main approaches, namely the angular integration (AI) approach pioneered by Lanir (1983), and the generalized structure tensor (GST) approach due to Gasser et al. (2006). We focus on the GST approach in this chapter and refer the reader to Holzapfel et al. (2015) for pointers to the literature.

2 Fundamentals of Continuum Mechanics

Here we summarize the key notation used for describing the kinematics associated with continuum deformation, followed by a brief account of the stress tensors used to describe the stress within a deformed material and the associated equilibrium equations. We do not analyze (time-dependent) motion in this chapter. For more details of the background for this section we refer to Ogden (1997) and Holzapfel (2000), for example.

2.1 The Geometry of Deformation

As is usual in continuum mechanics, we consider a material body which, when unloaded (i.e., when not subject to either surface tractions or body forces) occupies a *reference configuration*, which we denote by \mathcal{B}_r , the boundary of which is denoted $\partial\mathcal{B}_r$. Let an arbitrary point of \mathcal{B}_r be labeled by its position vector \mathbf{X} . After deformation the body occupies the *deformed configuration*, denoted \mathcal{B} , which has boundary $\partial\mathcal{B}$. The material point \mathbf{X} is then taken to the new position vector \mathbf{x} in \mathcal{B} , as depicted in Fig. 4.

Mathematically, the deformation is described by the *deformation function* χ , which is a one-to-one, onto mapping from \mathcal{B}_r to \mathcal{B} . Thus, we write

$$\mathbf{x} = \chi(\mathbf{X}) \quad \text{for all } \mathbf{X} \in \mathcal{B}_r, \quad (1)$$

and, without further comment, χ is assumed to possess sufficient regularity for the analysis in this chapter.

In standard notation the second-order tensor \mathbf{F} , the so-called *deformation gradient tensor*, denotes the gradient of $\mathbf{x} = \chi(\mathbf{X})$, explicitly

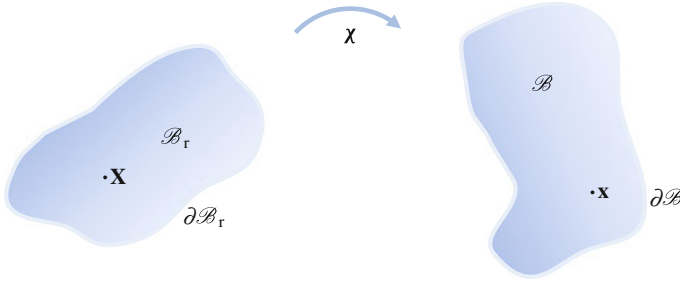


Fig. 4 On the *left-hand side* is depicted a body in its (unloaded) reference configuration \mathcal{B}_r , which has boundary $\partial\mathcal{B}_r$. As a result of the deformation χ the body occupies the deformed configuration \mathcal{B} , which has boundary $\partial\mathcal{B}$, as depicted on the *right-hand side*

$$\mathbf{F} = \text{Grad } \mathbf{x} = \text{Grad } \chi(\mathbf{X}), \tag{2}$$

where Grad denotes the gradient with respect to \mathbf{X} , as distinct from the gradient grad with respect to \mathbf{x} . Likewise Div and div denote the divergence operators with respect to \mathbf{X} and \mathbf{x} , respectively. We shall also use the notations $(\bullet)^T$ and $\text{tr}(\bullet)$, respectively, to denote the transpose and trace of a second-order tensor (\bullet) . With reference to a rectangular Cartesian coordinate system, we write the components of \mathbf{F} as $F_{i\alpha} = \partial x_i / \partial X_\alpha$, where x_i and X_α , $i, \alpha \in \{1, 2, 3\}$, are the components of \mathbf{x} and \mathbf{X} , respectively, Greek and Roman indices being associated with \mathcal{B}_r and \mathcal{B} , respectively.

We use the standard notation J for the determinant $\det \mathbf{F}$ of \mathbf{F} and, by convention, this is taken to be positive, i.e.,

$$J \equiv \det \mathbf{F} > 0, \tag{3}$$

which is clearly satisfied when \mathcal{B} coincides with \mathcal{B}_r since then $\mathbf{x} = \mathbf{X}$, $\mathbf{F} = \mathbf{I}_r$, the identity tensor in \mathcal{B}_r , and $\det \mathbf{F} = 1$. The physical interpretation of J is that it represents the local ratio of an infinitesimal volume element dv in \mathcal{B} to the corresponding volume element dV in \mathcal{B}_r based on \mathbf{X} in \mathcal{B}_r , i.e., $dv = JdV$.

Thus, for an isochoric (volume preserving) deformation $J = 1$, while for an incompressible material the constraint

$$J \equiv \det \mathbf{F} = 1 \tag{4}$$

must be satisfied at each \mathbf{X} in \mathcal{B}_r . This constraint is important here since many soft biological tissues, including artery walls, can be treated as incompressible.

We now define an important kinematical quantity known as the *stretch* $\lambda(\mathbf{M})$ in the direction of a unit vector \mathbf{M} based at \mathbf{X} in \mathcal{B}_r . Let dS be the length of an infinitesimal line element of material lying along the direction \mathbf{M} in \mathcal{B}_r . Under the deformation this becomes the infinitesimal line element $\mathbf{F}\mathbf{M}dS$ based at \mathbf{x} in \mathcal{B} , which has length $|\mathbf{F}\mathbf{M}|dS$. Thus, the ratio of deformed to undeformed length of the line element is

$|\mathbf{FM}|$, which defines the stretch in the direction \mathbf{M} :

$$\lambda(\mathbf{M}) = |\mathbf{FM}| = [(\mathbf{F}^T \mathbf{F} \mathbf{M}) \cdot \mathbf{M}]^{1/2}. \quad (5)$$

The product $\mathbf{F}^T \mathbf{F}$ in (5) defines the *right Cauchy–Green deformation tensor*, denoted \mathbf{C} , which has Cartesian components $C_{\alpha\beta} = F_{p\alpha} F_{p\beta}$, where the usual Einstein summation convention is used for repeated indices. Since $C_{\alpha\beta}$ has two Greek indices it is associated with \mathcal{B}_r , and \mathbf{C} is referred to as a Lagrangian tensor. This distinguishes it from its Eulerian counterpart, the *left Cauchy–Green deformation tensor* $\mathbf{B} = \mathbf{F} \mathbf{F}^T$, which has Cartesian components $B_{ij} = F_{i\alpha} F_{j\alpha}$ and is associated with \mathcal{B} . For future reference we record here the definitions

$$\mathbf{B} = \mathbf{F} \mathbf{F}^T, \quad \mathbf{C} = \mathbf{F}^T \mathbf{F}. \quad (6)$$

Scalar quantities known as the *principal invariants* of \mathbf{B} (the same as those of \mathbf{C}) are the coefficients I_1, I_2, I_3 in the identity

$$\mathbf{B}^3 - I_1 \mathbf{B}^2 + I_2 \mathbf{B} - I_3 \mathbf{I} = \mathbf{O}, \quad (7)$$

where \mathbf{O} is the zero tensor and \mathbf{I} the identity tensor in \mathcal{B} . This is the Cayley–Hamilton theorem, and I_1, I_2, I_3 are defined by

$$I_1 = \text{tr}(\mathbf{B}), \quad I_2 = \frac{1}{2}[I_1^2 - \text{tr}(\mathbf{B}^2)], \quad I_3 = \det \mathbf{B} \equiv J^2. \quad (8)$$

Since $I_3 = J^2$, we see that for an incompressible material $I_3 = 1$. Furthermore, for a plane strain deformation $I_2 = I_1$ and then, for an incompressible material, (7) factorizes as

$$(\mathbf{B} - \mathbf{I})[\mathbf{B}^2 - (I_1 - 1)\mathbf{B} + \mathbf{I}] = \mathbf{O}, \quad (9)$$

thus yielding the two-dimensional (plane strain) version of the Cayley–Hamilton theorem for an incompressible material, namely

$$\mathbf{B}^2 - (I_1 - 1)\mathbf{B} + \mathbf{I} = \mathbf{O}, \quad (10)$$

wherein the tensors are now two-dimensional.

Valuable further analysis of the local deformation governed by \mathbf{F} is provided by the *polar decomposition theorem*, which enables \mathbf{F} to be expressed in the two forms

$$\mathbf{F} = \mathbf{R} \mathbf{U} = \mathbf{V} \mathbf{R}, \quad (11)$$

each of which is uniquely defined. Here, \mathbf{R} is a proper orthogonal tensor, which represents a rotation, and \mathbf{U} and \mathbf{V} are positive definite and symmetric tensors, termed the *right* and *left stretch tensors*, respectively. Their symmetry allows us to introduce the spectral decompositions

$$\mathbf{U} = \sum_{i=1}^3 \lambda_i \mathbf{u}^{(i)} \otimes \mathbf{u}^{(i)}, \quad \mathbf{V} = \sum_{i=1}^3 \lambda_i \mathbf{v}^{(i)} \otimes \mathbf{v}^{(i)}, \quad (12)$$

where $\lambda_i > 0$, $i \in \{1, 2, 3\}$, are the *principal stretches*, $\mathbf{u}^{(i)}$ and $\mathbf{v}^{(i)}$ are the (unit) eigenvectors of \mathbf{U} and \mathbf{V} , respectively, and \otimes denotes the tensor product: $\mathbf{u}^{(i)}$ and $\mathbf{v}^{(i)}$ are referred to as the *Lagrangian principal axes* and *Eulerian principal axes*, respectively. By taking $\mathbf{M} = \mathbf{u}^{(i)}$ in the definition (5) of stretch, we see that $\lambda(\mathbf{u}^{(i)}) = \lambda_i$, the principal stretch corresponding to $\mathbf{u}^{(i)}$.

The connections

$$\mathbf{C} = \mathbf{U}^2, \quad \mathbf{B} = \mathbf{V}^2 \quad (13)$$

are also recorded here for later reference. These each have eigenvalues $\lambda_1^2, \lambda_2^2, \lambda_3^2$, and their principal invariants I_1, I_2, I_3 defined by (8) may now be expressed in terms of the principal stretches as

$$I_1 = \lambda_1^2 + \lambda_2^2 + \lambda_3^2, \quad I_2 = \lambda_2^2 \lambda_3^2 + \lambda_3^2 \lambda_1^2 + \lambda_1^2 \lambda_2^2, \quad I_3 = \lambda_1^2 \lambda_2^2 \lambda_3^2. \quad (14)$$

Note that these are symmetric functions of $\lambda_1, \lambda_2, \lambda_3$.

Finally in this section we note that from (3), (11) and (12) we may express J in the alternative forms

$$J = \det \mathbf{F} = \det \mathbf{U} = \det \mathbf{V} = \lambda_1 \lambda_2 \lambda_3. \quad (15)$$

In particular, for an incompressible material, the principal stretches satisfy the constraint

$$\lambda_1 \lambda_2 \lambda_3 = 1. \quad (16)$$

2.2 Stress and Equilibrium

While deformation is essentially concerned with geometry, the forces acting on a body that cause the deformation and changes in geometry are described in terms of stresses, and this section therefore introduces the notion of stress and its representation in terms of tensors. For this purpose we consider an arbitrary subdomain of \mathcal{B}_r , denoted \mathcal{D}_r , and its deformed counterpart \mathcal{D} in \mathcal{B} . Let $\partial \mathcal{D}_r$ and $\partial \mathcal{D}$ be the boundaries of \mathcal{D}_r and \mathcal{D} , respectively. An element of area dA on $\partial \mathcal{D}_r$ with unit outward normal \mathbf{N} is deformed into the area da on $\partial \mathcal{D}$ with unit normal \mathbf{n} , as depicted in Fig. 5.

According to Cauchy's stress theorem, the surface force acting on the area da due to its contact with the surrounding material depends linearly on the normal \mathbf{n} and may be written as $\boldsymbol{\sigma}^T \mathbf{n} da$, where $\boldsymbol{\sigma}$ is the *Cauchy stress tensor* (a second-order tensor). If the deformation results from the combined action of surface tractions on $\partial \mathcal{B}$ and a body force \mathbf{b} per unit mass then for equilibrium of the domain \mathcal{D} the total force on it must vanish, i.e.,

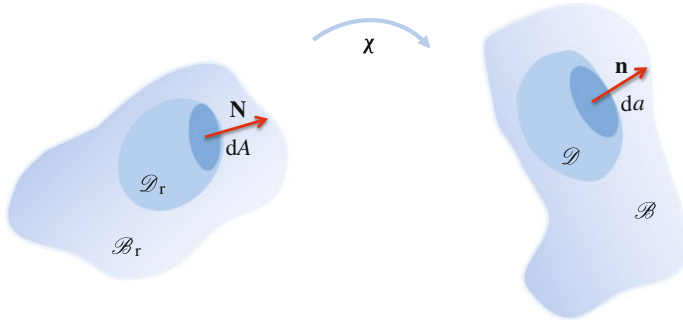


Fig. 5 An area element dA with unit outward normal \mathbf{N} on the boundary $\partial\mathcal{D}_r$ of the reference domain $\mathcal{D}_r \subset \mathcal{B}_r$ deforms into the area element da with unit outward normal \mathbf{n} on the boundary $\partial\mathcal{D}$ of the domain $\mathcal{D} \subset \mathcal{B}$ under the deformation χ

$$\int_{\partial\mathcal{D}} \boldsymbol{\sigma}^T \mathbf{n} \, da + \int_{\mathcal{D}} \rho \mathbf{b} \, dv \equiv \int_{\mathcal{D}} (\operatorname{div} \boldsymbol{\sigma} + \rho \mathbf{b}) \, dv = \mathbf{0}, \tag{17}$$

where ρ is the mass density per unit volume in \mathcal{D} , dv is an element of volume in \mathcal{D} , and the divergence theorem has been applied to the surface integral to obtain the volume integral on the right-hand side.

Assuming that the integrand on the right-hand side of (17) is continuous the arbitrariness of \mathcal{D} allows us to deduce the standard local form of the equilibrium equation, namely

$$\operatorname{div} \boldsymbol{\sigma} + \rho \mathbf{b} = \mathbf{0}. \tag{18}$$

If there are no intrinsic couple stresses in the material then symmetry of $\boldsymbol{\sigma}$ follows from the equilibrium of the moments of the forces acting on \mathcal{D} , so that $\boldsymbol{\sigma}^T = \boldsymbol{\sigma}$, and the transpose on $\boldsymbol{\sigma}$ is no longer needed.

The equilibrium equation (18) is Eulerian in nature since \mathbf{x} is the independent variable. The equation may also be expressed in Lagrangian form, with \mathbf{X} as the independent variable, by using the standard kinematic identity $\operatorname{Div} (J\mathbf{F}^{-1}) = \mathbf{0}$ and the definition

$$\mathbf{S} = J\mathbf{F}^{-1}\boldsymbol{\sigma} \tag{19}$$

of the so-called *nominal stress tensor*, which leads to the connection $\operatorname{Div} \mathbf{S} = J \operatorname{div} \boldsymbol{\sigma}$. By defining the mass density ρ_r per unit reference volume, invoking conservation of mass $\rho_r dV = \rho dv$ and recalling that $dv = JdV$, we obtain the connection

$$\rho_r = J\rho, \tag{20}$$

and hence the equilibrium equation (18) can be expressed in the equivalent form as

$$\operatorname{Div} \mathbf{S} + \rho_r \mathbf{b} = \mathbf{0}. \tag{21}$$

The transpose \mathbf{S}^T of \mathbf{S} is known as the *first Piola–Kirchhoff stress tensor*. For an isochoric deformation ($J = 1$) we have $\rho = \rho_r$, which becomes an identity for an incompressible material.

Note that, unlike $\boldsymbol{\sigma}$, \mathbf{S} is not in general symmetric but it follows from (19) and the symmetry of $\boldsymbol{\sigma}$ that

$$\mathbf{S}^T \mathbf{F}^T = \mathbf{F} \mathbf{S}. \quad (22)$$

Another stress tensor that is often used, particularly in the computational mechanics community, is the *second Piola–Kirchhoff stress tensor*, here denoted \mathbf{P} . It is symmetric and defined here for later reference through its connections with $\boldsymbol{\sigma}$ and \mathbf{S} , namely

$$\mathbf{P} = J \mathbf{F}^{-1} \boldsymbol{\sigma} \mathbf{F}^{-T} = \mathbf{S} \mathbf{F}^{-T}, \quad (23)$$

where $\mathbf{F}^{-T} = (\mathbf{F}^{-1})^T = (\mathbf{F}^T)^{-1}$.

2.2.1 Residual Stress

At this point we introduce the notion of *residual stress*. Here we adopt the definition of Hoger (1985) that residual stress is a stress distribution that exists in the reference configuration \mathcal{B}_r in the absence of loads, either surface tractions or body forces, and should be distinguished from other types of initial stresses (often referred to as prestresses) that are associated with loads. We denote the residual (Cauchy) stress by $\boldsymbol{\tau}$ and assume that there are no intrinsic couple stresses in \mathcal{B}_r , so that $\boldsymbol{\tau}$ is symmetric: $\boldsymbol{\tau}^T = \boldsymbol{\tau}$. The equilibrium equation that must be satisfied by $\boldsymbol{\tau}$ is, from (21) with $\mathbf{b} = \mathbf{0}$,

$$\text{Div } \boldsymbol{\tau} = \mathbf{0} \quad \text{in } \mathcal{B}_r. \quad (24)$$

Since there are no surface tractions, $\boldsymbol{\tau}$ must also satisfy the boundary condition

$$\boldsymbol{\tau} \mathbf{N} = \mathbf{0} \quad \text{on } \partial \mathcal{B}_r. \quad (25)$$

It is worth emphasizing at this point that residual stresses are necessarily nonuniform and a material with residual stress is itself inhomogeneous. This follows from the identity $\text{Div}(\boldsymbol{\tau} \otimes \mathbf{X}) = (\text{Div } \boldsymbol{\tau}) \otimes \mathbf{X} + \boldsymbol{\tau}$, the use of (24), application of the divergence theorem and then (25), which leads to

$$\int_{\mathcal{B}_r} \boldsymbol{\tau} \, dV = \mathbf{0}. \quad (26)$$

Clearly, a nontrivial $\boldsymbol{\tau}$ cannot be uniform, and the character of the inhomogeneity depends on the geometry of the considered material body.

3 Constitutive Theory

In this section we focus on the characterization of the elastic behavior of solids based on the existence of a *strain-energy function*. Materials which possess a strain-energy function are referred to as *hyperelastic*. First, by considering the virtual work of the forces acting on the body, we motivate the introduction of a strain-energy function. We then examine its general properties and its functional dependence for particular classes of material symmetry through the use of invariants. We also show how residual stress can affect the material response by its inclusion in the argument of the strain-energy function.

3.1 The Elastic Strain-Energy Function

Consider the work done by the forces acting on the region \mathcal{D} in a virtual displacement, i.e., a small increment in \mathbf{x} , which we denote by $\dot{\mathbf{x}}$. This work is

$$\int_{\partial\mathcal{D}} (\boldsymbol{\sigma}\mathbf{n}) \cdot \dot{\mathbf{x}} \, da + \int_{\mathcal{D}} \rho\mathbf{b} \cdot \dot{\mathbf{x}} \, dv = \int_{\mathcal{D}} \text{tr}(\boldsymbol{\sigma} \text{grad } \dot{\mathbf{x}}) \, dv, \quad (27)$$

where the right-hand side has been obtained by an application of the divergence theorem and use of the equilibrium equation (18). By means of the connections (19) and $dv = JdV$ this may also be written

$$\int_{\mathcal{D}_r} \text{tr}(\mathbf{S}\dot{\mathbf{F}}) \, dV, \quad (28)$$

where $\dot{\mathbf{F}} = \text{Grad } \dot{\mathbf{x}}$. The work done is converted into stored elastic energy if there exists a scalar function $W(\mathbf{F})$ such that

$$\dot{W} = \text{tr}(\mathbf{S}\dot{\mathbf{F}}), \quad (29)$$

in which case (28) represents the virtual change in the total elastic energy stored in \mathcal{D}_r . We assume that a strain-energy function $W(\mathbf{F})$ exists, defined per unit volume in \mathcal{D}_r . If the material is inhomogeneous then W also depends separately on \mathbf{X} , but for a homogeneous material the dependence on \mathbf{X} is through $\mathbf{F}(\mathbf{X})$ alone.

Because of (29) the nominal stress is considered to be *work conjugate* to the deformation gradient. If there are no constraints on \mathbf{F} then, since $\dot{\mathbf{F}}$ is arbitrary, we obtain the stress deformation relation

$$\mathbf{S} = \frac{\partial W}{\partial \mathbf{F}}, \quad (30)$$

or, in index notation,

$$S_{\alpha i} = \frac{\partial W}{\partial F_{i\alpha}}, \quad (31)$$

the latter defining the convention used here for the order of the indices when differentiating with respect to $F_{i\alpha}$.

If \mathbf{F} is subject to a constraint then its components are no longer independent and $\dot{\mathbf{F}}$ is not arbitrary so that (30) requires modification. In the case of the incompressibility constraint, for example, (30) is replaced by

$$\mathbf{S} = \frac{\partial W}{\partial \mathbf{F}} - p \mathbf{F}^{-1}, \quad \det \mathbf{F} = 1, \quad (32)$$

where p is a Lagrange multiplier associated with the constraint.

The corresponding Cauchy stress tensor is then obtained from (19) as

$$\boldsymbol{\sigma} = J^{-1} \mathbf{F} \frac{\partial W}{\partial \mathbf{F}}, \quad \boldsymbol{\sigma} = \mathbf{F} \frac{\partial W}{\partial \mathbf{F}} - p \mathbf{I}, \quad (33)$$

for unconstrained and incompressible materials, respectively, with $J = \det \mathbf{F} = 1$ in the latter, where \mathbf{I} is again the identity tensor in \mathcal{B} .

Let us take the strain energy to be measured from \mathcal{B}_r , where $\mathbf{F} = \mathbf{I}_r$, the identity tensor in \mathcal{B}_r . This imposes the condition

$$W(\mathbf{I}_r) = 0. \quad (34)$$

If the configuration \mathcal{B}_r is stress free then we have

$$\frac{\partial W}{\partial \mathbf{F}}(\mathbf{I}_r) = \mathbf{O}, \quad \frac{\partial W}{\partial \mathbf{F}}(\mathbf{I}_r) - p^{(r)} \mathbf{I}_r = \mathbf{O}, \quad (35)$$

for unconstrained and incompressible materials, respectively, where $p^{(r)}$ is the specialization of the Lagrange multiplier p to \mathcal{B}_r . The reference configuration \mathcal{B}_r is sometimes referred to as a *natural configuration* if the conditions (34) and (35)₁ (or (35)₂) hold simultaneously.

If \mathcal{B}_r is not stress free, but supports a residual stress $\boldsymbol{\tau}$ then (35) does not hold and \mathcal{B}_r is referred to as a *residually stressed configuration*. In this case W , still measured from \mathcal{B}_r , depends on $\boldsymbol{\tau}$ as well as \mathbf{F} . We therefore include $\boldsymbol{\tau}$ explicitly in the arguments of W and write

$$W = W(\mathbf{F}, \boldsymbol{\tau}). \quad (36)$$

We emphasize that $\boldsymbol{\tau}$, being inhomogeneous, depends on \mathbf{X} , and therefore the material itself is also inhomogeneous if it is residually stressed.

The formulas (30)–(33) are unaffected by the presence of $\boldsymbol{\tau}$ but we now include the dependence on $\boldsymbol{\tau}$ and write

$$\mathbf{S} = \frac{\partial W}{\partial \mathbf{F}}(\mathbf{F}, \boldsymbol{\tau}), \quad \boldsymbol{\sigma} = J^{-1} \mathbf{F} \mathbf{S} = J^{-1} \mathbf{F} \frac{\partial W}{\partial \mathbf{F}}(\mathbf{F}, \boldsymbol{\tau}) \quad (37)$$

for an unconstrained material, and

$$\mathbf{S} = \frac{\partial W}{\partial \mathbf{F}}(\mathbf{F}, \boldsymbol{\tau}) - p \mathbf{F}^{-1}, \quad \boldsymbol{\sigma} = \mathbf{F} \mathbf{S} = \mathbf{F} \frac{\partial W}{\partial \mathbf{F}}(\mathbf{F}, \boldsymbol{\tau}) - p \mathbf{I} \quad (38)$$

for an incompressible material.

In \mathcal{B}_r there is no distinction between different stress tensors and each one must reduce to the residual stress, in which case

$$\boldsymbol{\tau} = \frac{\partial W}{\partial \mathbf{F}}(\mathbf{I}_r, \boldsymbol{\tau}), \quad \boldsymbol{\tau} = \frac{\partial W}{\partial \mathbf{F}}(\mathbf{I}_r, \boldsymbol{\tau}) - p^{(r)} \mathbf{I}_r, \quad (39)$$

for an unconstrained and incompressible material, respectively, where again \mathbf{I}_r is the identity tensor in \mathcal{B}_r and $p^{(r)}$ represents the value of p in \mathcal{B}_r (see, for example, Shams et al. 2011). These equations can be thought of as conditions providing either constraints on the residual stress for a given strain-energy function or constraints on the properties of the strain-energy function for a known residual stress. Some specializations of these conditions will be seen in later sections. These are particular constraints that apply for a residually stressed material and should be respected when specific models are constructed. Forms of W should also be consistent with data obtained from experimental tests that elicit the elastic properties of materials they aim to model. Other constraints may arise from basic physical and mathematical considerations, but we do not address these here. However, a key constraint, which should always be adopted, arises from the notion of *objectivity*, otherwise referred to as *material frame indifference*, which we discuss in the following.

3.2 The Principle of Objectivity

For a residually stressed material a general strain-energy function must satisfy the conditions (39), but it is not as yet subject to any other restrictions. At each \mathbf{X} it depends on \mathbf{F} and $\boldsymbol{\tau}$ in an otherwise general way. However, not all candidates for $W(\mathbf{F}, \boldsymbol{\tau})$ are admissible, and, importantly, after deformation W should be unaffected by any superimposed rigid body transformation. Such a transformation has the form $\mathbf{x}^* = \mathbf{Q}\mathbf{x} + \mathbf{c}$, where, since we are not considering time dependence, \mathbf{Q} is an arbitrary constant rotation tensor and \mathbf{c} is an arbitrary constant vector. The deformation gradient $\mathbf{F}^* = \text{Grad } \mathbf{x}^*$ associated with this new deformation is then given by $\mathbf{F}^* = \mathbf{Q}\mathbf{F}$. Noting that $\boldsymbol{\tau}$ is defined in the reference configuration and is not therefore affected by the rotation in \mathcal{B} , the requirement imposed on W is that it must be invariant under this transformation, i.e.,

$$W(\mathbf{Q}\mathbf{F}, \boldsymbol{\tau}) = W(\mathbf{F}, \boldsymbol{\tau}) \quad (40)$$

for *arbitrary* proper orthogonal \mathbf{Q} and for any deformation gradient \mathbf{F} .

This restriction on W is referred to as the *principle of objectivity*, or just *objectivity* for brevity, and from now on we regard W as objective.

From the polar decomposition (11)₁ we obtain $\mathbf{QF} = \mathbf{QRU}$ and then by choosing $\mathbf{Q} = \mathbf{R}^T$, Eq. (40) yields $W(\mathbf{F}, \boldsymbol{\tau}) = W(\mathbf{U}, \boldsymbol{\tau})$, which shows that W is independent of the rotational part \mathbf{R} of the deformation gradient and depends on \mathbf{F} only through the stretch tensor \mathbf{U} . Equivalently, since $\mathbf{C} = \mathbf{U}^2$, we can regard W as a function of \mathbf{C} and $\boldsymbol{\tau}$. Each of \mathbf{C} and $\boldsymbol{\tau}$ is a Lagrangian tensor, unaffected by a rotation in \mathcal{B} , and therefore any function of these two tensors is necessarily objective. In particular, without changing the notation for W on changing its argument, we write the strain-energy function as

$$W(\mathbf{C}, \boldsymbol{\tau}), \tag{41}$$

which automatically accommodates the required objectivity.

From this form of W we obtain the second Piola–Kirchhoff stress tensor

$$\mathbf{P} = 2 \frac{\partial W}{\partial \mathbf{C}}, \quad \mathbf{P} = 2 \frac{\partial W}{\partial \mathbf{C}} - p \mathbf{C}^{-1} \tag{42}$$

for unconstrained and incompressible materials, respectively. We remark that \mathbf{P} and $\mathbf{C}/2$ are therefore work conjugate stress and deformation tensors. In this case the incompressibility constraint is $I_3 = \det \mathbf{C} = 1$.

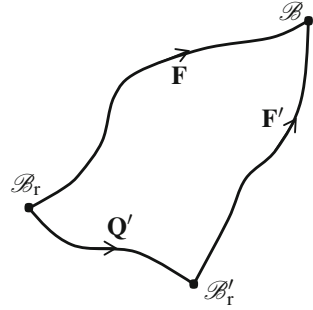
3.3 Material Symmetry (with no Residual Stress)

Objectivity applies irrespective of the material properties, but other restrictions arise that depend on the character of the material considered, and, in particular, the material may possess some intrinsic symmetry in its reference configuration. In order to examine such symmetry we consider $\boldsymbol{\tau} = \mathbf{O}$ since nonzero residual stresses complicate the arguments. For discussion of symmetry considerations in the presence of residual stress we refer to Hoger (1985) and Ogden (2003b).

If the material response is the same with respect to different reference configurations then this implies that the material has an intrinsic symmetry, and the transformation between the reference configurations is then known as a *symmetry transformation*.

To be specific, consider two reference configurations, denoted \mathcal{B}_r and \mathcal{B}'_r , and let a typical material point in these configurations have position vectors \mathbf{X} and \mathbf{X}' , respectively. Suppose the transformation (deformation) from \mathcal{B}_r to \mathcal{B}'_r has the deformation gradient $\mathbf{Q}' = \text{Grad } \mathbf{X}'$, which should be distinguished from the rotation \mathbf{Q} in \mathcal{B} . Then the deformation gradients of \mathcal{B} relative to \mathcal{B}_r and \mathcal{B}'_r , respectively, are \mathbf{F} and $\mathbf{F}' = \mathbf{FQ}'^{-1}$, as depicted in Fig. 6. In components the latter reads $\partial x_i / \partial X'_\alpha = (\partial x_i / \partial X_\beta)(\partial X_\beta / \partial X'_\alpha)$.

Fig. 6 Depiction of the reference configurations \mathcal{B}_r and \mathcal{B}'_r and the deformed configuration \mathcal{B} connected by the deformation gradients \mathbf{F} , \mathbf{F}' and \mathbf{Q}' , with $\mathbf{F} = \mathbf{F}'\mathbf{Q}'$ in the space of deformation gradients



The right Cauchy–Green tensor relative to \mathcal{B}_r is \mathbf{C} , and that relative to \mathcal{B}'_r is $\mathbf{C}' = \mathbf{F}'^T \mathbf{F}' = \mathbf{Q}'^{-T} \mathbf{C} \mathbf{Q}'^{-1}$. If the material properties, as characterized by the strain-energy function W , are independent of this change of reference configuration then we must have, for the given \mathbf{Q}' ,

$$W(\mathbf{Q}'^{-T} \mathbf{C} \mathbf{Q}'^{-1}) = W(\mathbf{C}) \tag{43}$$

for all right Cauchy–Green deformation tensors \mathbf{C} , where the argument $\boldsymbol{\tau} = \mathbf{O}$ has been omitted from W . Such a \mathbf{Q}' identifies a symmetry of the material in the original reference configuration \mathcal{B}_r .

The set of all such changes of reference configuration for which (43) holds, i.e., the set of \mathbf{Q}' satisfying (43) for all right Cauchy–Green deformation tensors \mathbf{C} , forms a group of transformations, called the *symmetry group of the material relative to the reference configuration \mathcal{B}_r* . In this chapter we consider only symmetries for which the \mathbf{Q}' 's are proper orthogonal transformations, so that $\mathbf{Q}'^{-1} = \mathbf{Q}'^T$. It should be emphasized that the rotation \mathbf{Q}' is applied in \mathcal{B}_r , whereas \mathbf{Q} is applied in \mathcal{B} . The two rotations are entirely independent. We now consider the consequences of (43) for some particular classes of symmetry groups.

3.3.1 Isotropy

With the restriction to proper orthogonal transformations, Eq. (43) becomes

$$W(\mathbf{Q}' \mathbf{C} \mathbf{Q}'^T) = W(\mathbf{C}). \tag{44}$$

An *isotropic elastic material* is one for which the symmetry group is the full *proper orthogonal group*, i.e., (44) holds for *arbitrary* proper orthogonal \mathbf{Q}' . Equation (44) implies that W is an *isotropic function* of \mathbf{C} . This means, in particular, that W depends on \mathbf{C} through just three scalar deformation variables, which typically are taken to be the three principal invariants I_1, I_2, I_3 defined in (8) in terms of the left Cauchy–Green tensor \mathbf{B} . For convenience we now repeat them here in terms of \mathbf{C} :

$$I_1 = \text{tr } \mathbf{C}, \quad I_2 = \frac{1}{2}[I_1^2 - \text{tr}(\mathbf{C}^2)], \quad I_3 = \det \mathbf{C}. \quad (45)$$

We now write $W = W(I_1, I_2, I_3)$, and from (30) the nominal stress is given by

$$\mathbf{S} = \frac{\partial W}{\partial \mathbf{F}} = \sum_{i=1}^3 W_i \frac{\partial I_i}{\partial \mathbf{F}}, \quad (46)$$

where we have used the shorthand notation $W_i = \partial W / \partial I_i$, $i = 1, 2, 3$. All the information about material properties is contained in the coefficients W_i , $i = 1, 2, 3$, while the derivatives $\partial I_i / \partial \mathbf{F}$ are purely kinematic quantities. The latter can be calculated simply from (45) as

$$\frac{\partial I_1}{\partial \mathbf{F}} = 2\mathbf{F}^T, \quad \frac{\partial I_2}{\partial \mathbf{F}} = 2(I_1\mathbf{F}^T - \mathbf{C}\mathbf{F}^T), \quad \frac{\partial I_3}{\partial \mathbf{F}} = 2I_3\mathbf{F}^{-1}, \quad (47)$$

and an expanded expression for \mathbf{S} then follows from (46). The corresponding Cauchy stress tensor $\boldsymbol{\sigma} = J^{-1}\mathbf{F}\mathbf{S}$ is then given by

$$J\boldsymbol{\sigma} = 2W_1\mathbf{B} + 2W_2(I_1\mathbf{B} - \mathbf{B}^2) + 2I_3W_3\mathbf{I}. \quad (48)$$

For an incompressible material $I_3 \equiv 1$, W depends only on I_1 and I_2 and, instead of (48), we have

$$\boldsymbol{\sigma} = 2W_1\mathbf{B} + 2W_2(I_1\mathbf{B} - \mathbf{B}^2) - p\mathbf{I}, \quad (49)$$

where p is the Lagrange multiplier (an arbitrary hydrostatic pressure) appearing in (33)₂.

Since, by (14), I_1, I_2, I_3 are symmetric functions of the stretches, we can also think of W as a symmetric function of the stretches and write $W = W(\lambda_1, \lambda_2, \lambda_3)$, and it follows that

$$\lambda_i \frac{\partial W}{\partial \lambda_i} = 2\lambda_i^2 W_1 + 2\lambda_i^2 (I_1 - \lambda_i^2) W_2 + 2I_3 W_3, \quad i = 1, 2, 3. \quad (50)$$

By (48) $\boldsymbol{\sigma}$ has the same principal axes as \mathbf{B} . Thus, (50) represents the principal components of (48) and enables the principal Cauchy stresses, denoted σ_i , $i = 1, 2, 3$, to be identified as

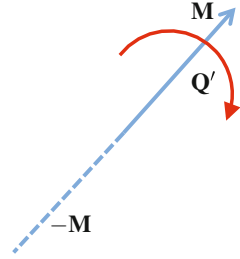
$$\sigma_i = J^{-1} \lambda_i \frac{\partial W}{\partial \lambda_i}, \quad i = 1, 2, 3, \quad (51)$$

for an unconstrained material. For an incompressible material this is replaced by

$$\sigma_i = \lambda_i \frac{\partial W}{\partial \lambda_i} - p, \quad i = 1, 2, 3, \quad (52)$$

which correspond to the eigenvalues of Eq. (49).

Fig. 7 Transverse isotropy with preferred direction \mathbf{M} in the reference configuration. The material properties are independent of rotations \mathbf{Q}' about \mathbf{M} and reversal of the direction of \mathbf{M} : $\mathbf{M} \rightarrow -\mathbf{M}$



3.3.2 One Preferred Direction (Transverse Isotropy)

If there is a single preferred direction in the material in its reference configuration, as in the case of a fiber-reinforced material with a single family of (locally) aligned fibers, then we identify that direction by the unit vector \mathbf{M} in \mathcal{B}_r , which in general depends on the point \mathbf{X} . Such a material is said to be *transversely isotropic* with direction of transverse isotropy \mathbf{M} . In the plane transverse to \mathbf{M} the material response is isotropic.

The material properties are invariant with respect to an arbitrary rotation about the direction \mathbf{M} and to reversal of \mathbf{M} , i.e., to rotations \mathbf{Q}' such that $\mathbf{Q}'\mathbf{M} = \pm\mathbf{M}$, as depicted in Fig. 7.

From the mathematical point of view the strain-energy function must satisfy (44) for all such \mathbf{Q}' . Thus, W depends on \mathbf{M} as well as \mathbf{C} and we may regard W as a function of both \mathbf{M} and \mathbf{C} , but since material properties are treated as independent of the sense of \mathbf{M} we can consider the \mathbf{M} dependence to be through the tensor product $\mathbf{M} \otimes \mathbf{M}$ and write $W(\mathbf{C}, \mathbf{M} \otimes \mathbf{M})$ instead of just $W(\mathbf{C})$, and note that $\mathbf{M} \otimes \mathbf{M}$ is unaffected by reversal of \mathbf{M} . In general, \mathbf{M} depends on \mathbf{X} , in which case the material is inhomogeneous. This is left implicit in $W(\mathbf{C}, \mathbf{M} \otimes \mathbf{M})$ since material symmetry is a local property.

It follows that transverse isotropy may be characterized by W being an *isotropic function* of the two symmetric tensors \mathbf{C} and $\mathbf{M} \otimes \mathbf{M}$ (Liu 1982); for general background on transverse isotropy and more generally on the theory of invariants we refer to Spencer (1971, 1972, 1984). Noting that $\mathbf{Q}'\mathbf{M} = \mathbf{M}\mathbf{Q}'^T$, the symmetry requirement is then

$$W(\mathbf{Q}'\mathbf{C}\mathbf{Q}'^T, \mathbf{Q}'\mathbf{M} \otimes \mathbf{Q}'\mathbf{M}) = W(\mathbf{C}, \mathbf{M} \otimes \mathbf{M}) \quad (53)$$

for *all* orthogonal \mathbf{Q}' . In this case there is no difference whether we restrict attention to *proper* orthogonal \mathbf{Q}' or consider all orthogonal \mathbf{Q}' since we may replace \mathbf{Q}' by $-\mathbf{Q}'$ in (53) without changing its consequences. Similarly in Eq. (44). The tensor $\mathbf{M} \otimes \mathbf{M}$ is referred to as a *structure tensor*.

The symmetry (53) is equivalent to W being a function of five independent invariants for an unconstrained material in three dimensions. These are, for example, the three isotropic invariants I_1, I_2, I_3 defined in (45) and two invariants that depend on \mathbf{M} and \mathbf{C} , these usually being denoted I_4 and I_5 . The choice of I_4 and I_5 is not unique

but, typically, they are defined by

$$I_4 = \mathbf{M} \cdot (\mathbf{CM}), \quad I_5 = \mathbf{M} \cdot (\mathbf{C}^2\mathbf{M}). \quad (54)$$

Note that in terms of the stretch $\lambda(\mathbf{M})$ defined in (5), $I_4 = \lambda(\mathbf{M})^2$, the square of the stretch in the direction \mathbf{M} . The invariant I_5 does not have a similar simple interpretation, and we refer to Merodio and Ogden (2002) for discussion of a related invariant which does have a direct physical interpretation.

Then, by expanding out the formula (30) based on the invariants I_1, \dots, I_5 , similarly to that in the isotropic case, and using again the derivatives (47), supplemented by the derivatives

$$\frac{\partial I_4}{\partial \mathbf{F}} = 2\mathbf{M} \otimes \mathbf{FM}, \quad \frac{\partial I_5}{\partial \mathbf{F}} = 2(\mathbf{M} \otimes \mathbf{BFM} + \mathbf{CM} \otimes \mathbf{FM}), \quad (55)$$

we obtain an expression for the nominal stress tensor \mathbf{S} , which we do not write here. The corresponding Cauchy stress tensor $\boldsymbol{\sigma} = J^{-1}\mathbf{FS}$ for a transversely isotropic material is then given by

$$J\boldsymbol{\sigma} = 2W_1\mathbf{B} + 2W_2(I_1\mathbf{B} - \mathbf{B}^2) + 2I_3W_3\mathbf{I} + 2W_4\mathbf{m} \otimes \mathbf{m} + 2W_5(\mathbf{m} \otimes \mathbf{Bm} + \mathbf{Bm} \otimes \mathbf{m}), \quad (56)$$

where $\mathbf{m} = \mathbf{FM}$ is the ‘push forward’ of \mathbf{M} from \mathcal{B}_r to \mathcal{B} and now $W_i = \partial W / \partial I_i$, $i = 1, \dots, 5$, with $W = W(I_1, I_2, I_3, I_4, I_5)$. This recovers the formula (48) for an isotropic material when $W_4 = W_5 = 0$.

For an incompressible material $I_3 \equiv 1$, so only the four independent invariants I_1, I_2, I_4, I_5 are required in W to characterize the material, with $W = W(I_1, I_2, I_4, I_5)$ in general. Then, instead of (56), we have

$$\boldsymbol{\sigma} = 2W_1\mathbf{B} + 2W_2(I_1\mathbf{B} - \mathbf{B}^2) + 2W_4\mathbf{m} \otimes \mathbf{m} + 2W_5(\mathbf{m} \otimes \mathbf{Bm} + \mathbf{Bm} \otimes \mathbf{m}) - p\mathbf{I}. \quad (57)$$

Plane Strain

If attention is restricted to plane strain deformations, for example, then the number of independent invariants is reduced. In particular, for plane strain with \mathbf{M} in the considered plane the connections

$$I_2 = I_1 + I_3 - 1, \quad I_5 = (I_1 - 1)I_4 - I_3 \quad (58)$$

may be deduced (Merodio and Ogden 2002, 2003), and only three independent invariants remain, which we can take as I_1, I_3 and I_4 , for example. In the incompressible case just two invariants remain, namely I_1 and I_4 , and we define the plane strain specialization of W , denoted \hat{W} , by

$$\hat{W}(I_1, I_4) = W(I_1, I_2, I_4, I_5) \quad \text{with} \quad I_2 = I_1, \quad I_5 = (I_1 - 1)I_4 - 1. \quad (59)$$

For plane strain $\mathbf{m} = \mathbf{FM}$ lies in the considered plane, and if we identify planar second-order tensors with a superposed hat $\hat{\cdot}$ then the plane strain version of Cauchy stress, denoted $\hat{\boldsymbol{\sigma}}$, becomes simply

$$\hat{\boldsymbol{\sigma}} = 2\hat{W}_1\hat{\mathbf{B}} + 2\hat{W}_4\mathbf{m} \otimes \mathbf{m} - \hat{p}\hat{\mathbf{I}}, \quad (60)$$

where $\hat{W}_1 = \partial\hat{W}/\partial I_1$ and $\hat{W}_4 = \partial\hat{W}/\partial I_4$ and \hat{p} is an adjusted form of p that includes various derivatives of W that contribute only hydrostatic terms to $\hat{\boldsymbol{\sigma}}$.

3.4 A General Invariant Formulation

As we have seen, both isotropy and transverse isotropy can be formulated in terms of invariants. More generally, suppose that there are N independent invariants associated with \mathbf{C} and the material structure. Let these be denoted by I_1, I_2, \dots, I_N . They depend on \mathbf{C} and the material structure but not otherwise on the properties of the material, i.e., not on the particular form of W . Thus, we can write $W = W(I_1, I_2, \dots, I_N)$, and for an unconstrained material the nominal and Cauchy stress tensors can be expanded as

$$\mathbf{S} = \sum_{i=1}^N W_i \frac{\partial I_i}{\partial \mathbf{F}}, \quad \boldsymbol{\sigma} = J^{-1} \mathbf{F} \sum_{i=1}^N W_i \frac{\partial I_i}{\partial \mathbf{F}}, \quad (61)$$

where we have extended the notation W_i to $i = 1, 2, \dots, N$. The corresponding expressions for an incompressible material are

$$\mathbf{S} = \sum_{i=1, i \neq 3}^N W_i \frac{\partial I_i}{\partial \mathbf{F}} - p \mathbf{F}^{-1}, \quad \boldsymbol{\sigma} = \mathbf{F} \sum_{i=1, i \neq 3}^N W_i \frac{\partial I_i}{\partial \mathbf{F}} - p \mathbf{I}. \quad (62)$$

In general, the derivatives W_i depend on the material properties through the strain-energy function W , but, independently of that, apart from the case of isotropy, some information about the material structure is also contained within the derivatives $\partial I_i / \partial \mathbf{F}$, as for a transversely isotropic material for which $\partial I_4 / \partial \mathbf{F}$ and $\partial I_5 / \partial \mathbf{F}$ depend on the structure through \mathbf{M} .

In the remainder of this section we apply the above first to a material with two preferred directions and second to a material with a general residual stress but no preferred directions.

3.4.1 Two Preferred Directions and the Special Case of Orthotropy

Consider the situation in which there are two preferred directions in the reference configuration \mathcal{B}_t of the material, identified by the unit vectors \mathbf{M} and \mathbf{M}' with associated structure tensors $\mathbf{M} \otimes \mathbf{M}$ and $\mathbf{M}' \otimes \mathbf{M}'$. The strain-energy function now depends on \mathbf{C} , $\mathbf{M} \otimes \mathbf{M}$ and $\mathbf{M}' \otimes \mathbf{M}'$, and we write $W(\mathbf{C}, \mathbf{M} \otimes \mathbf{M}, \mathbf{M}' \otimes \mathbf{M}')$. Similarly to the transversely isotropic model, W is an isotropic function of its three arguments, i.e., it must satisfy

$$W(\mathbf{Q}'\mathbf{C}\mathbf{Q}'^T, \mathbf{Q}'\mathbf{M} \otimes \mathbf{Q}'\mathbf{M}, \mathbf{Q}'\mathbf{M}' \otimes \mathbf{Q}'\mathbf{M}') = W(\mathbf{C}, \mathbf{M} \otimes \mathbf{M}, \mathbf{M}' \otimes \mathbf{M}') \quad (63)$$

for arbitrary orthogonal \mathbf{Q}' and for any right Cauchy–Green tensor \mathbf{C} .

This means that W can be expressed in terms of invariants of the three tensors and their combinations. For an unconstrained material this requires eight independent invariants. These are the invariants I_1, \dots, I_5 associated with \mathbf{C} and $\mathbf{M} \otimes \mathbf{M}$, but additionally the invariants combining \mathbf{C} and $\mathbf{M}' \otimes \mathbf{M}'$, denoted I_6, I_7 , analogously to I_4, I_5 , and defined by

$$I_6 = \mathbf{M}' \cdot (\mathbf{C}\mathbf{M}'), \quad I_7 = \mathbf{M}' \cdot (\mathbf{C}^2\mathbf{M}'). \quad (64)$$

Finally, there is the invariant $[\mathbf{M} \cdot (\mathbf{C}\mathbf{M}')] \mathbf{M} \cdot \mathbf{M}'$ that involves all three tensors when $\mathbf{M} \cdot \mathbf{M}' \neq 0$. However, it is more convenient in the analysis to use $\mathbf{M} \cdot (\mathbf{C}\mathbf{M}')$ without the geometric factor, and we denote this by I_8 . Thus,

$$I_8 = \mathbf{M} \cdot (\mathbf{C}\mathbf{M}'), \quad (65)$$

which is not strictly invariant since it changes sign if either \mathbf{M} or \mathbf{M}' is reversed. An alternative, which is invariant, is to use I_8^2 rather than I_8 itself, and in any case the strain-energy function should depend on I_8 through I_8^2 . In fact, for the special case in which $\mathbf{M} \cdot \mathbf{M}' = 0$, I_8^2 is not needed since it depends on the other invariants and is given by (Merodio and Ogden 2006)

$$I_8^2 = I_2 + I_5 + I_7 + I_4 I_6 - I_1(I_4 + I_6). \quad (66)$$

To form expressions for the stress tensors we require the derivatives of I_6, I_7 and I_8 with respect to \mathbf{F} in addition to those given in (47) and (55) for I_1, \dots, I_5 . These are

$$\frac{\partial I_6}{\partial \mathbf{F}} = 2\mathbf{M}' \otimes \mathbf{F}\mathbf{M}', \quad \frac{\partial I_7}{\partial \mathbf{F}} = 2(\mathbf{M}' \otimes \mathbf{B}\mathbf{F}\mathbf{M}' + \mathbf{C}\mathbf{M}' \otimes \mathbf{F}\mathbf{M}'), \quad (67)$$

and

$$\frac{\partial I_8}{\partial \mathbf{F}} = \mathbf{M} \otimes \mathbf{F}\mathbf{M}' + \mathbf{M}' \otimes \mathbf{F}\mathbf{M}. \quad (68)$$

These enable the Cauchy stress tensor $\boldsymbol{\sigma}$ for an unconstrained material to be given via

$$\begin{aligned}
J\boldsymbol{\sigma} = & 2W_1\mathbf{B} + 2W_2(I_1\mathbf{B} - \mathbf{B}^2) + 2I_3W_3\mathbf{I} + 2W_4\mathbf{m} \otimes \mathbf{m} + 2W_5(\mathbf{m} \otimes \mathbf{Bm} + \mathbf{Bm} \otimes \mathbf{m}) \\
& + 2W_6\mathbf{m}' \otimes \mathbf{m}' + 2W_7(\mathbf{m}' \otimes \mathbf{Bm}' + \mathbf{Bm}' \otimes \mathbf{m}') + W_8(\mathbf{m} \otimes \mathbf{m}' + \mathbf{m}' \otimes \mathbf{m}), \quad (69)
\end{aligned}$$

where $\mathbf{m} = \mathbf{FM}$ and $\mathbf{m}' = \mathbf{FM}'$ and the notation $W_i = \partial W / \partial I_i$ now applies for $i = 1, \dots, 8$.

For an incompressible material the list of invariants reduces by one to $I_1, I_2, I_4, \dots, I_8$ and the Cauchy stress is given by

$$\begin{aligned}
\boldsymbol{\sigma} = & 2W_1\mathbf{B} + 2W_2(I_1\mathbf{B} - \mathbf{B}^2) - p\mathbf{I} + 2W_4\mathbf{m} \otimes \mathbf{m} + 2W_5(\mathbf{m} \otimes \mathbf{Bm} + \mathbf{Bm} \otimes \mathbf{m}) \\
& + 2W_6\mathbf{m}' \otimes \mathbf{m}' + 2W_7(\mathbf{m}' \otimes \mathbf{Bm}' + \mathbf{Bm}' \otimes \mathbf{m}') + W_8(\mathbf{m} \otimes \mathbf{m}' + \mathbf{m}' \otimes \mathbf{m}), \quad (70)
\end{aligned}$$

the notation $W_i = \partial W / \partial I_i$ now applying for $i = 1, 2, 4, \dots, 8$.

In general, the material response associated with two preferred directions is not *orthotropic*, orthotropy being characterized locally by the existence of three mutually orthogonal planes of symmetry in the reference configuration of the material. There are two situations in which the response is orthotropic. The first situation arises in the special case in which the two directions are orthogonal and the second for which the preferred directions are mechanically equivalent (Spencer 1972).

In the second case, for example, the material properties are unaffected by interchange of \mathbf{M} and \mathbf{M}' , which implies that

$$W(I_1, I_2, I_3, I_4, I_5, I_6, I_7, I_8) = W(I_1, I_2, I_3, I_6, I_7, I_4, I_5, I_8). \quad (71)$$

Plane Strain

As for the case of transverse isotropy, the number of independent invariants is reduced for plane strain, and we have the connections given in (58) together with

$$I_7 = (I_1 - 1)I_6 - I_3, \quad I_8^2 = I_4I_6 - I_3|\mathbf{M} \times \mathbf{M}'|^2, \quad (72)$$

and there are only four independent invariants, such as I_1, I_3, I_4, I_6 . In the incompressible case we summarize the connections between the invariants as

$$I_2 = I_1, \quad I_5 = (I_1 - 1)I_4 - 1, \quad I_7 = (I_1 - 1)I_6 - 1, \quad I_8^2 = I_4I_6 - |\mathbf{M} \times \mathbf{M}'|^2, \quad (73)$$

and the strain-energy function depends on just three invariants: $W \rightarrow \hat{W}(I_1, I_4, I_6)$, and the (planar) Cauchy stress has the form

$$\hat{\boldsymbol{\sigma}} = 2\hat{W}_1\hat{\mathbf{B}} + 2\hat{W}_4\mathbf{m} \otimes \mathbf{m} + 2\hat{W}_6\mathbf{m}' \otimes \mathbf{m}' - \hat{p}\hat{\mathbf{I}}, \quad (74)$$

which generalizes the formula (60). Note that when $\mathbf{M} \cdot \mathbf{M}' = 0$, $I_8^2 = I_4I_6 - 1$, which is a special case of the three-dimensional formula (66).

3.4.2 Invariant Formulation with Residual Stress

We now consider the residual stress $\boldsymbol{\tau}$ within the invariant framework of Sect. 3.4. First, we note that since $\boldsymbol{\tau}$ is symmetric it can be written in spectral form as

$$\boldsymbol{\tau} = \sum_{i=1}^3 \tau_i \mathbf{M}_i \otimes \mathbf{M}_i, \quad (75)$$

where τ_i , $i = 1, 2, 3$, are its eigenvalues and \mathbf{M}_i , $i = 1, 2, 3$, are the corresponding eigenvectors. Each $\mathbf{M}_i \otimes \mathbf{M}_i$, $i = 1, 2, 3$, can be considered as a structure tensor, although they are not all independent since they satisfy

$$\sum_{i=1}^3 \mathbf{M}_i \otimes \mathbf{M}_i = \mathbf{I}_r. \quad (76)$$

Thus, $\boldsymbol{\tau}$ can be thought of as a generalized structure tensor, and we shall consider the combined invariants of the two tensors \mathbf{C} and $\boldsymbol{\tau}$, and without any other structure in the material. Thus, generalizing the condition (53), the strain-energy function of a residually stressed material must satisfy

$$W(\mathbf{Q}'\mathbf{C}\mathbf{Q}'^T, \mathbf{Q}'\boldsymbol{\tau}\mathbf{Q}'^T) = W(\mathbf{C}, \boldsymbol{\tau}) \quad (77)$$

for all orthogonal \mathbf{Q}' . Note that we are using the notation W for the strain-energy function irrespective of its arguments.

Since $\text{Div } \boldsymbol{\tau} = \mathbf{0}$ in \mathcal{B}_r and $\boldsymbol{\tau}\mathbf{N} = \mathbf{0}$ on $\partial\mathcal{B}_r$ it is easy to show that $\boldsymbol{\tau}$ cannot be purely isotropic (i.e., a hydrostatic stress); for a proof, see, for example, Ogden (2003b). Thus, the response of a residually stressed material relative to \mathcal{B}_r is necessarily anisotropic and the effect of $\boldsymbol{\tau}$ on the response is similar to, but more complex than, that of a single preferred direction. In particular, the condition (77) implies that W can be expressed in terms of invariants, in fact only 10 independent invariants in general, as discussed in Shams et al. (2011) and more generally, for a residually stressed transversely isotropic elastic material with 18 invariants, as derived by Hoger (1993) and used in the context of wave propagation by Ogden and Singh (2011).

Here we adopt the notation K_1, K_2, K_3 for the isotropic invariants, i.e.,

$$K_1 = \text{tr } \mathbf{C}, \quad K_2 = \frac{1}{2}[(\text{tr } \mathbf{C})^2 - \text{tr } (\mathbf{C}^2)], \quad K_3 = \det \mathbf{C} \quad (78)$$

instead of I_1, I_2, I_3 so as avoid a conflict with the notations for the remaining invariants with the notations I_4, I_5, \dots for the other invariants considered heretofore. The three invariants of $\boldsymbol{\tau}$, since they do not depend on \mathbf{C} , are collected conveniently as

$$K_4 \equiv \left\{ \text{tr } \boldsymbol{\tau}, \frac{1}{2}[(\text{tr } \boldsymbol{\tau})^2 - \text{tr } (\boldsymbol{\tau}^2)], \det \boldsymbol{\tau} \right\}, \quad (79)$$

and the set of independent invariants involving the combination of \mathbf{C} and $\boldsymbol{\tau}$ is taken to be

$$K_5 = \text{tr}(\boldsymbol{\tau}\mathbf{C}), \quad K_6 = \text{tr}(\boldsymbol{\tau}\mathbf{C}^2), \quad K_7 = \text{tr}(\boldsymbol{\tau}^2\mathbf{C}), \quad K_8 = \text{tr}(\boldsymbol{\tau}^2\mathbf{C}^2). \quad (80)$$

For a residually stressed material we therefore consider the strain-energy function $W = W(K_1, K_2, K_3, K_4, K_5, K_6, K_7, K_8)$, K_4 consisting of three separate invariants in general.

For an incompressible material, since $K_3 = 1$, nine independent invariants are required in general. For the specialization to plane strain with a planar residual stress the number of independent invariants is reduced, as was illustrated, for example, in Sect. 3.4.1 for two preferred directions. We refer to Merodio et al. (2013) for details.

Note that when evaluated in the reference configuration \mathcal{B}_r the invariants that depend on \mathbf{C} reduce to

$$K_1 = K_2 = 3, \quad K_3 = 1, \quad K_5 = K_6 = \text{tr} \boldsymbol{\tau}, \quad K_7 = K_8 = \text{tr}(\boldsymbol{\tau}^2). \quad (81)$$

Stress Tensors

With the considered set of invariants the expanded expressions for the stress tensors given in (61) become

$$\mathbf{S} = \sum_{i \in \mathcal{I}} W_i \frac{\partial K_i}{\partial \mathbf{F}}, \quad \boldsymbol{\sigma} = J^{-1} \mathbf{F} \mathbf{S}, \quad (82)$$

for an unconstrained material, where \mathcal{I} is the index set $\{1, 2, 3, 5, 6, 7, 8\}$, while for an incompressible material (62) reads

$$\mathbf{S} = \sum_{i \in \mathcal{I}} W_i \frac{\partial K_i}{\partial \mathbf{F}} - p \mathbf{F}^{-1}, \quad \boldsymbol{\sigma} = \mathbf{F} \mathbf{S}, \quad (83)$$

in which case the index set reduces to $\{1, 2, 5, 6, 7, 8\}$. Note that the derivative of K_4 with respect to \mathbf{F} vanishes and so is not included in the above expressions, although K_4 is included in the arguments of W . We emphasize here that in this section W_i stands for $\partial W / \partial K_i$ as distinct from $\partial W / \partial I_i$ used earlier. At this point we do not include both residual stress and structure associated with preferred directions.

In addition to the expressions $\partial K_i / \partial \mathbf{F}$ given by (47) for $i = 1, 2, 3$ with I_i replaced by K_i , we require the corresponding expressions for $i = 5, 6, 7, 8$. Similarly to the derivatives of I_4 and I_5 in (55), these are easily obtained as

$$\frac{\partial K_5}{\partial \mathbf{F}} = 2\boldsymbol{\tau}\mathbf{F}^T, \quad \frac{\partial K_6}{\partial \mathbf{F}} = 2(\boldsymbol{\tau}\mathbf{C}\mathbf{F}^T + \mathbf{C}\boldsymbol{\tau}\mathbf{F}^T), \quad (84)$$

$$\frac{\partial K_7}{\partial \mathbf{F}} = 2\boldsymbol{\tau}^2\mathbf{F}^T, \quad \frac{\partial K_8}{\partial \mathbf{F}} = 2(\boldsymbol{\tau}^2\mathbf{C}\mathbf{F}^T + \mathbf{C}\boldsymbol{\tau}^2\mathbf{F}^T). \quad (85)$$

Using these in (82) we obtain the expanded Cauchy stress via

$$\begin{aligned} J\boldsymbol{\sigma} = & 2W_1\mathbf{B} + 2W_2(I_1\mathbf{B} - \mathbf{B}^2) + 2I_3W_3\mathbf{I} + 2W_5\boldsymbol{\Sigma} + 2W_6(\boldsymbol{\Sigma}\mathbf{B} + \mathbf{B}\boldsymbol{\Sigma}) \\ & + 2W_7\boldsymbol{\Sigma}\mathbf{B}^{-1}\boldsymbol{\Sigma} + 2W_8(\boldsymbol{\Sigma}\mathbf{B}^{-1}\boldsymbol{\Sigma}\mathbf{B} + \mathbf{B}\boldsymbol{\Sigma}\mathbf{B}^{-1}\boldsymbol{\Sigma}), \end{aligned} \quad (86)$$

where we have introduced the notation $\boldsymbol{\Sigma} = \mathbf{F}\boldsymbol{\tau}\mathbf{F}^T$. This is the Eulerian counterpart of the Lagrangian residual stress tensor $\boldsymbol{\tau}$ and represents the push forward of $\boldsymbol{\tau}$ from \mathcal{B}_r to \mathcal{B} .

For an incompressible material we obtain similarly, from (83),

$$\begin{aligned} \boldsymbol{\sigma} = & 2W_1\mathbf{B} + 2W_2(I_1\mathbf{B} - \mathbf{B}^2) + 2W_5\boldsymbol{\Sigma} + 2W_6(\boldsymbol{\Sigma}\mathbf{B} + \mathbf{B}\boldsymbol{\Sigma}) \\ & + 2W_7\boldsymbol{\Sigma}\mathbf{B}^{-1}\boldsymbol{\Sigma} + 2W_8(\boldsymbol{\Sigma}\mathbf{B}^{-1}\boldsymbol{\Sigma}\mathbf{B} + \mathbf{B}\boldsymbol{\Sigma}\mathbf{B}^{-1}\boldsymbol{\Sigma}) - p\mathbf{I}. \end{aligned} \quad (87)$$

When evaluated in \mathcal{B}_r Eqs. (86) and (87) reduce to

$$\boldsymbol{\tau} = 2(W_1 + 2W_2 + W_3)\mathbf{I}_r + 2(W_5 + 2W_6)\boldsymbol{\tau} + 2(W_7 + 2W_8)\boldsymbol{\tau}^2 \quad (88)$$

and

$$\boldsymbol{\tau} = (2W_1 + 4W_2 - p^{(r)})\mathbf{I}_r + 2(W_5 + 2W_6)\boldsymbol{\tau} + 2(W_7 + 2W_8)\boldsymbol{\tau}^2, \quad (89)$$

respectively, wherein each W_i , $i \in \mathcal{I}$, is evaluated for the invariants given in \mathcal{B}_r by (81). These are the specializations of the general formulas in (39) to the present circumstances.

From (88) and (89) we deduce that in \mathcal{B}_r the conditions

$$W_1 + 2W_2 + W_3 = 0, \quad 2(W_5 + 2W_6) = 1, \quad W_7 + 2W_8 = 0 \quad (90)$$

and

$$2W_1 + 4W_2 - p^{(r)} = 0, \quad 2(W_5 + 2W_6) = 1, \quad W_7 + 2W_8 = 0, \quad (91)$$

must hold for an unconstrained and incompressible material, respectively, as derived by Shams et al. (2011).

Plane Strain

In the plane strain specialization, for example, in the (1, 2) plane with the residual stress having only the in-plane components τ_{11} , τ_{22} , τ_{12} and \mathbf{C} having nonzero components C_{11} , C_{22} , C_{12} , $C_{33} = 1$, considerable simplification is achieved and only the invariants K_1 , K_3 , K_4 , K_5 remain independent. They are given by

$$K_1 = C_{11} + C_{22} + 1, \quad K_3 = C_{11}C_{22} - C_{12}^2, \quad K_4 = \{\tau_{11} + \tau_{22}, \tau_{11}\tau_{22} - \tau_{12}^2, 0\}, \quad (92)$$

$$K_5 = C_{11}\tau_{11} + C_{22}\tau_{22} + 2C_{12}\tau_{12}, \quad (93)$$

and in terms of these the other invariants are given by

$$K_2 = K_1 + K_3 - 1, \quad K_6 = (K_1 - 1)K_5 - K_3(\tau_{11} + \tau_{22}), \quad (94)$$

$$K_7 = (\tau_{11} + \tau_{22})K_5 - (K_1 - 1)(\tau_{11}\tau_{22} - \tau_{12}^2), \quad (95)$$

$$K_8 = (K_1 - 1)K_7 - K_3[(\tau_{11} + \tau_{22})^2 - 2(\tau_{11}\tau_{22} - \tau_{12}^2)]. \quad (96)$$

Similarly to the plane strain cases considered in Sects. 3.3.2 and 3.4.1 the planar Cauchy stress $\hat{\sigma}$ is given in a simple form via

$$J\hat{\sigma} = 2\hat{W}_1\hat{\mathbf{B}} + 2K_3\hat{W}_3\hat{\mathbf{I}} + 2\hat{W}_5\hat{\Sigma}, \quad (97)$$

where $\hat{W}(K_1, K_3, K_4, K_5)$ is obtained from $W(K_1, K_2, K_3, K_4, K_5, K_6, K_7, K_8)$ with the specializations (92)–(96) and, as before, the hats refer to the plane specialization. For an incompressible material the details were given by Merodio et al. (2013) and in the above the invariants specialize with $K_3 = 1$, \hat{W} depends on just K_1, K_4, K_5 , and the plane Cauchy stress has the form

$$\hat{\sigma} = 2\hat{W}_1\hat{\mathbf{B}} + 2\hat{W}_5\hat{\Sigma} - \hat{p}\hat{\mathbf{I}}. \quad (98)$$

The latter formulation has been used in Merodio et al. (2013) in the analysis of the azimuthal shear deformation of a residually stressed circular cylindrical tube.

4 The Role of Homogeneous Deformations

For the experimental determination of the elastic properties of soft biological tissues homogeneous deformations play a key role. Theoretically they are exact deformations for which the deformation gradient \mathbf{F} is independent of position \mathbf{X} , but experimentally a uniform \mathbf{F} is only achievable approximately. Provided the tissue specimens are selected appropriately and the experiments are carefully conducted then the approximation can be considered sufficiently good to allow certain tissue properties to be elicited. In this connection homogeneous deformations have been discussed extensively for isotropic, transversely isotropic and orthotropic fiber-reinforced materials in the literature, and we refer to, for example, Ogden (2003b, 2009, 2015) and Holzapfel and Ogden (2009c) and references therein for details.

Rather than repeating full details here, we shall consider only the case of the homogeneous biaxial deformation of a thin rectangular sheet of material loaded in tension in the plane of the sheet. The sheet is assumed to contain two preferred directions that represent two families of parallel fibers, the two families being disposed symmetrically to the axes of biaxial tension, which are parallel to the sheet edges. This deformation is an example of a so-called *pure homogeneous strain*, which is defined in terms of rectangular Cartesian coordinates (X_1, X_2, X_3) and (x_1, x_2, x_3) in the reference and deformed configurations, respectively, by

$$x_1 = \lambda_1 X_1, \quad x_2 = \lambda_2 X_2, \quad x_3 = \lambda_3 X_3, \quad (99)$$

where the principal stretches $\lambda_1, \lambda_2, \lambda_3$ are constants, i.e., independent of (X_1, X_2, X_3) .

With respect to these coordinates \mathbf{F} and \mathbf{C} have diagonal forms $\text{diag}[\lambda_1, \lambda_2, \lambda_3]$ and $\text{diag}[\lambda_1^2, \lambda_2^2, \lambda_3^2]$, respectively, and for an incompressible material the constraint (16) must be satisfied. For convenience of reference in this section we repeat this here:

$$\lambda_1 \lambda_2 \lambda_3 = 1. \quad (100)$$

Note that for a homogeneous deformation there can be no residual stress.

4.1 Application to Fiber-Reinforced Materials

We now suppose that the preferred directions in the reference configuration, denoted \mathbf{M} and \mathbf{M}' , are given by

$$\mathbf{M} = \cos \varphi \mathbf{e}_1 + \sin \varphi \mathbf{e}_2, \quad \mathbf{M}' = \cos \varphi \mathbf{e}_1 - \sin \varphi \mathbf{e}_2, \quad (101)$$

where φ is a constant angle, as depicted in Fig. 8, and $\mathbf{e}_1, \mathbf{e}_2$ denote the in-plane Cartesian coordinate directions. The directions \mathbf{M} and \mathbf{M}' deform into the vectors \mathbf{m} and \mathbf{m}' , which are given by

$$\mathbf{m} = \lambda_1 \cos \varphi \mathbf{e}_1 + \lambda_2 \sin \varphi \mathbf{e}_2, \quad \mathbf{m}' = \lambda_1 \cos \varphi \mathbf{e}_1 - \lambda_2 \sin \varphi \mathbf{e}_2. \quad (102)$$

In terms of the principal stretches the invariants defined in (45), or (14), (54), (64) and (65) are, for an incompressible material,

$$I_1 = \lambda_1^2 + \lambda_2^2 + \lambda_1^{-2} \lambda_2^{-2}, \quad I_2 = \lambda_1^{-2} + \lambda_2^{-2} + \lambda_1^2 \lambda_2^2, \quad (103)$$

where (100) has been used to replace λ_3 in terms of λ_1 and λ_2 ,

$$I_4 = I_6 = \lambda_1^2 \cos^2 \varphi + \lambda_2^2 \sin^2 \varphi, \quad I_5 = I_7 = \lambda_1^4 \cos^2 \varphi + \lambda_2^4 \sin^2 \varphi, \quad (104)$$

and

$$I_8 = \lambda_1^2 \cos^2 \varphi - \lambda_2^2 \sin^2 \varphi. \quad (105)$$

In this situation, on applying the general formula (70) for the Cauchy stress tensor $\boldsymbol{\sigma}$, it can be seen that the components σ_{13} and σ_{23} are zero and the other components are given by

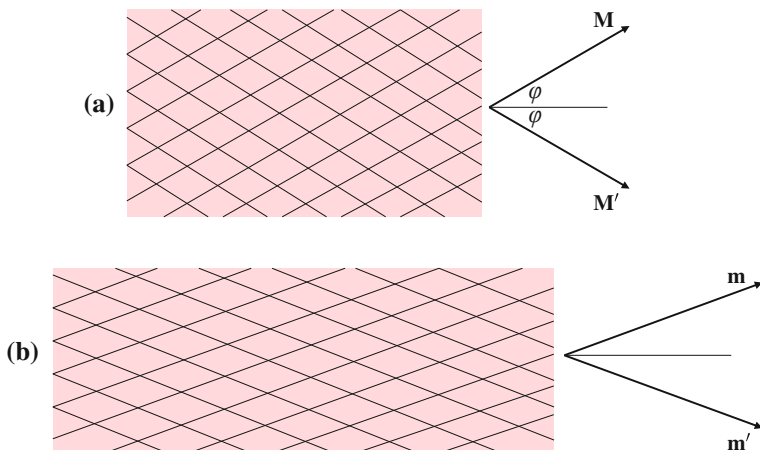


Fig. 8 Pure homogeneous strain of a thin sheet of material in the $(1, 2)$ plane with two in-plane symmetrically disposed families of fibers with directions \mathbf{M} and \mathbf{M}' in the reference configuration **(a)**, and \mathbf{m} and \mathbf{m}' in the deformed configuration **(b)**

$$\begin{aligned} \sigma_{11} = & 2W_1\lambda_1^2 + 2W_2(I_1\lambda_1^2 - \lambda_1^4) + 2(W_4 + W_6 + W_8)\lambda_1^2 \cos^2 \varphi \\ & + 4(W_5 + W_7)\lambda_1^4 \cos^2 \varphi - p, \end{aligned} \quad (106)$$

$$\begin{aligned} \sigma_{22} = & 2W_1\lambda_2^2 + 2W_2(I_1\lambda_2^2 - \lambda_2^4) + 2(W_4 + W_6 - W_8)\lambda_2^2 \sin^2 \varphi \\ & + 4(W_5 + W_7)\lambda_2^4 \sin^2 \varphi - p, \end{aligned} \quad (107)$$

$$\sigma_{12} = 2[W_4 - W_6 + (W_5 - W_7)(\lambda_1^2 + \lambda_2^2)]\lambda_1\lambda_2 \sin \varphi \cos \varphi, \quad (108)$$

$$\sigma_{33} = 2W_1\lambda_3^2 + 2W_2(I_1\lambda_3^2 - \lambda_3^4) - p. \quad (109)$$

Clearly, the invariants in this case depend on just the two independent stretches λ_1 and λ_2 and the angle φ and it is therefore convenient to reduce the dependence of W on the seven invariants to dependence on these three quantities by means of the notation $\tilde{W}(\lambda_1, \lambda_2, \varphi)$, which is defined by

$$\tilde{W}(\lambda_1, \lambda_2, \varphi) = W(I_1, I_2, I_4, I_5, I_6, I_7, I_8), \quad (110)$$

where $I_1, I_2, I_4, \dots, I_8$ are given by (103)–(105). Note that φ is a material property, not a deformation variable. For an isotropic material W depends on I_1 and I_2 only and in this case \tilde{W} is symmetric in λ_1 and λ_2 , but otherwise \tilde{W} is not symmetric except in the particular case $\varphi = \pi/4$. It is then easy to obtain the simple formulas

$$\sigma_{11} - \sigma_{33} = \lambda_1 \frac{\partial \tilde{W}}{\partial \lambda_1}, \quad \sigma_{22} - \sigma_{33} = \lambda_2 \frac{\partial \tilde{W}}{\partial \lambda_2}. \quad (111)$$

There is no corresponding simple formula for σ_{12} , which is not in general zero and hence, unlike σ_{33} , the normal stresses σ_{11} and σ_{22} are not in general principal stresses. However, there are particular circumstances in which they are principal stresses. First, if $\varphi = 0$ or $\pi/2$ the two preferred directions coincide and the material is transversely isotropic; second, if the two families of fibers have the same elastic properties and then, for the specific deformation considered here, since $I_4 = I_6$ and $I_5 = I_7$, $W_4 = W_6$ and $W_5 = W_7$ and $\sigma_{12} = 0$. In this second case the material is *orthotropic*, as indicated in Sect. 3.4.1, and the axes of orthotropy coincide with the Cartesian axes.

We emphasize at this point that, except in the case of incompressible isotropic materials, biaxial tests provide only limited information about tissue elastic properties, but they are nevertheless very useful since experimental setups in which more than two deformation components can be varied independently and the associated stress components measured are rare. Indeed, for an incompressible material there are seven constitutive functions $W_1, W_2, W_4, \dots, W_8$ that are required to be known in order to fully characterize material properties and at present it is not possible experimentally to distinguish the effects on the material behavior of all the different invariants and constitutive functions. As a result it is usual to specialize the dependence of the strain-energy function to a limited number of invariants that are able to capture the essence of the elastic behavior of tissues.

For the latter purpose strain-energy functions restricted to the invariants I_1, I_4 and I_6 are often considered and typically these have the general form

$$W(I_1, I_4, I_6) = W_{\text{iso}}(I_1) + W_{\text{aniso}}(I_4, I_6), \quad (112)$$

more particularly with the symmetry $W_{\text{aniso}}(I_4, I_6) = W_{\text{aniso}}(I_6, I_4)$, reflecting the fact that the two families of fibers have the same elastic properties. This decouples the isotropic part W_{iso} , which models the matrix, from the contributions of the collagen fibers embedded in the matrix and modeled by the anisotropic part W_{aniso} . A particular strain-energy function of this form has a neo-Hookean isotropic part

$$W_{\text{iso}}(I_1) = \frac{1}{2}\mu(I_1 - 3), \quad (113)$$

where $\mu (>0)$ is the shear modulus of the matrix in its reference configuration, and Fung-type exponentials associated with the fiber elasticity, namely

$$W_{\text{aniso}}(I_4, I_6) = \frac{k_1}{2k_2} \{ \exp[k_2(I_4 - 1)^2] + \exp[k_2(I_6 - 1)^2] - 2 \}, \quad (114)$$

where k_1 (with the dimension of stress) and k_2 (dimensionless) are material constants. In this case $\sigma_{12} = 0$ and the other stress components are given by

$$\sigma_{11} = \mu\lambda_1^2 + 4k_1(I_4 - 1) \exp[k_2(I_4 - 1)^2] \lambda_1^2 \cos^2 \varphi - p, \quad (115)$$

$$\sigma_{22} = \mu\lambda_2^2 + 4k_1(I_4 - 1) \exp[k_2(I_4 - 1)^2] \lambda_2^2 \sin^2 \varphi - p, \quad (116)$$

and $\sigma_{33} = \mu\lambda_3^2 - p$. On setting $\sigma_{33} = 0$ and eliminating p and λ_3 , we then obtain

$$\sigma_{11} = \mu(\lambda_1^2 - \lambda_1^{-2}\lambda_2^{-2}) + 4k_1(I_4 - 1) \exp[k_2(I_4 - 1)^2]\lambda_1^2 \cos^2 \varphi, \quad (117)$$

$$\sigma_{22} = \mu(\lambda_2^2 - \lambda_1^{-2}\lambda_2^{-2}) + 4k_1(I_4 - 1) \exp[k_2(I_4 - 1)^2]\lambda_2^2 \sin^2 \varphi, \quad (118)$$

equations for the in-plane stress components σ_{11} and σ_{22} in terms of the independent stretches λ_1 and λ_2 , I_4 being given by Eq.(104)₁.

To illustrate these formulas and, in particular, their dependence on the fiber angle we plot the dimensionless stress components $\bar{\sigma}_{11} = \sigma_{11}/\mu$ and $\bar{\sigma}_{22} = \sigma_{22}/\mu$ as functions of λ_1 for a fixed value of λ_2 in Figs. 9 and 10, respectively. Results are shown for the representative values $\lambda_2 = 1$ with $\bar{k}_1 = k_1/\mu = 1$ and $k_2 = 1$. Clearly, as is apparent from Fig. 9, the response becomes stiffer as the fiber become closer to the direction of the applied tension σ_{11} .

Fig. 9 Plot of the dimensionless stress $\bar{\sigma}_{11} = \sigma_{11}/\mu$ against λ_1 based on Eq. (117) for $\lambda_2 = 1$, dimensionless parameter values $\bar{k}_1 = k_1/\mu = 1$ and $k_2 = 1$ and the indicated values of the fiber angle φ together with the unmarked curve for $\varphi = \pi/2$ (which has the softest response)

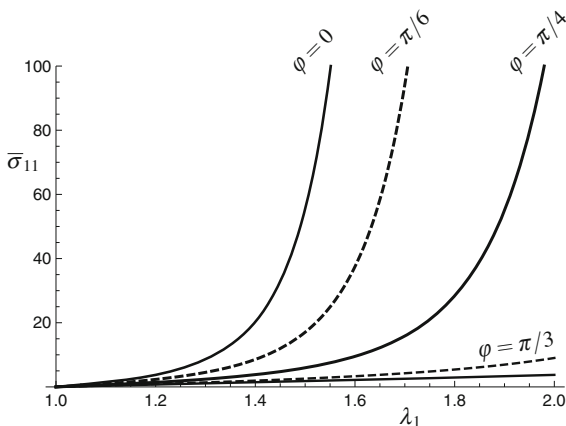
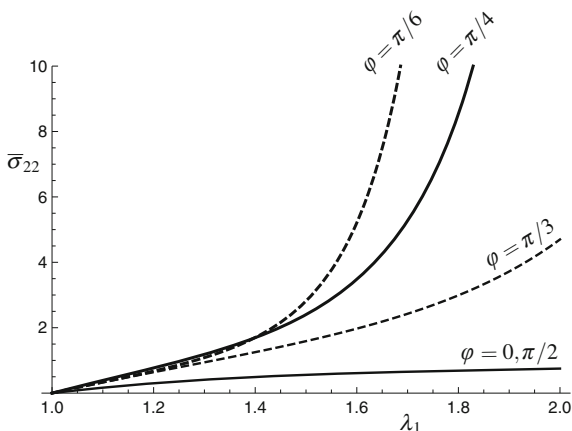


Fig. 10 Plot of the dimensionless stress $\bar{\sigma}_{22} = \sigma_{22}/\mu$ against λ_1 based on Eq. (118) for $\lambda_2 = 1$, dimensionless parameter values $\bar{k}_1 = k_1/\mu = 1$ and $k_2 = 1$ and the indicated values of the fiber angle φ



In Fig. 10 the behavior of the lateral stress is illustrated, also as a function of the active stretch λ_1 . These show a similar stiffening trend to that in Fig. 9 although there is some overlap of the curves for different values of φ . The curves for $\varphi = 0$ and $\varphi = \pi/2$ are identical since the anisotropic term vanishes, with $\varphi = 0$ and $I_4 = 1$, respectively, because we have chosen $\lambda_2 = 1$.

5 Extension and Inflation of an Artery

We now consider the elastic deformation of an artery, which is modeled as a thick-walled circular cylindrical tube. In particular, we restrict attention to the extension and inflation of an artery in which there are two symmetrically and helically arranged families of fibers with the two families having the same elastic properties. We obtain general expressions for the pressure and axial load on the artery in terms of the radial and axial stretches. As a special case, and as a first approximation, we examine the specialization of the results to a thin-walled (or membrane) tube. A membrane does not support residual stresses and in order to consider the effect of residual stresses on the elastic behavior of the tube we then return to consideration of the thick-walled model.

5.1 Geometry and Deformation

We consider first a thick-walled circular cylindrical tube with reference geometry defined in cylindrical polar coordinates R, Θ, Z by

$$0 < A \leq R \leq B, \quad 0 \leq \Theta \leq 2\pi, \quad 0 \leq Z \leq L, \quad (119)$$

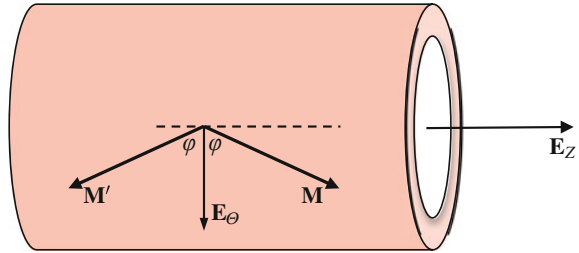
where A and $B > A$ are the inner and outer radii of the tube and L is its length. We consider that the unit tangents to the two families of continuously distributed fibers are given by

$$\mathbf{M} = \cos \varphi \mathbf{E}_\Theta + \sin \varphi \mathbf{E}_Z, \quad \mathbf{M}' = \cos \varphi \mathbf{E}_\Theta - \sin \varphi \mathbf{E}_Z, \quad (120)$$

locally with respect to unit basis vectors \mathbf{E}_Θ and \mathbf{E}_Z , as shown in Fig. 11, and symmetric with respect to the tube axis. In general we may take φ to depend on R , but in order to maintain radial symmetry we assume that it is independent of Θ and Z .

A particular significance of the prior consideration of the biaxial deformation in Sect. 4 is that locally (at each radius R) the deformation of the tube is biaxial and several of the formulas in Sect. 4.1 carry over to the present situation. Indeed, if the plane sheet shown in Fig. 8a is folded to form a cylinder then the straight lines (fiber directions) in the sheet become helices in the thin-walled cylinder so formed. The difference is that here the tube has a finite thickness and there is dependence on R .

Fig. 11 Unit vectors \mathbf{M} and \mathbf{M}' lying in the (Θ, Z) plane at radial distance R from the tube axis in the reference configuration and locally tangent to the two helically arranged families of fibers



It is generally considered that the material of artery walls is incompressible, and we therefore adopt the incompressibility assumption. Then, subject to the circular cylindrical shape being maintained during deformation (which requires the application of an appropriate internal pressure and axial load), the deformation of the tube can be described by the equations

$$r^2 = a^2 + \lambda_z^{-1}(R^2 - A^2), \quad \theta = \Theta, \quad z = \lambda_z Z, \tag{121}$$

where r, θ, z are cylindrical polar coordinates in the deformed configuration, λ_z is the constant (independent of R) axial stretch of the tube and a is its internal radius in the deformed configuration. The external deformed radius, denoted b , is given by

$$b^2 = a^2 + \lambda_z^{-1}(B^2 - A^2). \tag{122}$$

An advantage of the deformation defined in (121) is that, as is the case for homogeneous biaxial deformation, the principal axes of deformation do not rotate, which means that the radial, azimuthal, and axial directions are principal directions of the deformation. We denote by $\lambda_r, \lambda_\theta, \lambda_z$ the corresponding principal stretches, the first two of which are given by

$$\lambda_r = \lambda^{-1} \lambda_z^{-1}, \quad \lambda_\theta = \frac{r}{R}, \tag{123}$$

λ_r having been obtained from the incompressibility constraint, written here as

$$\lambda_r \lambda_\theta \lambda_z = 1. \tag{124}$$

We now adopt the notations

$$\lambda_a = a/A, \quad \lambda_b = b/B \tag{125}$$

for the values of λ_θ at $r = a$ and $r = b$, respectively, and we note that by expressing (121)₁ in terms of λ_θ we obtain

$$\lambda_a^2 \lambda_z - 1 = \frac{R^2}{A^2} (\lambda_\theta^2 \lambda_z - 1) = \frac{B^2}{A^2} (\lambda_b^2 \lambda_z - 1). \quad (126)$$

One implication of these connections is that the sign of $\lambda_\theta^2 \lambda_z - 1$ is independent of R , and, in particular, if $\lambda_\theta^2 \lambda_z - 1 = 0$ at one radius then this holds for *all* $R \in [A, B]$, so that λ_θ is independent of R and the deformation is homogeneous.

5.2 Stresses and Loads

Circular symmetry is maintained during the considered deformation, and because the two fiber families are symmetrically disposed and have the same elastic properties the (Cauchy) stresses required to maintain the deformation are the normal stresses in the r, θ, z directions, which we denote by $\sigma_{rr}, \sigma_{\theta\theta}$ and σ_{zz} . These are principal stresses, similarly to the situation for the homogeneous biaxial deformation discussed in Sect. 4.1. This means that the elastic response is orthotropic and the axes of orthotropy coincide with the cylindrical polar axes locally. For each radius R the considered deformation has the form of a pure homogeneous strain and hence the strain-energy function can be written as $\tilde{W}(\lambda_\theta, \lambda_z, \varphi)$, as in (110), except that λ_1 and λ_2 are replaced by λ_θ and λ_z , respectively.

Thus, similarly to (111), the principal stress differences take the forms

$$\sigma_{\theta\theta} - \sigma_{rr} = \lambda_\theta \frac{\partial \tilde{W}}{\partial \lambda_\theta}, \quad \sigma_{zz} - \sigma_{rr} = \lambda_z \frac{\partial \tilde{W}}{\partial \lambda_z}, \quad (127)$$

with the indices 1, 2, 3 corresponding to θ, z, r , respectively, and we emphasize that in general $\tilde{W}(\lambda_\theta, \lambda_z, \varphi) \neq \tilde{W}(\lambda_z, \lambda_\theta, \varphi)$.

The required invariants are

$$I_1 = \lambda_\theta^2 + \lambda_z^2 + \lambda_\theta^{-2} \lambda_z^{-2}, \quad I_2 = \lambda_\theta^{-2} + \lambda_z^{-2} + \lambda_\theta^2 \lambda_z^2, \quad (128)$$

$$I_4 = I_6 = \lambda_\theta^2 \cos^2 \varphi + \lambda_z^2 \sin^2 \varphi, \quad I_5 = I_7 = \lambda_\theta^4 \cos^2 \varphi + \lambda_z^4 \sin^2 \varphi, \quad (129)$$

$$I_8 = \lambda_\theta^2 \cos^2 \varphi - \lambda_z^2 \sin^2 \varphi, \quad (130)$$

which, with the identifications $\lambda_1 \leftrightarrow \lambda_\theta$ and $\lambda_2 \leftrightarrow \lambda_z$, can be seen to be the same as (103)–(105). In general, λ_θ depends on R so all the invariants also depend on R , as do the stress components $\sigma_{rr}, \sigma_{\theta\theta}$ and σ_{zz} .

We now apply the equilibrium equation (20) with body force $\mathbf{b} = \mathbf{0}$, which, by virtue of the radial symmetry (no dependence on θ or z), reduces to the radial equation

$$\frac{d\sigma_{rr}}{dr} + \frac{1}{r}(\sigma_{rr} - \sigma_{\theta\theta}) = 0. \quad (131)$$

Integration of this equation requires boundary conditions on the interior and exterior boundaries $r = a$ and $r = b$, and we assume that there is an internal pressure P (≥ 0) on $r = a$ but no traction on $r = b$. Thus, we set

$$\sigma_{rr} = \begin{cases} -P & \text{on } r = a \\ 0 & \text{on } r = b. \end{cases} \quad (132)$$

In order to maintain the deformation axial loads on the ends of the tube are needed in addition to the pressure P on $r = a$. At any cross section of the tube the resultant axial load, which is independent of z , is denoted N and given by

$$N = 2\pi \int_a^b \sigma_{zz} r \, dr. \quad (133)$$

On integration of (131) and use of (127)₁ and the boundary condition (132)₂ we obtain

$$\sigma_{rr} = - \int_r^b \lambda_\theta \frac{\partial \tilde{W}}{\partial \lambda_\theta} \frac{dr}{r}, \quad (134)$$

and then, on application of the boundary condition (132)₁, it follows that

$$P = \int_a^b \lambda_\theta \frac{\partial \tilde{W}}{\partial \lambda_\theta} \frac{dr}{r}. \quad (135)$$

For given A and B , noting that from (122) b depends on a and λ_z , Eq. (135) yields an expression for the P that is required to achieve the deformed internal radius a for any given λ_z .

On use of the expressions in (127) and the equilibrium equation (131) it is straightforward to show that N can be recast in the form

$$N = \pi \int_a^b \left(2\lambda_z \frac{\partial \tilde{W}}{\partial \lambda_z} - \lambda_\theta \frac{\partial \tilde{W}}{\partial \lambda_\theta} \right) r \, dr + \pi \int_a^b \frac{d}{dr} (r^2 \sigma_{rr}) \, dr. \quad (136)$$

Integration of the latter term and application of the boundary conditions (132) leads to

$$N = \pi \int_a^b \left(2\lambda_z \frac{\partial \tilde{W}}{\partial \lambda_z} - \lambda_\theta \frac{\partial \tilde{W}}{\partial \lambda_\theta} \right) r \, dr + \pi a^2 P. \quad (137)$$

Thus, N consists of two parts: the load that is applied on the ends between $r = a$ and $r = b$ and the contribution $\pi a^2 P$ of the pressure on the end area πa^2 of a tube with closed ends. The difference $N - \pi a^2 P$, which is the integral expression here, is known as the *reduced axial load*, and for this we adopt the notation $F = N - \pi a^2 P$.

5.2.1 Inclusion of Residual Stress

If residual stresses are included in the tube then some of the formulas in the previous section are essentially unchanged, as we now show. An axial residual stress is not compatible with the tube being circular cylindrical and a deformation independent of Θ and Z , so we restrict attention to radial and circumferential residual stresses, which we denote by τ_{RR} and $\tau_{\Theta\Theta}$. They satisfy the radial equation of equilibrium

$$\frac{d\tau_{RR}}{dR} + \frac{1}{R}(\tau_{RR} - \tau_{\Theta\Theta}) = 0, \quad (138)$$

which is associated with the boundary conditions

$$\tau_{RR} = 0 \quad \text{on } R = A \text{ and } B, \quad (139)$$

these being the specializations of (24) and (25), respectively, to the present geometry.

The invariants $I_1, I_2, I_4, I_5, I_6, I_7, I_8$ are again given by (128)–(130), the invariants K_4 in (79) reduce to just $\tau_{RR} + \tau_{\Theta\Theta}$ and $\tau_{RR}\tau_{\Theta\Theta}$, and

$$K_5 = \lambda_\theta^{-2}\lambda_z^{-2}\tau_{RR} + \lambda_\theta^2\tau_{\Theta\Theta}, \quad K_6 = \lambda_\theta^{-4}\lambda_z^{-4}\tau_{RR} + \lambda_\theta^4\tau_{\Theta\Theta}, \quad (140)$$

$$K_7 = \lambda_\theta^{-2}\lambda_z^{-2}\tau_{RR}^2 + \lambda_\theta^2\tau_{\Theta\Theta}^2, \quad K_8 = \lambda_\theta^{-4}\lambda_z^{-4}\tau_{RR}^2 + \lambda_\theta^4\tau_{\Theta\Theta}^2. \quad (141)$$

The strain-energy function can then be written in the form

$$\tilde{W}(\lambda_\theta, \lambda_z, \varphi, \tau_{RR} + \tau_{\Theta\Theta}, \tau_{RR}\tau_{\Theta\Theta}), \quad (142)$$

which is as in Sect. 5.2 except that $\tau_{RR} + \tau_{\Theta\Theta}$ and $\tau_{RR}\tau_{\Theta\Theta}$ are now included. With this change accounted for, the formulas for the Cauchy stress differences have exactly the same form as in (127), and likewise the formulas for P and N are given by (135) and (137). Only the content of \tilde{W} is different.

5.2.2 The Thin-Walled Approximation

As a first approximation arteries can be considered to be thin-walled tubes, which can be treated on the basis of membrane theory. Membranes do not support through-thickness stresses and, in particular, this means that $\sigma_{rr} = 0$ and there can be no residual stress. However, the membrane approximation does allow us to obtain (for general \tilde{W}) simple expressions for the pressure and axial load that do not involve integrals. The analysis is as follows. Introduce the small parameter $\varepsilon = (B - A)/A$, so the reference wall thickness $B - A$ is small compared with the inner radius A , and linearize (122) in ε to obtain, using the definitions $\lambda_a = a/A$, $\lambda_b = b/B$, the approximation

$$\lambda_b = \lambda_a - \varepsilon\lambda^{-1}\lambda_z^{-1}(\lambda^2\lambda_z - 1), \quad (143)$$

where, to first order in ε , λ , the membrane azimuthal stretch, can be chosen to be in $[\lambda_b, \lambda_a]$.

To the first order in ε , on application of the mean value theorem to Eq. (135) and use of (143), we obtain an approximation for P , namely

$$P = \varepsilon \lambda^{-1} \lambda_z^{-1} \frac{\partial \tilde{W}}{\partial \lambda}(\lambda, \lambda_z, \varphi). \quad (144)$$

Similarly, an approximation for the reduced axial load can be obtained from (137), which yields

$$F = \varepsilon \pi A^2 \lambda_z^{-1} \left[2\lambda_z \frac{\partial \tilde{W}}{\partial \lambda_z}(\lambda, \lambda_z, \varphi) - \lambda \frac{\partial \tilde{W}}{\partial \lambda}(\lambda, \lambda_z, \varphi) \right]. \quad (145)$$

Results for P and F in the case of a thick-walled tube will be illustrated in the following with and without residual stress, and also for the membrane approximation. In each case the results will be based on model constitutive equations, i.e., on special choices of \tilde{W} , which we discuss in the following section.

5.3 Constitutive Laws

We now illustrate the preceding theory by considering specific material models. In Sect. 5.3.1 we consider a strain-energy function for a fibrous material without residual stress, while in Sect. 5.3.2 we extend this to account for residual stress. This is followed by an illustration in which residual stresses and fiber reinforcement are combined.

5.3.1 Fiber Model

The fiber model is of the form (112) with (113) and (114). Thus, $\tilde{W}(\lambda_\theta, \lambda_z, \varphi)$ is given by

$$\begin{aligned} \tilde{W}(\lambda_\theta, \lambda_z, \varphi) &= \frac{1}{2} \mu (\lambda_\theta^2 + \lambda_z^2 + \lambda_\theta^{-2} \lambda_z^{-2} - 3) \\ &\quad + \frac{k_1}{k_2} \{ \exp[k_2 (\lambda_\theta^2 \cos^2 \varphi + \lambda_z^2 \sin^2 \varphi - 1)^2] - 1 \}, \end{aligned} \quad (146)$$

and hence

$$\lambda_\theta \frac{\partial \tilde{W}}{\partial \lambda_\theta} = \mu(\lambda_\theta^2 - \lambda_\theta^{-2} \lambda_z^{-2}) + 4k_1(\lambda_\theta^2 \cos^2 \varphi + \lambda_z^2 \sin^2 \varphi - 1) \lambda_\theta^2 \cos^2 \varphi \\ \times \exp[k_2(\lambda_\theta^2 \cos^2 \varphi + \lambda_z^2 \sin^2 \varphi - 1)^2], \quad (147)$$

and

$$\lambda_z \frac{\partial \tilde{W}}{\partial \lambda_z} = \mu(\lambda_z^2 - \lambda_\theta^{-2} \lambda_z^{-2}) + 4k_1(\lambda_\theta^2 \cos^2 \varphi + \lambda_z^2 \sin^2 \varphi - 1) \lambda_z^2 \sin^2 \varphi \\ \times \exp[k_2(\lambda_\theta^2 \cos^2 \varphi + \lambda_z^2 \sin^2 \varphi - 1)^2]. \quad (148)$$

This is applied first for a membrane tube and then for a thick-walled tube. In Fig. 12a, with $\lambda_z = 1$, the dimensionless pressure $P^* = P/\mu\varepsilon$ is plotted against λ for the model with four values of the fiber angle φ and for representative values of the material constants. Results for $\lambda_z > 1$ are qualitatively similar to those for $\lambda_z = 1$ and are not therefore plotted separately. For $\lambda_z < 1$, in the absence of internal pressure, the tube becomes unstable and this case is not therefore considered here. Figure 12a illustrates the strong dependence on fiber orientation. In particular, as the fibers approach the circumferential direction (decreasing φ) the pressure required to reach a given circumferential stretch increases, i.e., the fibers have a stronger restraining effect on inflation. In Fig. 12b the corresponding plots for a thick-walled tube are shown for comparison, with $\eta = 1.4$ and the same values of the material constants and for representative fiber angles. Qualitatively, these are very similar, but, of course, larger pressures are required to achieve the same level of inflation as for a membrane tube, although the dimensionless pressure is lower because of the different scaling used. The pressure curves exhibit qualitatively the typical response of artery walls. Note that the character of the curves in Fig. 12 is very similar to that evident for $\bar{\sigma}_{11}$ shown in Fig. 9 for the homogeneous deformation of a sheet.

For the thin-walled tube, the corresponding reduced axial load F is plotted against λ in Fig. 13a in the dimensionless form $F^* = F/(\pi A^2 \mu \varepsilon)$, also for $\lambda_z = 1$ and four values of the fiber angle φ . For the larger values of φ , i.e., for fibers closer to the axial direction than the circumferential direction, there is initially, as λ increases from 1 under pressure, a tendency for the pressure to shorten the tube and an increasing positive (tensile) value of F is required in order to maintain $\lambda_z = 1$. Then, as inflation continues, F reaches a maximum and then becomes negative, so the trend is reversed and the tube would elongate in the absence of the axial load. When the fibers are aligned closer to the circumferential direction, on the other hand, F becomes negative as soon as inflation begins and then decreases rapidly. Such ‘switching’ in response has been noted previously, both for isotropic materials (Haughton and Ogden 1979) and for a Fung-type model (Holzapfel and Gasser 2001). Some corresponding plots for a thick-walled tube are also shown in Fig. 13b for comparison. These are broadly similar.

Clearly, the membrane approximation gives a good qualitative picture of the pressure and axial load versus stretch behavior. However, the membrane approximation cannot account for the through-thickness stress distribution in artery walls and is

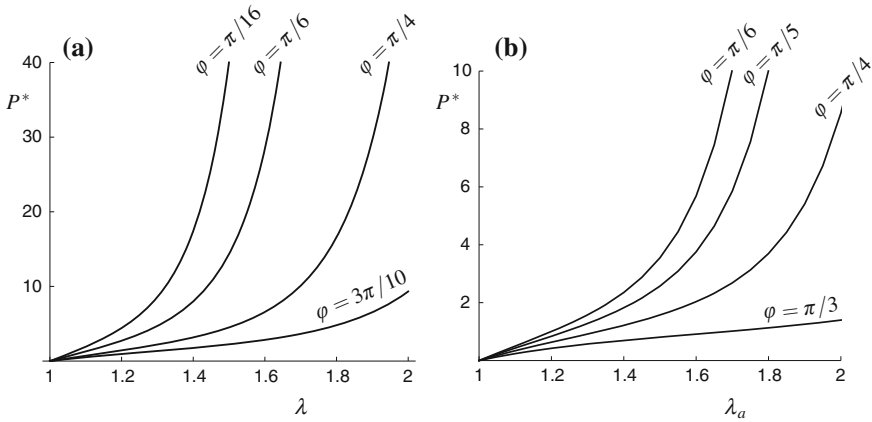


Fig. 12 **a** Plots of the dimensionless pressure $P^* = P/\mu\varepsilon$ versus the azimuthal stretch λ for the membrane approximate Eq. (144) for the strain-energy function given by (146) with $k_1/\mu = 1, k_2 = 1$ and $\varphi = \pi/16, \pi/6, \pi/4, 3\pi/10$. **b** Plots of $P^* = P/[\mu(\eta - 1)]$ versus the stretch λ_a , where $\eta = B/A = 1.4$ for a thick-walled tube based on Eq. (135), the same strain-energy function and material parameters and $\varphi = \pi/6, \pi/5, \pi/4, \pi/3$

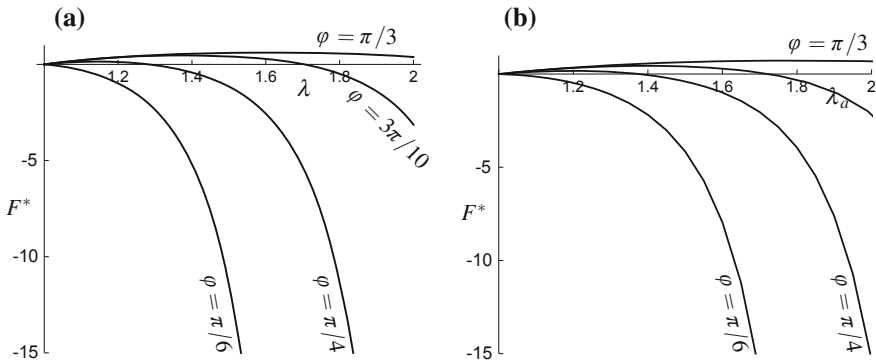


Fig. 13 **a** Plots of the dimensionless reduced axial load $F^* = F/(\pi A^2 \mu \varepsilon)$ versus the azimuthal stretch λ based on Eq. (145) with $k_1/\mu = 1, k_2 = 1$ and the values $\varphi = \pi/3, 3\pi/10, \pi/4, \pi/6$. **b** Plots of $F^* = (N - \pi a^2 P)/[\pi A^2 \mu(\eta - 1)]$ versus λ_a for the thick-walled case based on Eq. (137) with $\eta = 1.4$ and for the same values of the material constants, and $\varphi = \pi/3, \pi/4, \pi/6$

not able to support the residual stresses that have an important influence on the mechanical response of arteries. See, for example, the papers by Holzapfel et al. (2000), Ogden and Schulze-Bauer (2000) and Ogden (2003b) and references therein for detailed discussion of these features. In the following, therefore, we consider a thick-walled tube with residual stress.

5.3.2 Residual Stress Model

In order to illustrate the influence of residual stress on the material response we now specialize both the form of the residual stress and the strain-energy function. First, we choose a simple form of τ_{RR} satisfying the boundary conditions (139) and then use (138) to determine $\tau_{\theta\theta}$. Specifically, we take

$$\tau_{RR} = \alpha(R - A)(R - B), \tag{149}$$

where $\alpha (>0)$ is a constant, and obtain

$$\tau_{\theta\theta} = \alpha[3R^2 - 2(A + B)R + AB]. \tag{150}$$

Plots of τ_{RR} and $\tau_{\theta\theta}$ are shown in Fig. 14 for $\alpha = 1$. Since dependence on α is linear, curves for other values are obtained by appropriate scaling.

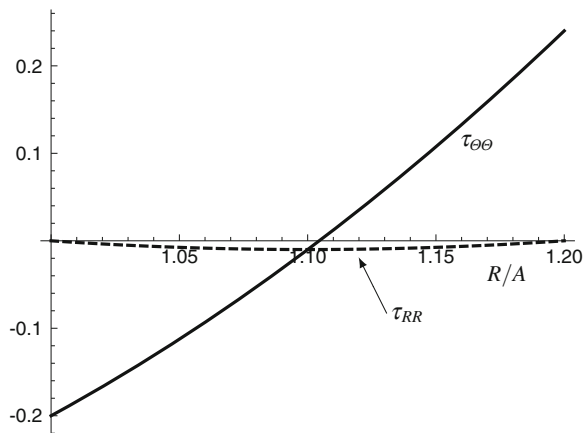
The characteristics of τ_{RR} and $\tau_{\theta\theta}$ shown in Fig. 14 are very similar to those obtained for a single layer from the so-called ‘opening angle’ method (Ogden 2003b) or from the assumption that the circumferential stress at a typical physiological pressure is uniform (Ogden and Schulze-Bauer 2000).

Recalling the constitutive law of a residually stressed material discussed in Sect. 3.4.2, we now specialize the strain-energy function to include the influence of residual stress with dependence only on the invariants K_1, K_4 and K_5 and without dependence on fibers. Then $W = W(K_1, K_4, K_5)$ and from (87) the expression for the Cauchy stress reduces to

$$\sigma = 2W_1\mathbf{B} + 2W_5\mathbf{\Sigma} - p\mathbf{I}, \tag{151}$$

and the restrictions (91) reduce to

Fig. 14 Residual stresses τ_{RR} (dashed curve) and $\tau_{\theta\theta}$ (continuous curve) plotted for $\alpha = 1$ based on Eqs. (149) and (150) as functions of R/A for $B/A = 1.2$, a typical value for artery walls



$$2W_1 - p^{(r)} = 0, \quad 2W_5 = 1 \quad (152)$$

in \mathcal{B}_r . Consistently with (152) we now consider the prototype model strain-energy function given by

$$W = \frac{1}{2}\mu(K_1 - 3) + \frac{1}{2}(K_5 - \text{tr } \boldsymbol{\tau}), \quad (153)$$

so that $W = 0$ in \mathcal{B}_r and (152) is satisfied with $p^{(r)} = \mu$, where $\mu (>0)$ is a constant.

For the considered problem the strain-energy function (142), on omission of φ , becomes

$$\begin{aligned} \tilde{W}(\lambda_\theta, \lambda_z, \tau_{RR}, \tau_{\Theta\Theta}) &= \frac{1}{2}\mu(\lambda_\theta^2 + \lambda_z^2 + \lambda_\theta^{-2}\lambda_z^{-2} - 3) \\ &\quad + \frac{1}{2}[\lambda_\theta^{-2}\lambda_z^{-2}\tau_{RR} + \lambda_\theta^2\tau_{\Theta\Theta} - (\tau_{RR} + \tau_{\Theta\Theta})], \end{aligned} \quad (154)$$

and the stress differences (127) specialize to

$$\sigma_{\theta\theta} - \sigma_{rr} = \lambda_\theta \frac{\partial \tilde{W}}{\partial \lambda_\theta} = \mu(\lambda_\theta^2 - \lambda_\theta^{-2}\lambda_z^{-2}) + \lambda_\theta^2\tau_{\Theta\Theta} - \lambda_\theta^{-2}\lambda_z^{-2}\tau_{RR}, \quad (155)$$

and

$$\sigma_{zz} - \sigma_{rr} = \lambda_z \frac{\partial \tilde{W}}{\partial \lambda_z} = \mu(\lambda_z^2 - \lambda_\theta^{-2}\lambda_z^{-2}) - \lambda_\theta^{-2}\lambda_z^{-2}\tau_{RR}. \quad (156)$$

The next step is to evaluate the integrals in the expressions for the pressure P and the reduced axial load $F = N - \pi a^2 P$ from the integrals in (135) and (137). This requires the expressions

$$\begin{aligned} \lambda_\theta \frac{\partial \tilde{W}}{\partial \lambda_\theta} &= (\mu + \alpha AB)(\lambda_\theta^2 - \lambda_\theta^{-2}\lambda_z^{-2}) - \alpha(A + B)R(2\lambda_\theta^2 - \lambda_\theta^{-2}\lambda_z^{-2}) \\ &\quad + \alpha R^2(3\lambda_\theta^2 - \lambda_\theta^{-2}\lambda_z^{-2}), \end{aligned} \quad (157)$$

$$\begin{aligned} 2\lambda_z \frac{\partial \tilde{W}}{\partial \lambda_z} - \lambda_\theta \frac{\partial \tilde{W}}{\partial \lambda_\theta} &= 2\mu\lambda_z^2 - (\mu + \alpha AB)(\lambda_\theta^2 + \lambda_\theta^{-2}\lambda_z^{-2}) \\ &\quad + \alpha(A + B)R(2\lambda_\theta^2 + \lambda_\theta^{-2}\lambda_z^{-2}) - \alpha R^2(3\lambda_\theta^2 + \lambda_\theta^{-2}\lambda_z^{-2}), \end{aligned} \quad (158)$$

which are obtained by substituting for the expressions (149) and (150) into (155) and (156).

The integrals are evaluated, with the help of the definition $\lambda_\theta = r/R$, using the radial part (121)₁ of the deformation in the form $r^2 - \lambda_z^{-1/2}R^2 = c$, where the notation $c = a^2 - \lambda_z^{-1}A^2 = b^2 - \lambda_z^{-1}B^2$ has been introduced for brevity. The resulting expressions for P and F , after some manipulation, are obtained as

$$\begin{aligned}
 P = & (\mu + \alpha AB)\lambda_z^{-1} \log\left(\frac{aB}{Ab}\right) + \frac{1}{2}\mu c\lambda_z^{-2} \frac{B^2 - A^2}{a^2b^2} + 2\alpha c \log\left(\frac{b}{a}\right) \\
 & - \frac{3}{2}\alpha\sqrt{c}(A+B)\lambda_z^{-1/2} \left[\tan^{-1}\left(\frac{\lambda_z^{1/2}\sqrt{c}}{A}\right) - \tan^{-1}\left(\frac{\lambda_z^{1/2}\sqrt{c}}{B}\right) \right] \quad (159)
 \end{aligned}$$

and

$$\begin{aligned}
 F = & \pi\mu(B^2 - A^2)(\lambda_z - \lambda_z^{-2}) + \pi c \left\{ (\mu + \alpha AB)\lambda_z^{-1} \log\left(\frac{bA}{aB}\right) - \alpha c \log\left(\frac{b}{a}\right) \right. \\
 & \left. + \alpha\sqrt{c}(A+B)\lambda_z^{-1/2} \left[\tan^{-1}\left(\frac{B}{\lambda_z^{1/2}\sqrt{c}}\right) - \tan^{-1}\left(\frac{A}{\lambda_z^{1/2}\sqrt{c}}\right) \right] \right\}. \quad (160)
 \end{aligned}$$

In the case $\lambda_z = 1$ these formulas were given in Ogden (2015).

For numerical purposes we now nondimensionalize all the quantities in the above two equations but restricted to the case $\lambda_z = 1$.

First, we set $P^* = P/\mu$ and $F^* = F/(\pi A^2\mu)$, which are different from the nondimensionalizations used for the membrane model in Sect. 5.2.2. We also introduce the notations

$$\eta = \frac{B}{A}, \quad \alpha^* = \frac{\alpha A^2}{\mu}, \quad (161)$$

and, as a measure of the radial inflation,

$$e = \frac{\sqrt{c}}{A} \equiv \sqrt{\lambda_a^2 - 1}. \quad (162)$$

The connections

$$\frac{b^2}{a^2} = \frac{\eta^2 + e^2}{1 + e^2}, \quad \lambda_b^2 = 1 + \eta^{-2}e^2 \quad (163)$$

then follow and hence P^* and F^* can be written

$$\begin{aligned}
 P^* = & \frac{1}{2}(1 + \alpha^*\eta) \log\left[\frac{(1 + e^2)\eta^2}{\eta^2 + e^2}\right] + \alpha^*e^2 \log\left(\frac{\eta^2 + e^2}{1 + e^2}\right) \\
 & + \frac{1}{2} \frac{(\eta^2 - 1)e^2}{(\eta^2 + e^2)(1 + e^2)} - \frac{3}{2}\alpha^*(1 + \eta)e \tan^{-1}\left[\frac{(\eta - 1)e}{\eta + e^2}\right], \quad (164)
 \end{aligned}$$

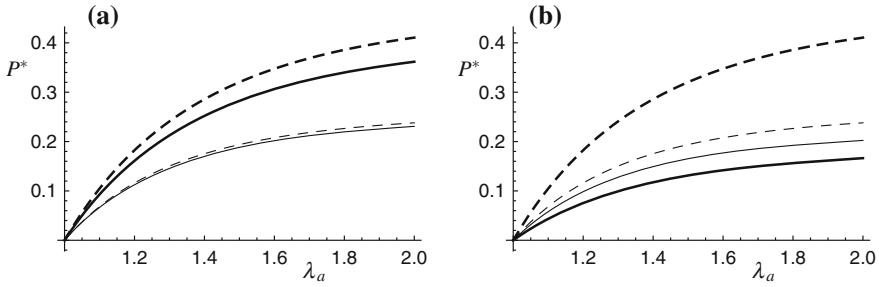


Fig. 15 Plots of $P^* = P/\mu$ versus λ_a based on Eq. (164) for **a** $\alpha^* = 2$ and **b** $\alpha^* = 10$ with $\eta = 1.3, 1.6$ in each case (*continuous curves*)—thin for $\eta = 1.3$ and thick for $\eta = 1.6$. Also shown are the corresponding curves without residual stress ($\alpha^* = 0$ —*dashed* for $\eta = 1.3$, *thick dashed* for $\eta = 1.6$)

$$\begin{aligned}
 F^* = & -\frac{1}{2}(1 + \alpha^*\eta)e^2 \log \left[\frac{(1 + e^2)\eta^2}{\eta^2 + e^2} \right] - \frac{1}{2}\alpha^*e^4 \log \left(\frac{\eta^2 + e^2}{1 + e^2} \right) \\
 & + \alpha^*(1 + \eta)e^3 \tan^{-1} \left[\frac{(\eta - 1)e}{\eta + e^2} \right]. \quad (165)
 \end{aligned}$$

Illustrative plots of P^* versus λ_a are shown in Fig. 15a, b for a residual stress with $\alpha^* = 2$ and $\alpha^* = 10$, respectively, and compared with corresponding plots without residual stress. In each case we choose $\eta = 1.3$ and $\eta = 1.6$. For thin-walled tubes with η between 1 and about 1.2 the effect of residual stress is small. For larger values of η and α^* it becomes more significant. Note that for larger α^* and/or larger values of η the negative value of the final term in (164) becomes significant and causes a reduction in the pressure. In particular, by comparing Fig. 15a, b we see that the pressure is larger for $\eta = 1.6$ than for $\eta = 1.3$ in Fig. 15a but the reverse is true in Fig. 15b. The effect of residual stress is to reduce the pressure required to achieve a given level of inflation compared with the case without residual stress. Moreover, if the residual stress has a very large magnitude the pressure becomes negative, which is unrealistic. Note: there is a typo in the sign of the final term in the corresponding expressions for P and P^* in Ogden (2015).

Plots of F^* are illustrated in Fig. 16a, b for $\alpha^* = 2$ and $\alpha^* = 10$, respectively, and compared with corresponding results without residual stress. The character of F^* changes because of the competing effects of the positive and negative terms in (165). As Fig. 16a shows, for $\alpha^* = 2$, F^* is negative for the considered values of η and increases in magnitude as η increases (only curves for $\eta = 1.3$ and $\eta = 1.6$ are shown). In this case F^* is slightly less negative than in the absence of residual stress. The tube has a tendency to elongate under pressure. But for larger α^* , F^* turns from negative to positive for the thicker walled tubes, exemplified by $\eta = 2$ in Fig. 16b, in which case the tube has a tendency to shorten under pressure.

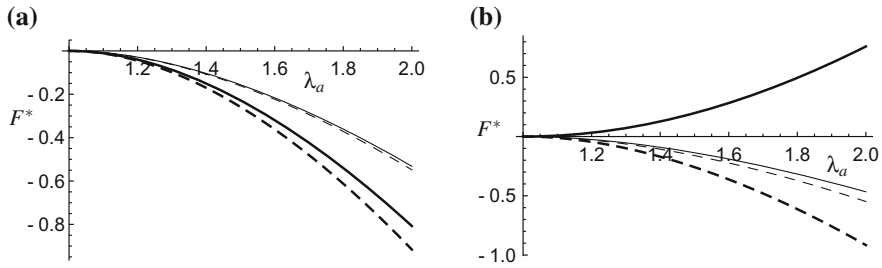


Fig. 16 Plots of $F^* = F/(\pi A^2 \mu)$ versus λ_a based on Eq. (165) for **a** $\alpha^* = 2$ with $\eta = 1.3, 1.6$ (continuous curves)—thin for $\eta = 1.3$ and thick for $\eta = 1.6$, and **b** $\alpha^* = 10$, with $\eta = 1.3, 2$ (continuous curves)—thin for $\eta = 1.3$ and thick for $\eta = 2$. Also shown are the corresponding curves without residual stress $\alpha^* = 0$: **a** dashed for $\eta = 1.3$, thick dashed for $\eta = 1.6$; **b** dashed for $\eta = 1.3$, thick dashed for $\eta = 2$

With both fibers and residual stress included in the strain-energy function we combine (146) and (154) to obtain

$$\begin{aligned} \tilde{W}(\lambda_\theta, \lambda_z, \varphi, \tau_{RR}, \tau_{\theta\theta}) &= \frac{1}{2} \mu (\lambda_\theta^2 + \lambda_z^2 + \lambda_\theta^{-2} \lambda_z^{-2} - 3) \\ &\quad + \frac{k_1}{k_2} \{ \exp[k_2 (\lambda_\theta^2 \cos^2 \varphi + \lambda_z^2 \sin^2 \varphi - 1)^2] - 1 \} \\ &\quad + \frac{1}{2} [\lambda_\theta^{-2} \lambda_z^{-2} \tau_{RR} + \lambda_\theta^2 \tau_{\theta\theta} - (\tau_{RR} + \tau_{\theta\theta})], \end{aligned} \quad (166)$$

and the associated

$$\begin{aligned} \lambda_\theta \frac{\partial \tilde{W}}{\partial \lambda_\theta} &= \mu (\lambda_\theta^2 - \lambda_\theta^{-2} \lambda_z^{-2}) + 4k_1 (\lambda_\theta^2 \cos^2 \varphi + \lambda_z^2 \sin^2 \varphi - 1) \lambda_\theta^2 \cos^2 \varphi \\ &\quad \times \exp[k_2 (\lambda_\theta^2 \cos^2 \varphi + \lambda_z^2 \sin^2 \varphi - 1)^2] + \lambda_\theta^2 \tau_{\theta\theta} - \lambda_\theta^{-2} \lambda_z^{-2} \tau_{RR}, \end{aligned} \quad (167)$$

$$\begin{aligned} \lambda_z \frac{\partial \tilde{W}}{\partial \lambda_z} &= \mu (\lambda_z^2 - \lambda_\theta^{-2} \lambda_z^{-2}) + 4k_1 (\lambda_\theta^2 \cos^2 \varphi + \lambda_z^2 \sin^2 \varphi - 1) \lambda_z^2 \sin^2 \varphi \\ &\quad \times \exp[k_2 (\lambda_\theta^2 \cos^2 \varphi + \lambda_z^2 \sin^2 \varphi - 1)^2] - \lambda_\theta^{-2} \lambda_z^{-2} \tau_{RR}. \end{aligned} \quad (168)$$

Based on the general formulas (135) and (137) we now exemplify the characters of P^* and F^* . First, in Fig. 17, $P^* = P/[\mu(\eta - 1)]$ is plotted for the representative parameter values $\alpha^* = 2$, $\eta = 1.4$, $k_1/\mu = k_2 = 1$, and for four values of φ , as indicated in the figure caption. For comparison, curves are also shown for $\alpha^* = 0$ (no residual stress) in order to illustrate the effect of residual stress. The residual stress has a significant effect on P^* only for fiber directions relatively close to the axial direction, as illustrated for $\varphi = \pi/3$ in Fig. 17a, in which case the presence of residual stress requires a significantly larger value of P^* to achieve a given level

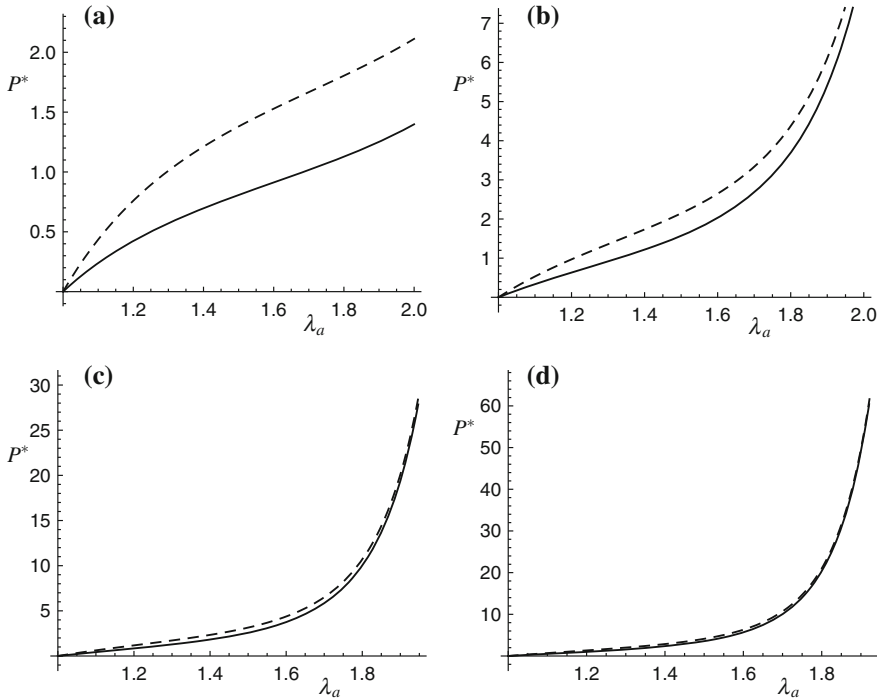


Fig. 17 Plots of $P^* = P/[\mu(\eta - 1)]$ versus λ_a based on (135) with (167) and parameters $\alpha^* = 2$, $\eta = 1.4$, $k_1/\mu = k_2 = 1$ for **a** $\varphi = \pi/3$, **b** $\varphi = \pi/4$, **c** $\varphi = \pi/5$, **d** $\varphi = \pi/6$ (dashed curves), and corresponding plots for $\alpha^* = 0$ (continuous curves)

of inflation than in the absence of residual stress. As the fiber direction approaches circumferential the residual stress has a smaller and smaller influence. The pattern is very similar for larger values of α^* and details are not therefore included here.

In Fig. 18a, b representative plots of $F^* = F/[\pi A^2 \mu(\eta - 1)]$ are shown for the same parameter values as for P^* . In Fig. 18c and d corresponding plots are shown for $\alpha^* = 20$ in order to illustrate that larger values of α^* have only a marginal effect on the character of the curves. In each case the curves are compared with those obtained in the absence of residual stress. For smaller values of φ there is only very little difference between the curves with and without residual stress, and as for P^* it is only for fiber directions close to axial that the residual stress has a significant effect. While the residual stress has the effect of increasing the value of P^* required to achieve a given inflation it reduces the magnitude of F^* .

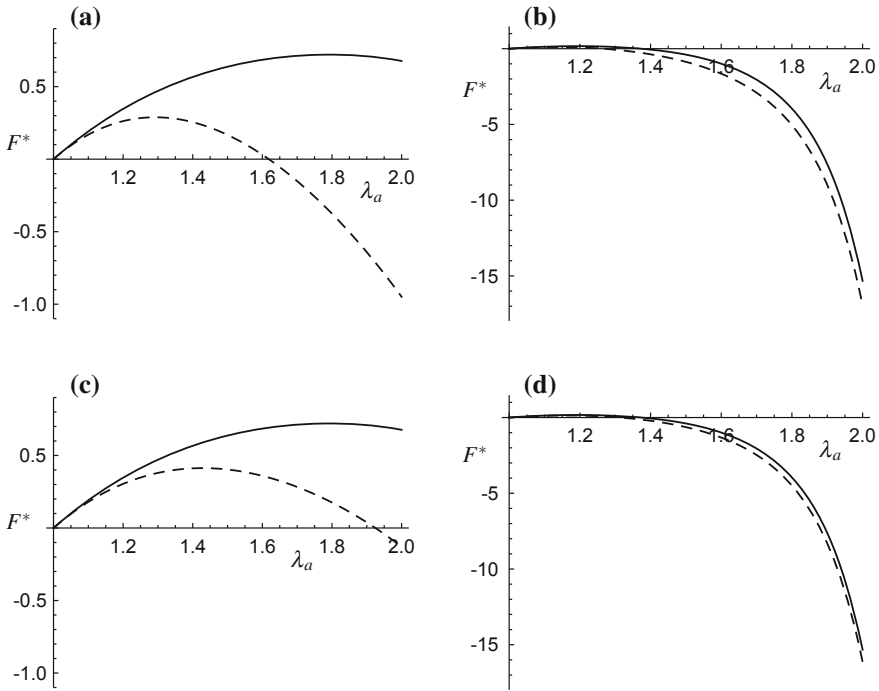


Fig. 18 Plots of $F^* = F/[\pi A^2 \mu (\eta - 1)]$ versus λ_a based on (137) with (167) and (168) and parameters $\eta = 1.4$, $k_1/\mu = k_2 = 1$ for **a** $\varphi = \pi/3$, **b** $\varphi = \pi/4$, with $\alpha^* = 2$, and **c** $\varphi = \pi/3$, **d** $\varphi = \pi/4$, with $\alpha^* = 20$ (dashed curves), and corresponding plots for $\alpha^* = 0$ (continuous curves)

6 The Effect of Fiber Dispersion

The model discussed in the preceding section assumes that all fibers within a given family are oriented in the same direction. This is patently not the case for actual arteries. There is dispersion in the orientations of collagen fibers within each family, as exemplified by histological data from human coronary and brain arteries obtained by Canham et al. (1989), Finlay et al. (1995, 1998). In particular, it was found that there is wider dispersion in the intimal and adventitial layers than in the medial layer. This is reflected in uniaxial test data obtained for the separate layers of aged human coronary arteries by Holzapfel et al. (2005). Mean data for such tests on strip specimens from the circumferential and axial directions of intimal, adventitial and medial layers are illustrated in Fig. 19. In the media, where the mean fiber direction is closer to the circumferential direction than the axial direction, the uniaxial response is stiffest in the circumferential direction, while for the intima and adventitia the reverse is the case.

The model discussed in Sect. 5.3.1 gives a good representation of the data for the media (and also for the intact, layer-unseparated artery, which behaves very similarly

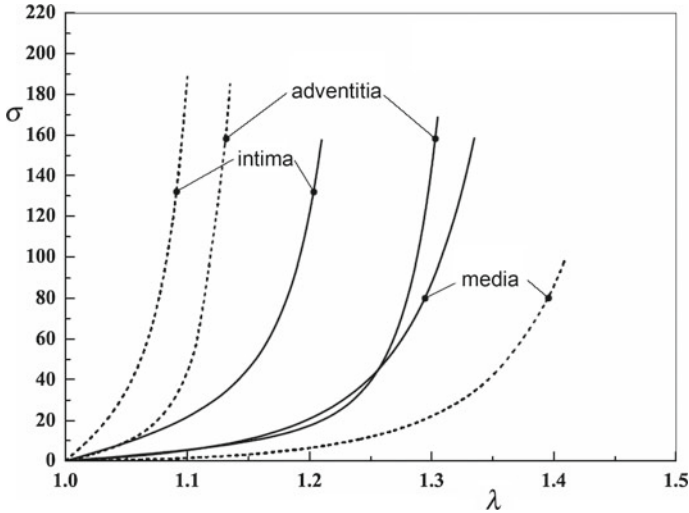


Fig. 19 Plots of the uniaxial Cauchy stress σ (kPa) versus the stretch λ based on mean data for intimal, medial, and adventitial strips from uniaxial tension experiments on aged human coronary arteries (Holzapfel et al. 2005). The tests were performed on strips from the circumferential direction (*continuous curves*) and axial direction (*dashed curves*). Based on Holzapfel et al. (2005), Fig. 7, with permission

to the media), but not of the data for the intima or adventitia. In Gasser et al. (2006) this difference was attributed to the greater level of dispersion in the latter two layers and led to the development of a model based on a so-called *generalized structure tensor*, which takes account of the dispersion and generalizes the model in Sect. 5.3.1. This is discussed in the following.

6.1 A Model of Fiber Dispersion in Three Dimensions

Consider a fiber dispersion with a general fiber direction \mathbf{N} within the dispersion referred to spherical polar angles Θ and Φ in the reference configuration, as depicted in Fig. 20 with respect to rectangular Cartesian basis vectors \mathbf{e}_1 , \mathbf{e}_2 , \mathbf{e}_3 . Thus, we have

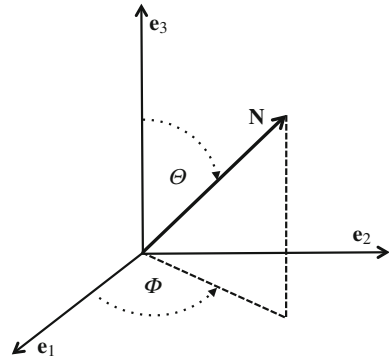
$$\mathbf{N}(\Theta, \Phi) = \sin \Theta \cos \Phi \mathbf{e}_1 + \sin \Theta \sin \Phi \mathbf{e}_2 + \cos \Theta \mathbf{e}_3, \quad (169)$$

where $\Theta \in [0, \pi]$ and $\Phi \in [0, 2\pi]$.

It is assumed that the fiber orientations in the reference configuration are distributed according to an *orientation density function* (or probability density function), which we denote by $\rho = \rho(\Theta, \Phi)$, and it is also assumed that this is unaffected by reversal of \mathbf{N} , so that $\rho(\pi - \Theta, \pi + \Phi) \equiv \rho(\Theta, \Phi)$.

The density is normalized according to

Fig. 20 Unit vector \mathbf{N} representing the orientation of a fiber within a dispersion in the reference configuration in terms of spherical polar angles Θ and Φ relative to background rectangular Cartesian axes $\mathbf{e}_1, \mathbf{e}_2, \mathbf{e}_3$



$$\frac{1}{4\pi} \int_{\Omega} \rho(\Theta, \Phi) d\Omega = 1, \tag{170}$$

where Ω is the unit sphere $\{(\Theta, \Phi) \mid \Theta \in [0, \pi], \Phi \in [0, 2\pi]\}$, and the proportion of fibers within the solid angle $d\Omega = \sin \Theta d\Theta d\Phi$ is $\rho(\Theta, \Phi) d\Omega$.

If there is no dispersion and all fibers in a family are aligned in the direction \mathbf{M} then the structure tensor $\mathbf{M} \otimes \mathbf{M}$ can be used to construct the invariants I_4 and I_5 , as in Sect. 3.3.2. This notion of a structure tensor is now generalized to form a *generalized structure tensor*, denoted \mathbf{H} , which is an average of $\mathbf{N} \otimes \mathbf{N}$ weighted by $\rho(\Theta, \Phi)$ over the unit sphere, i.e., it is defined by

$$\mathbf{H} = \frac{1}{4\pi} \int_{\Omega} \rho(\Theta, \Phi) \mathbf{N} \otimes \mathbf{N} d\Omega. \tag{171}$$

Clearly, \mathbf{H} is symmetric, and because \mathbf{N} is a unit vector it follows from (170) and (171) that

$$\text{tr } \mathbf{H} = 1. \tag{172}$$

Thus, in three dimensions \mathbf{H} has five independent components in general, and when the expression (171) is expanded using (169) the five components of \mathbf{H} with respect to the Cartesian basis $\mathbf{e}_1, \mathbf{e}_2, \mathbf{e}_3$ are

$$H_{11} = \frac{1}{4\pi} \int_{\Omega} \rho \sin^3 \Theta \cos^2 \Phi d\Theta d\Phi, \tag{173}$$

$$H_{22} = \frac{1}{4\pi} \int_{\Omega} \rho \sin^3 \Theta \sin^2 \Phi d\Theta d\Phi, \tag{174}$$

$$H_{12} = \frac{1}{4\pi} \int_{\Omega} \rho \sin^3 \Theta \sin \Phi \cos \Phi d\Theta d\Phi, \tag{175}$$

$$H_{23} = \frac{1}{4\pi} \int_{\Omega} \rho \sin^2 \Theta \cos \Theta \sin \Phi d\Theta d\Phi, \tag{176}$$

$$H_{13} = \frac{1}{4\pi} \int_{\Omega} \rho \sin^2 \Theta \cos \Theta \cos \Phi d\Theta d\Phi, \quad (177)$$

with $H_{ij} = H_{ji}$, $i, j \in \{1, 2, 3\}$, and from (172) we also have $H_{33} = 1 - H_{11} - H_{22}$.

6.1.1 Fiber Dispersion with Rotational Symmetry

In Gasser et al. (2006) the focus was on the special case in which ρ is independent of Φ , and we therefore omit the dependence of Φ and write $\rho = \rho(\Theta)$. Then, the fiber dispersion has rotational symmetry about the direction \mathbf{e}_3 , and the normalization condition (170) reduces to

$$\frac{1}{2} \int_0^\pi \rho(\Theta) \sin \Theta d\Theta = 1. \quad (178)$$

This dispersion is sometimes referred to as a *transversely isotropic dispersion*, and in this case \mathbf{e}_3 is the mean fiber direction.

Now there is only one independent component of \mathbf{H} , and its components can be written compactly as

$$H_{11} = H_{22} = \kappa, \quad H_{33} = 1 - 2\kappa, \quad H_{ij} = 0, \quad i \neq j, \quad (179)$$

where κ , which is a measure of dispersion, is defined by

$$\kappa = \frac{1}{4} \int_0^\pi \rho(\Theta) \sin^3 \Theta d\Theta. \quad (180)$$

This allows the tensor \mathbf{H} to be represented in the form

$$\mathbf{H} = \kappa \mathbf{I}_r + (1 - 3\kappa) \mathbf{M} \otimes \mathbf{M}, \quad (181)$$

where \mathbf{I}_r is again the identity tensor in \mathcal{B}_r and \mathbf{M} is a unit vector denoting the mean fiber direction, which, in terms of the considered Cartesian axes, is $\mathbf{M} = \mathbf{e}_3$. More generally, without specifying the axes, (181) represents a rotationally symmetric distribution about the mean direction \mathbf{M} .

In general κ must lie in the interval $[0, 1/2]$. The limiting value $\kappa = 0$ corresponds to the case where all fibers are aligned and there is no dispersion, in which case $\mathbf{H} = \mathbf{M} \otimes \mathbf{M}$ (ρ being a delta function). The intermediate value $\kappa = 1/3$ corresponds to an isotropic fiber dispersion, i.e., the fibers are dispersed uniformly in all directions in three dimensions, $\rho = 1$ and $\mathbf{H} = \mathbf{I}_r/3$. For the upper limit $\kappa = 1/2$ the fiber dispersion is isotropic in two dimensions in the plane normal to \mathbf{M} (and ρ is again a delta function). We note that in some circumstances values of κ in the range $(1/3, 1/2]$ lead to unphysical results, as pointed out in Holzapfel and Ogden (2010); see also Melnik et al. (2015).

Dispersion Represented as a von Mises Distribution

The fiber dispersion can be measured approximately by imaging histological samples and represented using a probability density function. In particular, it has been found reasonable to represent $\rho(\Theta)$ by a π -periodic von Mises distribution (Gasser et al. 2006; Holzapfel et al. 2015) based on the exponential function $\exp[\cos(2\Theta)]$. Here we write it in the form

$$\rho(\Theta) = 4\sqrt{\frac{b}{2\pi}} \frac{\exp(2b \cos^2 \Theta)}{\operatorname{erfi}(\sqrt{2b})}, \tag{182}$$

which is symmetrical about $\Theta = 0$ and the constant factor is needed to satisfy the normalization (178), where erfi is the imaginary error function related to the standard error function erf by $\operatorname{erfi}(x) = -i \operatorname{erf}(ix)$, erf being defined by

$$\operatorname{erf}(x) = \frac{2}{\sqrt{\pi}} \int_0^x \exp(-u^2) du, \tag{183}$$

and b is the so-called *concentration parameter*. Plots of $\rho(\Theta)$ versus Θ are shown in Fig. 21 for several values of b , with larger values of b giving a more concentrated distribution about $\Theta = 0$, tending to a delta function as $b \rightarrow \infty$, in which case there is no dispersion. For ease of viewing $\rho(\Theta)$ is plotted for the range $\Theta \in [-\pi/2, \pi/2]$ instead of $[0, \pi]$.

The integral in (180) can be evaluated explicitly to give κ as a function of b in the form

$$\kappa = \frac{1}{2} + \frac{1}{8b} - \frac{1}{4} \sqrt{\frac{2}{\pi b}} \frac{\exp(2b)}{\operatorname{erfi}(\sqrt{2b})}, \tag{184}$$

and Fig. 22 provides a plot of this function. This shows, in particular, that $\kappa \rightarrow 0$ as $b \rightarrow \infty$ and the isotropic case corresponds to $b = 0$ and $\kappa = 1/3$.

Fig. 21 Plot of $\rho(\Theta)$ versus Θ for the von Mises distribution (182) for $b = 2, 5, 8$, the dashed, continuous and thick dashed curves, respectively

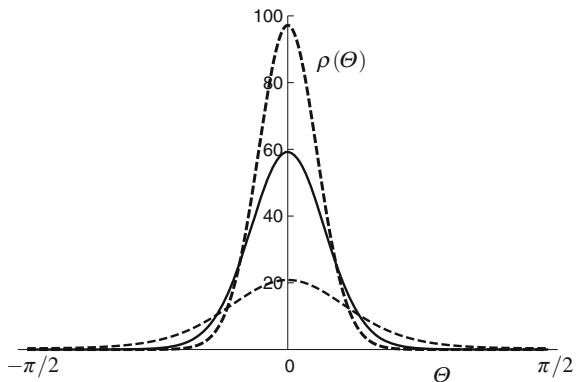
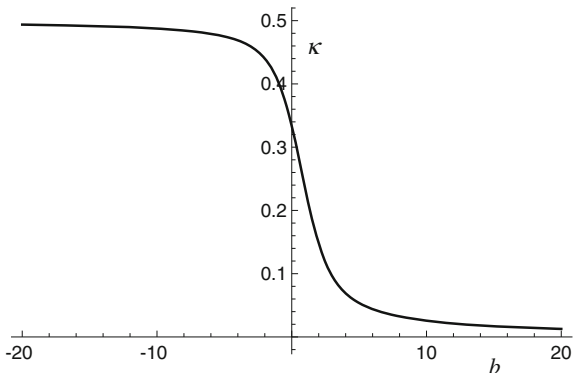


Fig. 22 Plot of the dispersion parameter κ as a function of the concentration parameter b based on the formula (184)



Generalized Invariants

Let us now recall the definition of the invariants I_4 and I_5 given in (54). These may equivalently be written as

$$I_4 = \text{tr}(\mathbf{C}\mathbf{M} \otimes \mathbf{M}), \quad I_5 = \text{tr}(\mathbf{C}^2\mathbf{M} \otimes \mathbf{M}). \tag{185}$$

These motivate the introduction of *generalized invariants*, which we denote by I_4^* and I_5^* , based on the generalized structure tensor \mathbf{H} in (181). These are defined by

$$I_4^* = \text{tr}(\mathbf{C}\mathbf{H}), \quad I_5^* = \text{tr}(\mathbf{C}^2\mathbf{H}), \tag{186}$$

and from (181) and (45) it follows that

$$I_4^* = \kappa I_1 + (1 - 3\kappa)I_4, \quad I_5^* = \kappa(I_1^2 - 2I_2) + (1 - 3\kappa)I_5, \tag{187}$$

in which we have used the definitions (185) with \mathbf{M} now being the mean fiber direction. Thus, for the considered rotationally symmetric fiber dispersion the generalized invariants I_4^* and I_5^* are combinations of isotropic and transversely isotropic invariants, weighted with respect to the dispersion parameter κ . Implicit in this consideration is that at a given point \mathbf{X} in \mathcal{B}_t the deformation gradient \mathbf{F} applies to each fiber in the dispersion at \mathbf{X} .

The generalized invariants do not, of course, capture complete information about the dispersion. Further information on the structure can be obtained by considering higher order structure tensors, an example of which is the fourth-order structure tensor \mathcal{H} with components given by

$$\mathcal{H}_{ijkl} = \frac{1}{4\pi} \int_0^\pi \rho(\Theta) \int_0^{2\pi} N_i N_j N_k N_l \sin \Theta d\Theta d\Phi, \tag{188}$$

which has complete i, j, k, l symmetry and satisfies (in the summation convention)

$$\mathcal{H}_{iijj} = 1, \quad \mathcal{H}_{11jj} = \mathcal{H}_{22jj} = \kappa, \quad \mathcal{H}_{33jj} = 1 - 2\kappa, \quad (189)$$

and also introduces an additional dispersion parameter, denoted κ_1 and defined by

$$\kappa_1 = \frac{1}{4} \int_0^\pi \rho(\Theta) \sin^5 \Theta d\Theta. \quad (190)$$

The only nonzero components of \mathcal{H} are

$$\mathcal{H}_{1111} = \mathcal{H}_{2222} = 3\mathcal{H}_{1122} = \frac{3}{4}\kappa_1, \quad \mathcal{H}_{1133} = \mathcal{H}_{2233} = \kappa - \kappa_1 \quad (191)$$

and

$$\mathcal{H}_{3333} = 1 - 4\kappa + 2\kappa_1. \quad (192)$$

Clearly, additional generalized invariants based on \mathcal{H} and involving κ_1 can be constructed; indeed, extension to higher order structure tensors would introduce yet more dispersion parameters. However, for our purposes it suffices to restrict attention to \mathbf{H} and its associated generalized invariants.

6.1.2 A Strain-Energy Function for a Rotationally Symmetric Dispersion

In Sect. 3.3.2, for an incompressible material with a single preferred direction \mathbf{M} , we considered the strain-energy function to depend on the invariants I_1, I_2, I_4, I_5 : $W(I_1, I_2, I_4, I_5)$. In view of the dependence noted in (187) this can be considered to remain the case when there is a rotationally symmetric fiber dispersion with the proviso concerning higher order generalized structure tensors mentioned above, except that \mathbf{M} in the definitions in (185) is now the mean fiber direction.

Thus, to account for the dispersion in the strain-energy function of an incompressible elastic material with a single rotationally symmetric dispersion it suffices to replace I_4 and I_5 by I_4^* and I_5^* , and we write the strain-energy function as $W^*(I_1, I_2, I_4^*, I_5^*)$, which depends on κ as well as (I_1, I_2, I_4, I_5) .

The Cauchy stress is then calculated from (57) with the help of (187) as

$$\boldsymbol{\sigma} = 2W_1^* \mathbf{B} + 2W_2^* (I_1 \mathbf{B} - \mathbf{B}^2) + 2W_4^* \mathbf{h} + 2W_5^* (\mathbf{B}\mathbf{h} + \mathbf{h}\mathbf{B}) - p\mathbf{I}, \quad (193)$$

where $W_1^* = \partial W^*/\partial I_1$, $W_2^* = \partial W^*/\partial I_2$, $W_4^* = \partial W^*/\partial I_4^*$, $W_5^* = \partial W^*/\partial I_5^*$ and $\mathbf{h} = \mathbf{F}\mathbf{H}\mathbf{F}^T$, the latter being the push forward of \mathbf{H} to \mathcal{B} . Thus, compared with (57) the role of $\mathbf{m} \otimes \mathbf{m}$ is taken by \mathbf{h} . For a material with two families of dispersed fibers with mean fiber directions \mathbf{M} and \mathbf{M}' additional invariants $I_6 = \mathbf{M}' \cdot (\mathbf{C}\mathbf{M}')$, $I_7 = \mathbf{M}' \cdot (\mathbf{C}^2\mathbf{M}')$ and $I_8 = \mathbf{M} \cdot (\mathbf{C}\mathbf{M}')$ can be defined as in (64) and (65) with the new interpretation of \mathbf{M} and \mathbf{M}' , and an expression for the Cauchy stress formed, extending (193).

However, it is sufficient in what follows to restrict attention to the dependence of W on I_1, I_4, I_6 instead of $I_1, I_2, I_4, I_5, I_6, I_7, I_8$ in order to capture the effect of two fiber families. For this purpose we introduce the notation $W^*(I_1, I_4^*, I_6^*) = W(I_1, I_4, I_6)$, where, analogously to (187),

$$I_6^* = \kappa' I_1 + (1 - 3\kappa') I_6, \quad (194)$$

with $I_6^* = \text{tr}(\mathbf{C}\mathbf{H}')$ and $\mathbf{H}' = \kappa' \mathbf{I}_r + (1 - 3\kappa') \mathbf{M}' \otimes \mathbf{M}'$, κ' being the dispersion parameter associated with \mathbf{M}' .

The Cauchy stress then has the form

$$\boldsymbol{\sigma} = 2W_1^* \mathbf{B} + 2W_4^* \mathbf{h} + 2W_6^* \mathbf{h}' - p \mathbf{I}, \quad (195)$$

where $\mathbf{h}' = \mathbf{F}\mathbf{H}'\mathbf{F}^T$.

We now recall the strain-energy function with the structure given by (112) in terms of I_1, I_4, I_6 , i.e.,

$$W = W_{\text{iso}}(I_1) + W_{\text{aniso}}(I_4, I_6), \quad (196)$$

and extend this to account for fiber dispersion by writing

$$W^* = W_{\text{iso}}^*(I_1) + W_{\text{aniso}}^*(I_4^*, I_6^*), \quad (197)$$

where $W_{\text{iso}}^*(I_1)$ characterizes the properties of the isotropic matrix in which the fibers are embedded and $W_{\text{aniso}}^*(I_4^*, I_6^*)$ characterizes the properties of the fiber dispersions.

As in (113) the isotropic part is taken to have the neo-Hookean form

$$W_{\text{iso}}^* = \frac{1}{2} \mu (I_1 - 3) \quad (198)$$

with the shear modulus $\mu (>0)$. The anisotropic part of (197) is now

$$W_{\text{aniso}}^* = \frac{k_1}{2k_2} \sum_{i=4,6} \{\exp[k_2(I_i^* - 1)^2] - 1\}, \quad (199)$$

which is obtained from (114) by replacing I_4 and I_6 by I_4^* and I_6^* , respectively. In particular, we note that when $\kappa' = \kappa$ the two families of dispersed fibers have the same elastic properties. The material constants $k_1 (>0)$ and $k_2 (>0)$ have the same interpretation as in (114).

The strain-energy function (197) with (198) and (199) was introduced by Gasser et al. (2006), and, in particular, we note that the anisotropic contribution (199) involves the isotropic invariant I_1 as well as the anisotropic ones I_4 and I_6 . We also note that it was assumed in Gasser et al. (2006) that the anisotropic term in I_4^* only contributes to the energy and the stress if $I_4 > 1$ and similarly the term in I_6^* only contributes to the energy and the stress if $I_6 > 1$, i.e., if the mean fiber direction is extended in one or other family of fibers. In the case when there is no dispersion

this is because it is assumed that individual fibers cannot support compression. When there is dispersion, on the other hand, that the mean fiber direction is extended does not in general mean that all fibers in a dispersion are extended and those that are compressed should therefore be omitted from contributing to the energy and stress if it is again assumed that compressed fibers do not support compression. Whether this is the case or not is open to debate since closely packed fibers may well support some compression. Equally, if, for example, $I_4 \leq 1$ then this does not in general mean that all fibers in the dispersed family are under compression, so to omit the contribution of the I_4^* term may not then be appropriate. See the discussion in Holzapfel and Ogden (2015) and Melnik et al. (2015), for example. This is an issue that requires further investigation.

6.2 Fiber Dispersion in Two Dimensions

In two-dimensional problems such as for plane strain or plane stress it is appropriate to consider planar dispersions, and toward the analysis of such dispersions we confine attention to the plane defined by the unit basis vectors \mathbf{e}_1 and \mathbf{e}_2 . We follow the analysis in Ogden (2009) and Holzapfel and Ogden (2010) but with different notation. Let the direction of a general fiber lying in this plane be represented by the unit vector \mathbf{N} in the reference configuration, where

$$\mathbf{N} = \cos \Theta \mathbf{e}_1 + \sin \Theta \mathbf{e}_2. \quad (200)$$

Suppose that the fiber dispersion is symmetric about \mathbf{e}_1 , which is then the mean fiber direction. The orientation density ρ then depends only on Θ and satisfies $\rho(-\Theta) = \rho(\Theta)$.

The counterpart of the three-dimensional normalization in the considered two dimensions is

$$\frac{1}{\pi} \int_{-\pi/2}^{\pi/2} \rho(\Theta) d\Theta = 1, \quad (201)$$

and the (two-dimensional) generalized structure tensor is defined by

$$\hat{\mathbf{H}} = \frac{1}{\pi} \int_{-\pi/2}^{\pi/2} \rho(\Theta) \mathbf{N} \otimes \mathbf{N} d\Theta, \quad (202)$$

where the hat is used to indicate the two-dimensional restriction. The only nonzero components of $\hat{\mathbf{H}}$ are \hat{H}_{11} and \hat{H}_{22} , which satisfy $\hat{H}_{11} + \hat{H}_{22} = 1$, where

$$\hat{H}_{22} = \frac{1}{\pi} \int_{-\pi/2}^{\pi/2} \rho(\Theta) \sin^2 \Theta d\Theta. \quad (203)$$

Let us introduce the notation $\hat{H}_{22} = \kappa$ as a characteristic parameter of the dispersion, similarly to the three-dimensional situation. Then $\hat{\mathbf{H}}$ can be expanded in the form

$$\hat{\mathbf{H}} = \kappa \hat{\mathbf{I}}_r + (1 - 2\kappa) \mathbf{e}_1 \otimes \mathbf{e}_1, \quad (204)$$

where $\hat{\mathbf{I}}_r$ is the two-dimensional identity in the reference configuration of the considered plane.

More generally, if \mathbf{M} is the mean fiber direction in the plane and the dispersion is symmetric about \mathbf{M} then (204) generalizes slightly to

$$\hat{\mathbf{H}} = \kappa \hat{\mathbf{I}}_r + (1 - 2\kappa) \mathbf{M} \otimes \mathbf{M}. \quad (205)$$

By way of illustration we now apply this to the case of plane strain for an incompressible material. In respect of a single preferred direction, we recall the plane strain connections $I_2 = I_1$ and $I_5 = (I_1 - 1)I_4 - 1$ given in (59) and the expression

$$\hat{\sigma} = 2\hat{W}_1 \hat{\mathbf{B}} + 2\hat{W}_4 \mathbf{m} \otimes \mathbf{m} - \hat{p} \hat{\mathbf{I}} \quad (206)$$

from (60) for the planar Cauchy stress, where $\hat{W} = \hat{W}(I_1, I_4)$.

Similarly to the three-dimensional model considered in the preceding section we accommodate the dispersion by replacing I_4 by $I_4^* = \text{tr}(\mathbf{C}\hat{\mathbf{H}})$, which in this case is given by

$$I_4^* = \kappa(I_1 - 1) + (1 - 2\kappa)I_4, \quad (207)$$

with $\hat{W}^*(I_1, I_4^*) = \hat{W}(I_1, I_4)$. A short calculation then leads to the planar Cauchy stress

$$\hat{\sigma} = 2\hat{W}_1^* \hat{\mathbf{B}} + 2\hat{W}_4^* \hat{\mathbf{h}} - \hat{p} \hat{\mathbf{I}}, \quad (208)$$

where $\hat{\mathbf{h}} = \mathbf{F}\hat{\mathbf{H}}\mathbf{F}^T$, and, analogously to (195), if there are two fiber families with mean fiber directions \mathbf{M} and \mathbf{M}' in the plane, corresponding generalized invariants I_4^* and I_6^* and dispersion parameters κ and κ' , (208) extends to

$$\hat{\sigma} = 2\hat{W}_1^* \hat{\mathbf{B}} + 2\hat{W}_4^* \hat{\mathbf{h}} + 2\hat{W}_6^* \hat{\mathbf{h}}' - \hat{p} \hat{\mathbf{I}}, \quad (209)$$

where $\hat{W}^* = \hat{W}^*(I_1, I_4^*, I_6^*)$,

$$\hat{\mathbf{h}}' = \mathbf{F}[\kappa' \hat{\mathbf{I}}_r + (1 - 2\kappa') \mathbf{M}' \otimes \mathbf{M}'] \mathbf{F}^T, \quad (210)$$

and $I_6^* = \kappa'(I_1 - 1) + (1 - 2\kappa')I_6$.

6.3 The Influence of Fiber Dispersion on the Response of an Artery

Again we denote the mean orientations of the two fiber families by \mathbf{M} and \mathbf{M}' and we assume that each dispersion is rotationally symmetric about its mean direction with the same dispersion parameter κ . We take the mean fiber directions to be symmetrically disposed, making equal angles φ with the circumferential direction and to lie in the tangential (Θ, Z) plane locally, as illustrated in Fig. 23. Hence,

$$\mathbf{M} = \cos \varphi \mathbf{E}_\Theta + \sin \varphi \mathbf{E}_Z, \quad \mathbf{M}' = -\cos \varphi \mathbf{E}_\Theta + \sin \varphi \mathbf{E}_Z. \tag{211}$$

Note that with respect to Fig. 11 the sense of \mathbf{M}' has been reversed here.

Then, for the deformation described in Sect. 5.1 we again have

$$I_1 = \lambda_\theta^2 + \lambda_z^2 + \lambda_\theta^{-2} \lambda_z^{-2}, \quad I_4 = I_6 = \lambda_\theta^2 \cos^2 \varphi + \lambda_z^2 \sin^2 \varphi, \tag{212}$$

and the invariants I_4^* and I_6^* are

$$I_4^* = I_6^* = \kappa I_1 + (1 - 3\kappa)I_4. \tag{213}$$

We again adopt the strain-energy function (197) with (198) and (199), which, under the present assumptions, specializes to

$$W^* = \frac{1}{2} \mu (I_1 - 3) + \frac{k_1}{k_2} \{ \exp[k_2 (I_4^* - 1)^2] - 1 \}. \tag{214}$$

In order to illustrate the effect of the fiber dispersion it suffices to consider the membrane equations for P and F given by (144) and (145), respectively, but now with the strain-energy function \tilde{W} in (146) replaced by \tilde{W}^* obtained from (214) as

Fig. 23 Mean fiber directions \mathbf{M} and \mathbf{M}' locally in (Θ, Z) planes at radial location R through the tube wall, with an indication of the rotationally symmetric fiber dispersions about \mathbf{M} and \mathbf{M}'

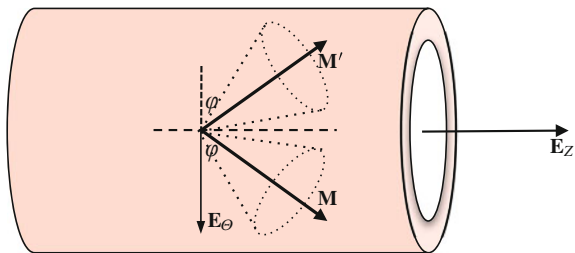
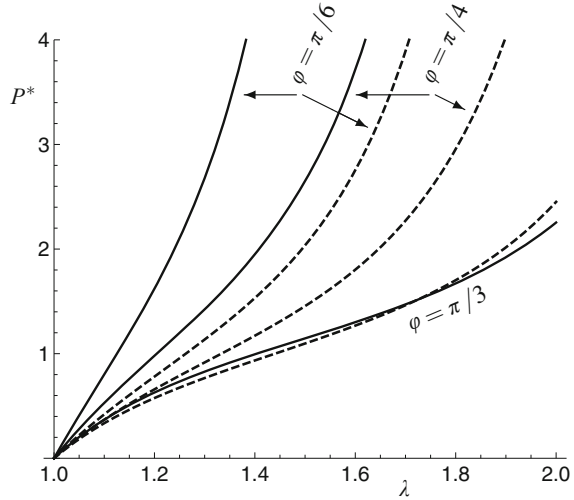


Fig. 24 Plot of the dimensionless pressure $P^* = P/\mu\varepsilon$ against λ for the strain-energy function (215) with $\lambda_z = 1$, material parameters $k_1/\mu = 1, k_2 = 1$ and dispersion parameters $\kappa = 0.2$ (dashed curves) and $\kappa = 0$ (continuous curves—no dispersion), and angles $\varphi = \pi/6, \pi/4, \pi/3$, based on the thin-wall approximation (144)



$$\begin{aligned} \tilde{W}^*(\lambda_\theta, \lambda_z, \varphi, \kappa) = & \frac{1}{2}\mu(\lambda_\theta^2 + \lambda_z^2 + \lambda_\theta^{-2}\lambda_z^{-2} - 3) \\ & + \frac{k_1}{k_2} \left[\exp\{k_2[\kappa(\lambda_\theta^2 + \lambda_z^2 + \lambda_\theta^{-2}\lambda_z^{-2}) \right. \\ & \left. + (1 - 3\kappa)(\lambda_\theta^2 \cos^2 \varphi + \lambda_z^2 \sin^2 \varphi) - 1\}^2 - 1 \right]. \quad (215) \end{aligned}$$

In Fig. 24 the dimensionless pressure $P^* = P/\mu\varepsilon$ is plotted as a function of λ for the representative axial stretch $\lambda_z = 1$, dispersion parameter $\kappa = 0.2$ and material parameters $k_1/\mu = k_2 = 1$, with the three different values of the mean fiber angle $\varphi = \pi/6, \pi/4, \pi/3$. These are the dashed curves in the figure and are compared with corresponding results in the absence of dispersion (the continuous curves). The latter are the same as the curves in Fig. 12a but the vertical scale has been reduced here in order to highlight the significant difference that dispersion makes to the pressure response for $\varphi = \pi/6, \pi/4$, in particular for mean fiber directions relatively close to circumferential.

When the mean fiber direction is closer to axial the effect of dispersion is considerably reduced. For larger values of κ our calculations show that the response becomes less stiff and as κ approaches $1/3$ (the isotropic case) the three dispersion curves merge. The chosen values of $\lambda_z, k_1/\mu$ and k_2 serve to illustrate the main features of the pressure response in the presence of dispersed fibers, and results for other values of these parameters are qualitatively similar. Examples with different parameter values corresponding to fitting to arterial wall data can be found in Gasser et al. (2006) and Ogden (2009) in which P and/or P^* is plotted against λ for fixed λ_z or for $F = 0$ and against λ_z for $F = 0$.

Next, in Fig. 25, corresponding plots of the dimensionless reduced axial load $F^* = F/(\pi A^2 \mu \varepsilon)$ as a function of λ are illustrated for the same parameters as in

Fig. 25 Plot of the dimensionless reduced axial load $F^* = F/(\pi A^2 \mu \varepsilon)$ against λ for the strain-energy function (215) with $\lambda_z = 1$, material parameters $k_1/\mu = 1, k_2 = 1$ and dispersion parameters $\kappa = 0.2$ (dashed curves) and $\kappa = 0$ (continuous curves—no dispersion), and angles $\varphi = \pi/6, \pi/4, \pi/3$, based on the thin-wall approximation (145)

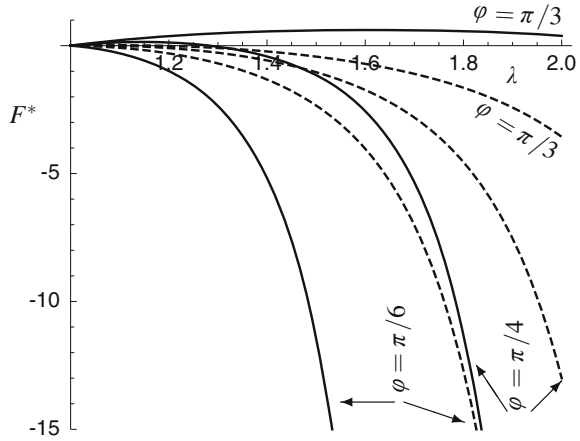


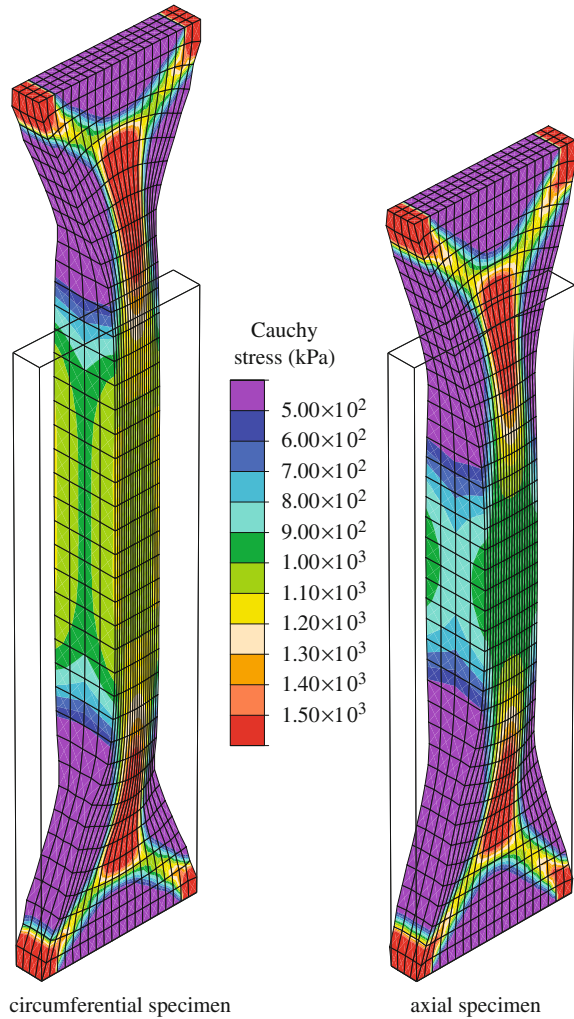
Fig. 24. In this case the dispersion has a significant effect for all values of φ , and, in particular, for $\varphi = \pi/3$, F^* changes from positive to negative as a result of dispersion for the considered range of values of λ .

As a final example in this section we illustrate the influence of fiber dispersion on circumferential and axial strips subjected to uniaxial tensile load with the ends of the strips constrained so that the resulting deformations and stress distributions are nonuniform. Based on data relating to an iliac adventitia, finite element results were presented in Gasser et al. (2006) for a uniaxial tension of 1 N, with material parameter $\mu = 7.64$ kPa for the soft (neo-Hookean) matrix and $k_1 = 996.6$ kPa, $k_2 = 524.6$. Here we show a small selection of their results, for full details of which we refer to Gasser et al. (2006).

In Fig. 26 we show the distribution of the component of Cauchy stress in the direction of the applied load for the case of no fiber dispersion ($\kappa = 0$) with fibers oriented at an angle $\varphi = 49.98^\circ$ relative to the circumferential direction. Clearly, the circumferential specimen, shown on the left of the figure, extends more than the axial specimen because the stiff fibers are oriented closer to the axial than the circumferential direction. For each specimen there is a significant lateral contraction in the width of the specimens caused by rotation of the fibers, which tends to squeeze the material in the width. This is accompanied by an expansion in the thickness direction in which the stretch is, by incompressibility, $\lambda_3 = \lambda_1^{-1} \lambda_2^{-1} > 1$, although this is less evident near the ends of the specimens because of the end constraints.

Figure 27 shows the corresponding results for a case with fiber dispersion and dispersion parameter $\kappa = 0.226$ and mean fiber angle $\varphi = 49.98^\circ$. In this case the thickness is approximately constant and the uniaxial response is stiffer. Clearly, the dispersion has a significant effect on the response.

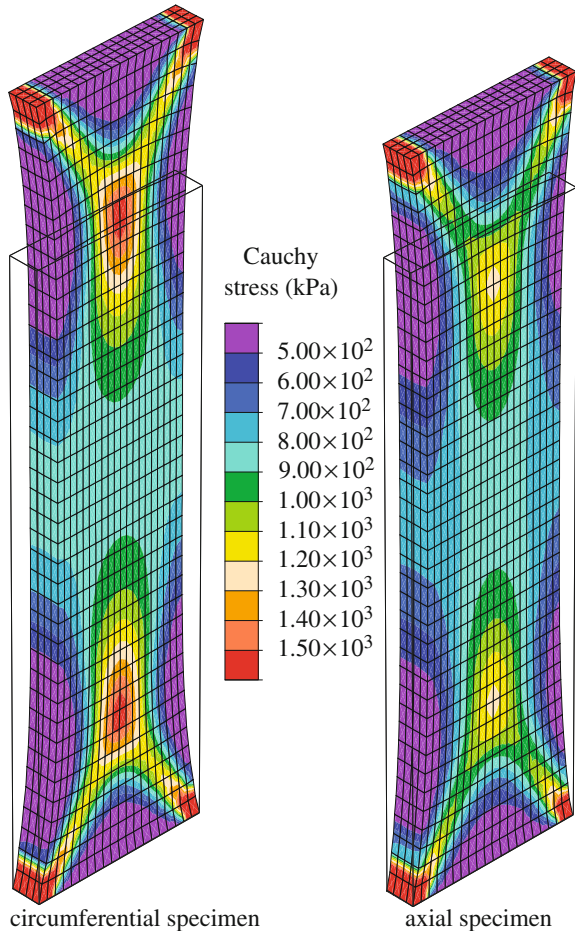
Fig. 26 Finite element computation showing the component of the Cauchy stress distribution in the direction of the applied load for a uniaxial tensile load of 1 N applied to strips in the circumferential and axial directions with no fiber dispersion ($\kappa = 0$). Reproduced from Fig. 9 of Gasser et al. (2006) with permission



6.4 Nonsymmetric Fiber Dispersion

Recent extensive experiments of Schriefl et al. (2012) have characterized the in-plane (circumferential–axial) dispersion of collagen fibers in the intima, media, and adventitia of human non-atherosclerotic thoracic and abdominal aortas and common iliac arteries. They also measured out-of-plane (radial) fiber angles for each layer and found that the out-of-plane dispersions are similar at all anatomic locations for each layer. In particular, they determined that for each (three-dimensional) dispersion the mean fiber angle was very close to tangential, and that the out-of-plane component was very small. These results show that it is inappropriate to adopt rotationally

Fig. 27 Finite element computation showing the component of the Cauchy stress distribution in the direction of the applied load for a uniaxial tensile load of 1 N applied to strips in the circumferential and axial directions with fiber dispersion parameter $\kappa = 0.226$. Reproduced from Fig. 12 of Gasser et al. (2006) with permission



symmetric dispersions for the two fiber families with mean fiber direction in the circumferential–axial plane. The purpose of this section, therefore, is to provide a modification of the rotationally symmetric dispersion model that takes account of these new results. Our analysis here is based on the recent paper by Holzapfel et al. (2015), but for consistency with the previous sections herein some of the notation has been changed.

With reference to Fig. 20 we again assume that a general fiber direction \mathbf{N} within a dispersion is given by (169), which we repeat here for ease of reference as

$$\mathbf{N}(\Theta, \Phi) = \sin \Theta \cos \Phi \mathbf{e}_1 + \sin \Theta \sin \Phi \mathbf{e}_2 + \cos \Theta \mathbf{e}_3, \tag{216}$$

with $\Theta \in [0, \pi]$, $\Phi \in [0, 2\pi]$, and, locally, for a circular cylinder, $\mathbf{e}_1, \mathbf{e}_2$ defining the tangential plane of a cylindrical coordinate system, \mathbf{e}_1 being the circumferential direction and \mathbf{e}_2 the axial direction. Thus, \mathbf{e}_3 is the outward radial direction.

We again adopt the notation $\rho(\Theta, \Phi)$ for the fiber orientation density, and this is normalized according to (170). The requirement that ρ is independent of the sense of \mathbf{N} again gives $\rho(\pi - \Theta, \pi + \Phi) = \rho(\Theta, \Phi)$. The experimental results of Schrieffer et al. (2012) suggest two additional symmetries, the in-plane symmetry $\rho(\Theta, \pi + \Phi) = \rho(\Theta, \Phi)$, and the out-of-plane symmetry $\rho(\pi - \Theta, \Phi) = \rho(\Theta, \Phi)$, as a result of which we can now focus on the ranges of values $\Theta \in [0, \pi/2]$ and $\Phi \in [0, \pi]$.

Again we assume that the material properties are independent of the sense of \mathbf{N} , so that the strain-energy function depends on \mathbf{N} via the tensor product $\mathbf{N} \otimes \mathbf{N}$, as in Sect. 6.1, through the (symmetric) generalized structure tensor \mathbf{H} defined in (171), which, in view of the symmetries mentioned above, we now write as

$$\mathbf{H} = \frac{1}{\pi} \int_{\Omega'} \rho(\Theta, \Phi) \mathbf{N} \otimes \mathbf{N} \sin \Theta d\Theta d\Phi, \quad (217)$$

where $\Omega' = \{(\Theta, \Phi) \mid \Theta \in [0, \pi/2], \Phi \in [0, \pi]\}$.

With reference to the basis $\mathbf{e}_1, \mathbf{e}_2, \mathbf{e}_3$ we denote the components of \mathbf{H} by $H_{ij} = H_{ji}$, so that (in the summation convention) $\mathbf{H} = H_{ij} \mathbf{e}_i \otimes \mathbf{e}_j$. However, the symmetries of ρ identified above ensure that $H_{13} = H_{23} = 0$. In view of the restriction (172) there remain only three independent components of \mathbf{H} . Thus, we consider

$$H_{11}, \quad H_{22}, \quad H_{12}, \quad \text{with} \quad H_{33} = 1 - H_{11} - H_{22}. \quad (218)$$

It was found in Schrieffer et al. (2012) that the in-plane and out-of-plane dispersions are essentially independent, which means that $\rho(\Theta, \Phi)$ can be decoupled as

$$\rho(\Theta, \Phi) = \rho_{\text{op}}(\Theta) \rho_{\text{ip}}(\Phi), \quad (219)$$

where $\rho_{\text{op}}(\Theta)$ and $\rho_{\text{ip}}(\Phi)$ are the out-of-plane and in-plane fiber orientation densities, respectively. The symmetries discussed above then impose the conditions

$$\rho_{\text{op}}(\pi - \Theta) = \rho_{\text{op}}(\Theta), \quad \rho_{\text{ip}}(\pi + \Phi) = \rho_{\text{ip}}(\Phi). \quad (220)$$

As a result, with the symmetries accounted for, the normalization (170) gives

$$\frac{1}{\pi} \int_0^{\pi/2} \rho_{\text{op}}(\Theta) \sin \Theta d\Theta \int_0^{\pi} \rho_{\text{ip}}(\Phi) d\Phi = 1. \quad (221)$$

Clearly, the out-of-plane dispersion has rotational symmetry, and guided therefore by the normalization (178) in the case of rotational symmetry, we assume that $\rho_{\text{op}}(\Theta)$ is normalized according to

$$\int_0^{\pi/2} \rho_{\text{op}}(\Theta) \sin \Theta d\Theta = 1, \tag{222}$$

which leaves the normalization of $\rho_{\text{ip}}(\Phi)$ in the form

$$\frac{1}{\pi} \int_0^\pi \rho_{\text{ip}}(\Phi) d\Phi = 1. \tag{223}$$

Analogously to the dispersion parameter κ defined in (180) we now define the out-of-plane dispersion parameter κ_{op} by

$$\kappa_{\text{op}} = \frac{1}{2} \int_0^{\pi/2} \rho_{\text{op}}(\Theta) \sin^3 \Theta d\Theta, \tag{224}$$

which lies in the range of values

$$0 \leq \kappa_{\text{op}} \leq 1/2, \tag{225}$$

as discussed in Sect. 6.1.1 in respect of κ . Thus, in particular, $\kappa_{\text{op}} = 1/3$ corresponds to an isotropic dispersion with $\rho_{\text{op}} = 1$.

Note that (223) is automatically satisfied if $\rho_{\text{ip}}(\Phi) \equiv 1$, which corresponds to in-plane isotropy, in which case $H_{12} = 0$, $H_{11} = H_{22} = \kappa_{\text{op}}$, and $H_{33} = 1 - 2\kappa_{\text{op}}$, so that the dispersion is rotationally symmetric with mean fiber direction \mathbf{e}_3 . Three-dimensional isotropy arises if $\rho_{\text{op}}(\Theta) = \rho_{\text{ip}}(\Phi) = 1$ and $\kappa_{\text{op}} = 1/3$.

Having considered the out-of-plane dispersion in terms of κ_{op} , we now discuss the in-plane dispersion. From the definitions (217), (226) and (227) with Eq. (219) the components of \mathbf{H} are calculated simply as

$$H_{ij} = 2\kappa_{\text{op}}\bar{\kappa}_{ij}, \quad i, j \in \{1, 2\}, \quad H_{11} + H_{22} = 2\kappa_{\text{op}}, \quad H_{33} = 1 - 2\kappa_{\text{op}}, \tag{226}$$

where $\bar{\kappa}_{11}$, $\bar{\kappa}_{22}$ and $\bar{\kappa}_{12}$ are given by

$$\bar{\kappa}_{11} = \frac{1}{\pi} \int_0^\pi \rho_{\text{ip}}(\Phi) \cos^2 \Phi d\Phi, \quad \bar{\kappa}_{22} = \frac{1}{\pi} \int_0^\pi \rho_{\text{ip}}(\Phi) \sin^2 \Phi d\Phi, \tag{227}$$

$$\bar{\kappa}_{12} = \frac{1}{\pi} \int_0^\pi \rho_{\text{ip}}(\Phi) \sin \Phi \cos \Phi d\Phi. \tag{228}$$

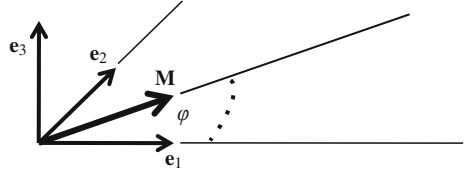
It follows from (223) that

$$\bar{\kappa}_{11} + \bar{\kappa}_{22} = 1. \tag{229}$$

Note that in the case of in-plane isotropy, $\rho_{\text{ip}}(\Phi) \equiv 1$, it follows that $\bar{\kappa}_{12} = 0$ and $\bar{\kappa}_{11} = \bar{\kappa}_{22} = 1/2$.

If the mean in-plane fiber direction coincides with \mathbf{e}_1 or \mathbf{e}_2 then we also have $\bar{\kappa}_{12} = 0$. We then consider a mean in-plane fiber direction \mathbf{M} , as depicted in Fig. 28, with

Fig. 28 Schematic of the in-plane mean fiber direction $\mathbf{M} = \cos \varphi \mathbf{e}_1 + \sin \varphi \mathbf{e}_2$, with in-plane unit vectors \mathbf{e}_1 (circumferential) and \mathbf{e}_2 (axial) and plane normal \mathbf{e}_3



the dispersion symmetric about \mathbf{M} , which is a unit vector given by $\mathbf{M} = \cos \varphi \mathbf{e}_1 + \sin \varphi \mathbf{e}_2$, φ being the angle between \mathbf{M} and the circumferential direction \mathbf{e}_1 . With respect to axes aligned with $\mathbf{e}'_1 = \mathbf{M}$ and $\mathbf{e}'_2 = -\sin \varphi \mathbf{e}_1 + \cos \varphi \mathbf{e}_2$, we denote the dispersion parameters by $\bar{\kappa}'_{ij}$ and in this case also $\bar{\kappa}'_{12} = 0$. In such a case we drop the bars and use the notation κ_{11} and κ_{22} , noting that $\kappa_{11} + \kappa_{22} = 1$.

Then, the dispersion components $\bar{\kappa}_{ij}$ are related to κ_{ij} , $i, j \in \{1, 2\}$, and the angle φ by

$$\bar{\kappa}_{11} = \kappa_{11} \cos^2 \varphi + \kappa_{22} \sin^2 \varphi, \quad \bar{\kappa}_{12} = (\kappa_{11} - \kappa_{22}) \sin \varphi \cos \varphi, \quad (230)$$

with $\bar{\kappa}_{22}$ given by (229), and hence

$$\tan 2\varphi = \frac{2\bar{\kappa}_{12}}{\bar{\kappa}_{11} - \bar{\kappa}_{22}}. \quad (231)$$

Note that

$$(\bar{\kappa}_{11} - \bar{\kappa}_{22})^2 + 4\bar{\kappa}_{12}^2 = (\kappa_{11} - \kappa_{22})^2 \quad (232)$$

is an invariant, i.e., independent of φ . Clearly then, given the angle φ , there is only one independent in-plane dispersion parameter. We take this to be κ_{22} , which we denote by κ_{ip} henceforth.

Now let us refer the structure tensor \mathbf{H} to the axes $\mathbf{e}'_1, \mathbf{e}'_2$ identified above, along with $\mathbf{e}'_3 = \mathbf{e}_3$, and let H'_{ij} be the corresponding components of \mathbf{H} , where

$$H'_{11} = 2\kappa_{op}(1 - \kappa_{ip}), \quad H'_{22} = 2\kappa_{op}\kappa_{ip}, \quad H'_{33} = 1 - 2\kappa_{op} \quad (233)$$

and $H'_{ij} = 0$, $i \neq j$. By using the identity $\mathbf{e}'_1 \otimes \mathbf{e}'_1 + \mathbf{e}'_2 \otimes \mathbf{e}'_2 + \mathbf{e}'_3 \otimes \mathbf{e}'_3 = \mathbf{I}_r$, the spectral form of \mathbf{H} , i.e.,

$$\mathbf{H} = H'_{11} \mathbf{e}'_1 \otimes \mathbf{e}'_1 + H'_{22} \mathbf{e}'_2 \otimes \mathbf{e}'_2 + H'_{33} \mathbf{e}'_3 \otimes \mathbf{e}'_3, \quad (234)$$

can be rewritten as

$$\mathbf{H} = 2\kappa_{op}\kappa_{ip}\mathbf{I}_r + 2\kappa_{op}(1 - 2\kappa_{ip})\mathbf{M} \otimes \mathbf{M} + (1 - 2\kappa_{op} - 2\kappa_{op}\kappa_{ip})\mathbf{M}_n \otimes \mathbf{M}_n, \quad (235)$$

where the unit vector \mathbf{M}_n is now used in place of \mathbf{e}_3 . This is the generalized structure tensor associated with a fiber dispersion that has a single in-plane mean direction

\mathbf{M} , and because of the considered symmetries \mathbf{M} is also the mean direction of the three-dimensional dispersion.

We emphasize that \mathbf{H} involves just two independent dispersion parameters, κ_{op} and κ_{ip} , and κ_{op} can be calculated when ρ_{op} is prescribed, while $\bar{\kappa}_{11}$, $\bar{\kappa}_{22}$ and $\bar{\kappa}_{12}$ can be determined from a given form of ρ_{ip} . The latter lead to the angle φ via (231). The calculations are exemplified in the following section by considering ρ_{op} and ρ_{ip} to be von Mises distributions.

Special Cases

It is worthwhile at this point to identify the values of κ_{op} and κ_{ip} for which the structure tensor (235) reduces to the particular structure tensors considered previously. First, by taking $\kappa_{ip} = 1/2$, we obtain

$$\mathbf{H} = \kappa_{op} \mathbf{I}_r + (1 - 3\kappa_{op}) \mathbf{M}_n \otimes \mathbf{M}_n, \tag{236}$$

which is the structure tensor of a rotationally symmetric dispersion with mean fiber direction \mathbf{M}_n . Alternatively, we may obtain

$$\mathbf{H} = \kappa \mathbf{I}_r + (1 - 3\kappa) \mathbf{M} \otimes \mathbf{M} \tag{237}$$

by setting $\kappa = 2\kappa_{op}\kappa_{ip} = 1 - 2\kappa_{op}$, which is the structure tensor of a rotationally symmetric dispersion with mean fiber direction \mathbf{M} . If there is no dispersion then by taking $\kappa_{op} = 0$ and $\kappa = 0$, respectively, in these two cases we obtain $\mathbf{H} = \mathbf{M}_n \otimes \mathbf{M}_n$ and $\mathbf{H} = \mathbf{M} \otimes \mathbf{M}$. The structure tensor for an isotropic dispersion of fibers is obtained by taking either $\kappa_{op} = 1/3$ in (236) or $\kappa = 1/3$ in (237).

The structure tensor $\hat{\mathbf{H}}$ for a two-dimensional dispersion given in (205) is obtained from (235) by setting $\kappa_{op} = 1/2$ and $\kappa_{ip} = \kappa$, and noting that the in-plane identity is given by $\hat{\mathbf{I}}_r = \mathbf{I}_r - \mathbf{M}_n \otimes \mathbf{M}_n$. Then, with $\kappa = 1/2$, we obtain the structure tensor for an isotropic in-plane dispersion, namely $\hat{\mathbf{H}} = \hat{\mathbf{I}}_r/2$.

6.4.1 Describing Dispersions in Terms of von Mises Distributions

We consider π -periodic von Mises distributions that account for the symmetries identified at the beginning of Sect. 6.4. For general details of von Mises distributions we refer to Fisher et al. (1987). We begin by representing the out-of-plane orientation density $\rho_{op}(\Theta)$ as a von Mises distribution of the form

$$\rho_{op}(\Theta) = 4\sqrt{\frac{b}{2\pi}} \frac{\exp(-2b \cos^2 \Theta)}{\operatorname{erf}(\sqrt{2b})}. \tag{238}$$

This can be obtained from the $\rho(\Theta)$ given in (182) in Sect. 6.1.1 by replacing b by $-b$ and leads to the closed-form expression for κ_{op} given by

$$\kappa_{\text{op}} = \frac{1}{2} - \frac{1}{8b} + \frac{1}{4} \sqrt{\frac{2}{\pi b}} \frac{\exp(-2b)}{\text{erf}(\sqrt{2b})}, \quad (239)$$

which has the character shown in Fig. 22 as for κ in (184) but with b and $-b$ interchanged.

For $\rho_{\text{ip}}(\Phi)$ we consider the von Mises distribution

$$\rho_{\text{ip}}(\Phi) = \frac{\exp(-a \cos 2\Phi)}{I_0(a)}, \quad (240)$$

which has a different normalization from $\rho_{\text{op}}(\Theta)$, where the constant a is again a concentration parameter, while $I_0(a)$ is the modified Bessel function of the first kind of order 0 defined by

$$I_0(x) = \frac{1}{\pi} \int_0^\pi \exp(x \cos \alpha) d\alpha. \quad (241)$$

The distribution (240) is slightly different from that used in Holzapfel et al. (2015) and is chosen to have its maximum at the center $\Phi = \pi/2$ of the integration interval. The forms of the curves of $\rho_{\text{ip}}(\Phi)$ for different values of a are, apart from the different scale, identical to those shown in Fig. 21. When $a \rightarrow \infty$, $\rho_{\text{ip}}(\Phi)$ becomes a delta function.

It is instructive to visualize the dispersion in three dimensions by plotting $\rho(\Theta, \Phi)\mathbf{N} = \rho_{\text{op}}(\Theta)\rho_{\text{ip}}(\Phi)\mathbf{N}$. Thus, Fig. 29 shows this for the different cases of dispersions considered, as described in the figure caption.

Since the distribution (240) is symmetric about $\Phi = 0$ it follows from the definition (228) that $\bar{\kappa}_{12} = 0$, and from (227), on dropping the bars, that κ_{11} and κ_{22} can be obtained in the closed forms

$$\kappa_{11} = \frac{1}{2} - \frac{I_1(a)}{2I_0(a)}, \quad \kappa_{22} = \kappa_{\text{ip}} = \frac{1}{2} + \frac{I_1(a)}{2I_0(a)}, \quad (242)$$

where

$$I_1(x) = \frac{1}{\pi} \int_0^\pi \exp(x \cos \alpha) \cos \alpha d\alpha \quad (243)$$

is the modified Bessel function of the first kind of order 1. Note that the expressions for κ_{11} and κ_{22} are reversed compared with those given in Holzapfel et al. (2015) because of the different form of $\rho_{\text{ip}}(\Phi)$ adopted here. Each of κ_{11} and κ_{22} lies in the range $[0, 1]$ subject to $\kappa_{11} + \kappa_{22} = 1$ and plots of them as functions of a are shown in Fig. 30. The character of κ_{22} is very similar to that of κ shown in Fig. 22 although the range of values is different.

If κ_{11} and κ_{22} are the dispersion parameters corresponding to a mean fiber direction at an angle φ to the \mathbf{e}_1 direction (see Fig. 28) then the dispersion parameters $\bar{\kappa}_{11}$, $\bar{\kappa}_{22}$ and $\bar{\kappa}_{12}$ are given by (229) and (230).

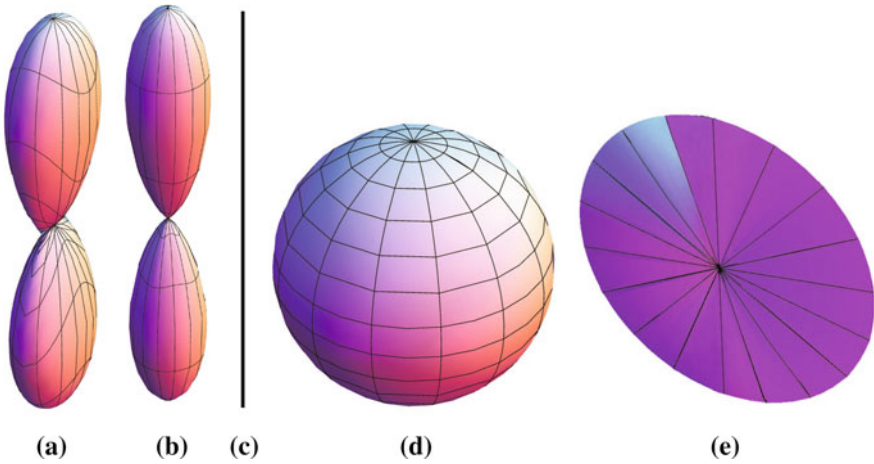
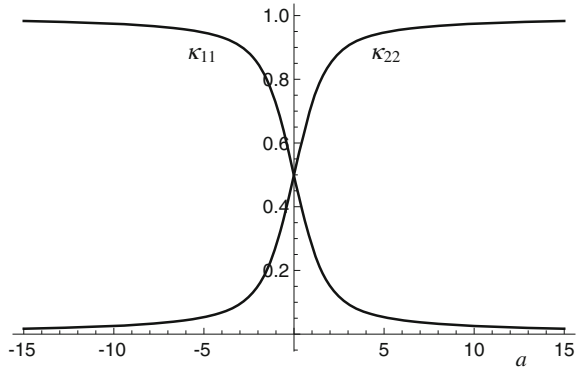


Fig. 29 Visualization of the fiber dispersion defined by $\rho(\Theta, \Phi)\mathbf{N} = \rho_{op}(\Theta)\rho_{ip}(\Phi)\mathbf{N}$ based on the von Mises distributions (238) and (240). The plots have been scaled differently and represent **a** a nonrotationally symmetric dispersion, **b** a rotationally symmetric dispersion, **c** perfectly aligned fibers, **d** a 3D isotropic dispersion and **e** a planar dispersion. The planar isotropic case corresponds to a circle in e. Except for case c the distance from the center to the surface represents the probability of finding a fiber in the direction \mathbf{N} . Reproduced from Fig. 6 of Holzapfel et al. (2015) with permission

Fig. 30 Plots of κ_{11} and κ_{22} versus a based on the formulas in (242)



6.4.2 Consideration of Data from Schriefl et al. (2012)

We now illustrate the results from Schriefl et al. (2012) by considering the angular dispersion data from a single adventitial specimen of a human non-atherosclerotic abdominal aorta which were included in the average data set in Fig. 5 of their paper. In Fig. 31 we show the data as a probability density for the out-of-plane dispersion together with a curve obtained by fitting $\rho_{op}(\Theta)$ obtained from (238) to the data for which the concentration parameter was found to be $b = 19.44$. Incidentally, the

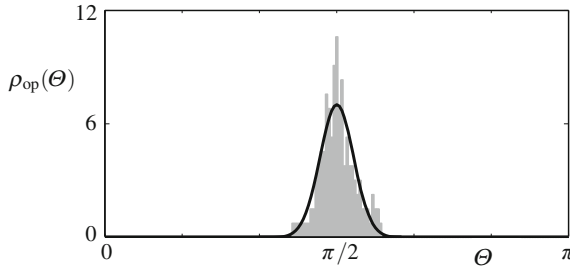
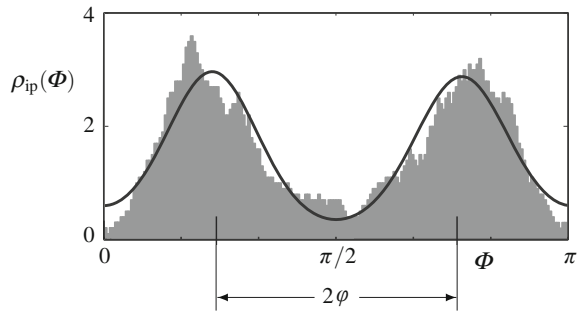


Fig. 31 Representative set of out-of-plane fiber angular dispersion data from Schrieffl et al. (2012) and the fit to these data with the orientation density function (238) with concentration parameter $b = 19.44$ and with $\rho_{\text{op}}(\Theta)$ plotted against Θ . Based on Fig. 5b in Holzapfel et al. (2015), with permission

Fig. 32 Representative set of in-plane fiber angular dispersion data from Schrieffl et al. (2012) and the fit to these data with the orientation density function (240) with concentration parameter $a = 2.54$ and angle $\varphi = 47.99^\circ$ and with $\rho_{\text{ip}}(\Phi)$ plotted against Φ . Based on Fig. 5a in Holzapfel et al. (2015), with permission



vertical scale shown in the corresponding figure (Fig. 5b) in Holzapfel et al. (2015) is incorrect, and Fig. 31 corrects this.

In Fig. 32 we show the data of the in-plane bimodal dispersion, the data being fitted by the curve shown using $\rho_{\text{ip}}(\Phi)$ from (240) with Φ replaced by $\Phi + \varphi$ and $\Phi - \varphi$ together, φ being determined as $\varphi = 47.99^\circ$, and the concentration parameter as $a = 2.54$.

Note that the data shown in Figs. 31 and 32 are centered on $\Theta = \pi/2$ rather than the $\Theta = 0$ used in Holzapfel et al. (2015).

From the formulas (239) and (242)₂ with the values of b and a above we then obtain the corresponding values of κ_{op} and κ_{ip} as $\kappa_{\text{op}} = 0.494$ and $\kappa_{\text{ip}} = 0.885$. Note that in Holzapfel et al. (2015) the value of κ_{op} was 0.493 and, because we are using a slightly different version of ρ_{ip} here κ_{ip} in Holzapfel et al. (2015) was 0.116, whereas the value of κ_{11} here is 0.115.

6.4.3 An Extended Constitutive Law

We recall the generalized structure tensor defined in (235) as

$$\mathbf{H} = 2\kappa_{\text{op}}\kappa_{\text{ip}}\mathbf{I}_r + 2\kappa_{\text{op}}(1 - 2\kappa_{\text{ip}})\mathbf{M} \otimes \mathbf{M} + (1 - 2\kappa_{\text{op}} - 2\kappa_{\text{op}}\kappa_{\text{ip}})\mathbf{M}_n \otimes \mathbf{M}_n, \quad (244)$$

for a single family of dispersed fibers. We now consider a second family with mean fiber direction \mathbf{M}' and the same material properties with structure tensor

$$\mathbf{H}' = 2\kappa_{\text{op}}\kappa_{\text{ip}}\mathbf{I}_r + 2\kappa_{\text{op}}(1 - 2\kappa_{\text{ip}})\mathbf{M}' \otimes \mathbf{M}' + (1 - 2\kappa_{\text{op}} - 2\kappa_{\text{op}}\kappa_{\text{ip}})\mathbf{M}_n \otimes \mathbf{M}_n, \quad (245)$$

\mathbf{M} and \mathbf{M}' lying in the $(\mathbf{e}_1, \mathbf{e}_2)$ plane and symmetrically arranged with respect to the axes, and $\mathbf{M}_n = \mathbf{e}_3$ normal to that plane, as depicted in Fig. 33. Thus,

$$\mathbf{M} = \cos \varphi \mathbf{e}_1 + \sin \varphi \mathbf{e}_2, \quad \mathbf{M}' = \cos \varphi \mathbf{e}_1 - \sin \varphi \mathbf{e}_2. \quad (246)$$

Note, with reference to Fig. 11, that \mathbf{e}_1 and \mathbf{e}_2 may be identified with \mathbf{E}_Θ and \mathbf{E}_Z , respectively.

The associated generalized invariants are denoted I_4^* and I_6^* , generalizing the definitions used in (186)₁ and (194), the latter with $\kappa' = \kappa$, and given by

$$I_4^* = \text{tr}(\mathbf{CH}) = 2\kappa_{\text{op}}\kappa_{\text{ip}}I_1 + 2\kappa_{\text{op}}(1 - 2\kappa_{\text{ip}})I_4 + (1 - 2\kappa_{\text{op}} - 2\kappa_{\text{op}}\kappa_{\text{ip}})I_n, \quad (247)$$

$$I_6^* = \text{tr}(\mathbf{CH}') = 2\kappa_{\text{op}}\kappa_{\text{ip}}I_1 + 2\kappa_{\text{op}}(1 - 2\kappa_{\text{ip}})I_6 + (1 - 2\kappa_{\text{op}} - 2\kappa_{\text{op}}\kappa_{\text{ip}})I_n, \quad (248)$$

where $I_n = \mathbf{M}_n \cdot (\mathbf{CM}_n)$

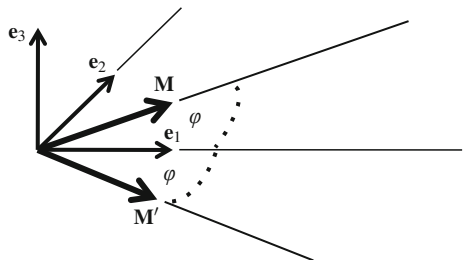
Note, by considering the (orthogonal) unit bisectors of \mathbf{M} and \mathbf{M}' , namely $\mathbf{e}_1 = (\mathbf{M} + \mathbf{M}')/2 \cos \varphi$ and $\mathbf{e}_2 = (\mathbf{M} - \mathbf{M}')/2 \sin \varphi$, where 2φ is the angle between \mathbf{M} and \mathbf{M}' , and using the identity

$$\mathbf{e}_1 \otimes \mathbf{e}_1 + \mathbf{e}_2 \otimes \mathbf{e}_2 + \mathbf{e}_3 \otimes \mathbf{e}_3 = \mathbf{I}_r, \quad (249)$$

we obtain

$$I_n = I_1 - \frac{I_4 + I_6 - 2I_8 \cos 2\varphi}{\sin^2 2\varphi}, \quad (250)$$

Fig. 33 Schematic of the in-plane mean fiber directions $\mathbf{M} = \cos \varphi \mathbf{e}_1 + \sin \varphi \mathbf{e}_2$ and $\mathbf{M}' = \cos \varphi \mathbf{e}_1 - \sin \varphi \mathbf{e}_2$, with in-plane unit vectors \mathbf{e}_1 (circumferential) and \mathbf{e}_2 (axial) and plane normal \mathbf{e}_3



where I_8 is defined by (65). Thus, I_n is in general an independent invariant, i.e., independent of I_1, I_4, I_6 , except in the special case in which \mathbf{M} and \mathbf{M}' are themselves orthogonal, and the above reduces to $I_n = I_1 - (I_4 + I_6)$.

Now, instead of treating W as a function of just I_1, I_4, I_6 we append the invariant I_n , which appears only in I_4^* and I_6^* , and consider $W(I_1, I_4, I_6, I_n) = W^*(I_1, I_4^*, I_6^*)$. Recalling the connections (23) and the formula (42)₂, the second Piola–Kirchhoff stress tensor \mathbf{P} is then given by

$$\mathbf{P} = 2 \frac{\partial W}{\partial \mathbf{C}} - p \mathbf{C}^{-1} = 2(W_1 \mathbf{I}_F + W_4 \mathbf{M} \otimes \mathbf{M} + W_6 \mathbf{M}' \otimes \mathbf{M}' + W_n \mathbf{M}_n \otimes \mathbf{M}_n) - p \mathbf{C}^{-1}, \quad (251)$$

and the Cauchy stress tensor is obtained from $\boldsymbol{\sigma} = \mathbf{F} \mathbf{P} \mathbf{F}^T$. When expressed in terms of $W^*(I_1, I_4^*, I_6^*)$ it can then be shown that the Cauchy stress is given by

$$\boldsymbol{\sigma} = -p \mathbf{I} + 2W_1^* \mathbf{B} + 2W_4^* \mathbf{h} + 2W_6^* \mathbf{h}', \quad (252)$$

the same formula as in (195), where $\mathbf{h} = \mathbf{F} \mathbf{H} \mathbf{F}^T$ and $\mathbf{h}' = \mathbf{F} \mathbf{H}' \mathbf{F}^T$, but \mathbf{H} and \mathbf{H}' are now given by (244) and (245). Hence

$$\mathbf{h} = 2\kappa_{\text{op}} \kappa_{\text{ip}} \mathbf{B} + 2\kappa_{\text{op}} (1 - 2\kappa_{\text{ip}}) \mathbf{m} \otimes \mathbf{m} + (1 - 2\kappa_{\text{op}} - 2\kappa_{\text{op}} \kappa_{\text{ip}}) \mathbf{m}_n \otimes \mathbf{m}_n, \quad (253)$$

$$\mathbf{h}' = 2\kappa_{\text{op}} \kappa_{\text{ip}} \mathbf{B} + 2\kappa_{\text{op}} (1 - 2\kappa_{\text{ip}}) \mathbf{m}' \otimes \mathbf{m}' + (1 - 2\kappa_{\text{op}} - 2\kappa_{\text{op}} \kappa_{\text{ip}}) \mathbf{m}_n \otimes \mathbf{m}_n, \quad (254)$$

with $\mathbf{m} = \mathbf{F} \mathbf{M}$, $\mathbf{m}' = \mathbf{F} \mathbf{M}'$, $\mathbf{m}_n = \mathbf{F} \mathbf{M}_n$.

We now extend the decomposition of the strain-energy function given in (197) to the present situation by writing it as

$$W^*(I_1, I_4^*, I_6^*) = W_{\text{iso}}^*(I_1) + W_{\text{aniso}}^*(I_4^*, I_6^*), \quad (255)$$

but now with I_4^* and I_6^* given by (247) and (248). With this change, as in (198) and (199), we take

$$W_{\text{iso}}^* = \frac{1}{2} \mu (I_1 - 3) \quad (256)$$

and

$$W_{\text{aniso}}^* = \frac{k_1}{2k_2} \sum_{i=4,6} \{\exp[k_2 (I_i^* - 1)^2] - 1\}. \quad (257)$$

Following Holzapfel et al. (2000), we make the common assumption that the fibers do not resist any compression and are only active in tension. In this respect the invariants I_4 and I_6 act as switches between fiber compression and tension so that W_{aniso}^* only contributes to the strain energy if either $I_4 > 1$ or $I_6 > 1$. Thus, if one or both of these conditions is not satisfied then the corresponding part of W_{aniso}^* is omitted. If neither condition is satisfied then the tissue response is purely isotropic.

For discussion of subtle points regarding the choice of switching criteria, we refer to Holzapfel and Ogden (2015).

6.4.4 Material Parameter Identification

For the particular data considered in Sect. 6.4.2 the dispersion parameters κ_{op} and κ_{ip} and the angle φ , and hence the mean fiber directions \mathbf{M} and \mathbf{M}' , were determined on the basis of histology and imaging. Thus, for the model (255) with (256) and (257), it remains to determine the material parameters μ , k_1 and k_2 . In Holzapfel et al. (2015) they were determined by fitting the model to uniaxial data.

To review this we first refer to the definition of pure homogeneous strain in (99) in terms of the principal stretches $\lambda_1, \lambda_2, \lambda_3$, which satisfy the incompressibility constraint $\lambda_1 \lambda_2 \lambda_3 = 1$, in which context \mathbf{M} and \mathbf{M}' were given by (101), the same formulas as in (246). Correspondingly, \mathbf{m} and \mathbf{m}' are given by (102) and $\mathbf{m}_n = \lambda_3 \mathbf{M}_n = \lambda_3 \mathbf{e}_3$.

From (103) and (104)₁, the invariants I_1, I_4, I_6 are given by

$$I_1 = \lambda_1^2 + \lambda_2^2 + \lambda_3^2, \quad I_4 = I_6 = \lambda_1^2 \cos^2 \varphi + \lambda_2^2 \sin^2 \varphi, \quad (258)$$

while $I_n = \lambda_3^2$.

The nonzero components of \mathbf{h} and \mathbf{h}' are calculated as

$$h_{11} = h'_{11} = 2\kappa_{\text{op}}[\kappa_{\text{ip}} + (1 - 2\kappa_{\text{ip}}) \cos^2 \varphi] \lambda_1^2, \quad (259)$$

$$h_{22} = h'_{22} = 2\kappa_{\text{op}}[\kappa_{\text{ip}} + (1 - 2\kappa_{\text{ip}}) \sin^2 \varphi] \lambda_2^2, \quad (260)$$

$$h_{33} = h'_{33} = (1 - 2\kappa_{\text{op}}) \lambda_3^2, \quad (261)$$

$$h_{12} = -h'_{12} = 2\kappa_{\text{op}}(1 - 2\kappa_{\text{ip}}) \lambda_1 \lambda_2 \sin \varphi \cos \varphi, \quad (262)$$

and hence I_4^* and I_6^* can be written simply as

$$I_4^* = I_6^* = h_{11} + h_{22} + h_{33}. \quad (263)$$

The nonzero components of the Cauchy stress tensor are obtained from (252) as

$$\sigma_{11} = \mu \lambda_1^2 + 4k_1(I_4^* - 1) \exp[k_2(I_4^* - 1)^2] h_{11} - p, \quad (264)$$

$$\sigma_{22} = \mu \lambda_2^2 + 4k_1(I_4^* - 1) \exp[k_2(I_4^* - 1)^2] h_{22} - p, \quad (265)$$

$$\sigma_{33} = \mu \lambda_3^2 + 4k_1(I_4^* - 1) \exp[k_2(I_4^* - 1)^2] h_{33} - p. \quad (266)$$

On specializing to the case of simple tension with $\sigma_{22} = \sigma_{33} = 0$, elimination of p from (264)–(266) leaves two equations, namely the incompressibility condition $\lambda_1 \lambda_2 \lambda_3 = 1$ and the implicit equation $\sigma_{22} - \sigma_{33} = 0$, which determine λ_2 and λ_3 in terms of λ_1 , so that σ_{11} can be expressed in terms of λ_1 , the material parameters μ , k_1 and k_2 and the structural parameters κ_{ip} , κ_{op} and φ . To determine the material

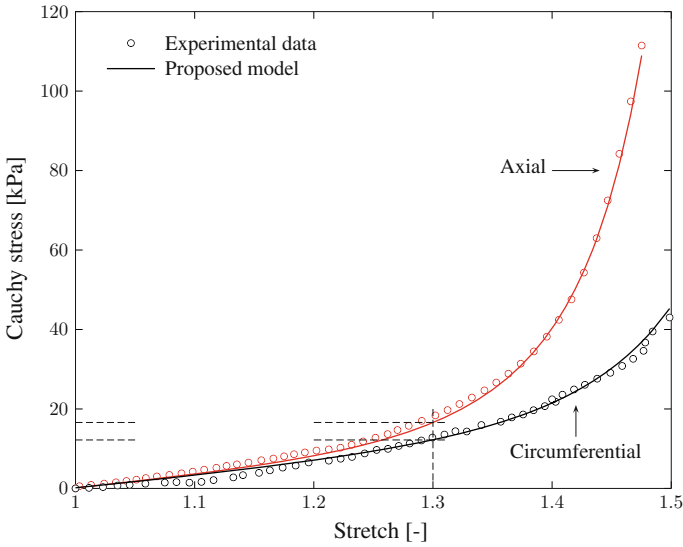


Fig. 34 Fitting of the model (255)–(257) to the results of uniaxial tension tests. The Cauchy stresses at a stretch of 1.3 are 16.6 kPa (axial) and 12.2 kPa (circumferential) and are identified here for reference to values determined in a finite element simulation of a uniaxial tension test illustrated in Fig. 35. Reproduced from Fig. 8 of Holzapfel et al. (2015) with permission

parameters, the values of the structural parameters given in Sect. 6.4.2 are used in conjunction with (unpublished) experimental data from uniaxial tension tests performed in the Graz lab on an adventitial layer of a human non-atherosclerotic abdominal aorta cut along the axial and circumferential directions. Following Holzapfel et al. (2015), and bearing in mind the different definitions of ρ_{op} and ρ_{ip} herein, we use the values $\varphi = \pm 47.99^\circ$, $\kappa_{op} = 0.493$, $\kappa_{ip} = 0.116$ for this exercise.

Full details of the fitting procedure are given in Holzapfel et al. (2015) wherein the material parameters $\mu = 10.07$ kPa, $k_1 = 5.89$ kPa, $k_2 = 21.62$ (dimensionless) were obtained, giving an excellent fit to the data, as shown in Fig. 34.

6.4.5 Application to the Extension of Adventitial Strips

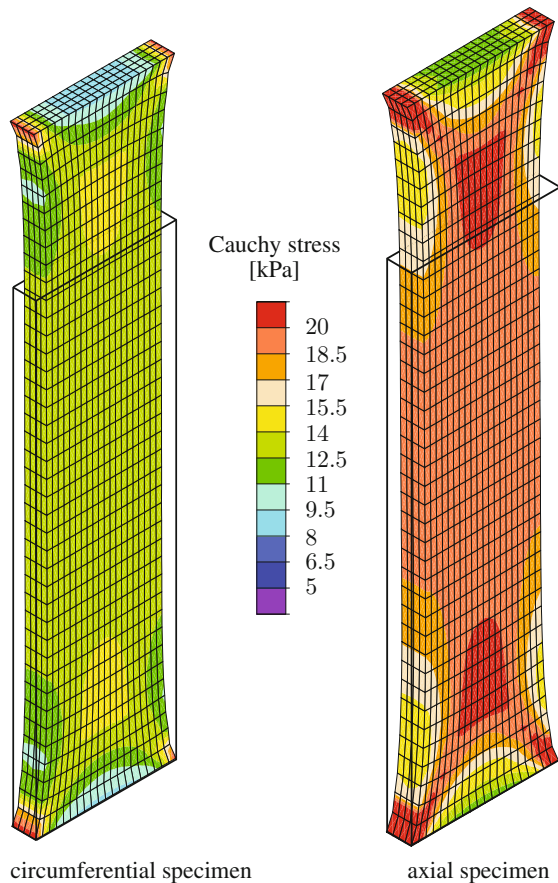
In this section we illustrate the results of a finite element implementation of the constitutive model (255)–(257) in which uniaxial extension tests related to the aforementioned experiments on strips in the circumferential and axial directions of an adventitial layer of a human non-atherosclerotic abdominal aorta are simulated. For the implementation each strip was assumed to have initial length, width and thickness of 10.0, 3.0 and 0.5 mm, respectively, and was subjected to a stretch of 1.3. The ends of each strip were fixed as if in the mounting of a testing machine and

were not allowed to deform, as a result of which the deformation of each strip was nonhomogeneous.

We adopt the material parameters determined in Holzapfel et al. (2015) and take them to be uniform over each strip. The two considered fiber families with symmetric dispersions and mean fiber directions are assumed to make angles φ of $\pm 47.99^\circ$ with the circumferential direction, as indicated in Fig. 33, with dispersion parameters $\kappa_{ip} = 0.116$ and $\kappa_{op} = 0.493$. The implementation, details of which are described in Holzapfel et al. (2015), was performed using the finite element analysis program FEAP (2013). Specifically, numerical results were obtained for the distribution of Cauchy stress component in the direction of the applied stretch for each nonhomogeneous extension, which was fixed at a stretch of 1.3.

The results are illustrated in Fig. 35 for both circumferential and axial specimens. For both specimens the Cauchy stresses were found to be within the range of values determined from the experimental results in Fig. 34. In fact, in the center of each

Fig. 35 Finite element results for circumferential and axial specimens based on data from an adventitia, subjected to a stretch of 1.3. The distribution of the component of the Cauchy stress in the direction of the applied stretch is shown in each case. The undeformed (initial) configuration is indicated by *solid lines*. Reproduced from Fig. 11 of Holzapfel et al. (2015) with permission



specimen the values of the Cauchy stress in the direction of the applied stretch were found to be marginally higher than the stresses at the same value (1.3) of the (homogeneous) stretch noted in Fig. 34. This difference is attributed to the effect of the boundary constraints on the ends.

7 Concluding Remarks

This chapter was in part aimed at illustrating the general value of using nonlinear continuum mechanics as a mathematical modeling framework for describing and predicting the mechanical, in particular the elastic, properties of fibrous soft biological tissues. The approach adopted here is based on the notion of structure tensors, which are used to characterize fiber directions within the tissues. In the present context the starting point was the paper by Holzapfel et al. (2000), which incorporated the fibrous structure into constitutive models of tissues. As more experimental evidence, and more structural information, became available this allowed us to build up the level of complexity of the model, first by incorporating dispersion into the model (Gasser et al. 2006). On the basis of imaging and histology more detailed information on the angular fiber dispersion was revealed in the work of Schriefel et al. (2012), which determined, in particular, various structural parameters, showing that the dispersion is not rotationally symmetric, and these new findings were incorporated into the recent model of Holzapfel et al. (2015). The fact that the structure tensor approach can also be used to incorporate residual stresses into the constitutive theory has also been highlighted. The problem of extension and inflation of an artery, treated simply as a circular cylindrical tube, has been considered throughout the chapter as an example application of the models to a prototype boundary-value problem.

The modeling allows us to define strain-energy functions from which the stress and the elasticity tensors can be computed, and these form the basis for implementing the model within a finite element framework, although this is not the concern of the present chapter. Expressions for the elasticity tensors have not been included here but can be found in, for example, Holzapfel et al. (2015). For a more detailed discussion we refer to Holzapfel (2000). Nevertheless, some examples of the results produced by finite element computations have been illustrated in Sect. 6.

For artery walls many more data are needed to determine finer details of the collagen fiber structure, in particular the dispersion of collagen fibers, and the inelastic behavior of the tissues in both health and disease in order to inform further development of the modeling process. This applies also to a range of other soft biological tissues, in particular those for which the experimental and modeling activities have not thus far been so extensive. In vivo data are really needed as a basis for constructing more realistic models of tissue and organ mechanics.

References

- Canham, P.B., Finlay, H.M., Dixon, J.G., Boughner, D.R., Chen, A.: Measurements from light and polarised light microscopy of human coronary arteries fixed at distending pressure. *Cardiovasc. Res.* **23**, 973–982 (1989)
- Chuong, C.J., Fung, Y.C.: Residual stress in arteries. In: Schmid-Schönbein, G.W., Woo, S.L.-Y., Zweifach, B.W. (eds.) *Frontiers in Biomechanics*, pp. 117–129. Springer, New York (1986)
- FEAP. A finite element analysis program, Version 8.4, User manual. University of California at Berkeley, California (2013)
- Finlay, H.M., McCullough, L., Canham, P.B.: Three-dimensional collagen organization of human brain arteries at different transmural pressures. *J. Vasc. Res.* **32**, 301–312 (1995)
- Finlay, H.M., Whittaker, P., Canham, P.B.: Collagen organization in the branching region of human brain arteries. *Stroke* **29**, 1595–1601 (1998)
- Fisher, N.I., Lewis, T.L., Embleton, B.J.J.: *Statistical Analysis of Spherical Data*. Cambridge University Press, Cambridge (1987)
- Fu, Y.B., Ogden, R.W.: *Nonlinear Elasticity: Theory and Applications*. Cambridge University Press, Cambridge (2001)
- Fung, Y.C.: *Biomechanics: Mechanical Properties of Living Tissue*, 2nd edn. Springer, New York (1993)
- Gasser, T.C., Ogden, R.W., Holzapfel, G.A.: Hyperelastic modelling of arterial layers with distributed collagen fibre orientations. *J. R. Soc. Interface* **3**, 15–35 (2006)
- Haughton, D.M., Ogden, R.W.: Bifurcation of inflated circular cylinders of elastic material under axial loading - I. Membrane theory for thin-walled tubes. *J. Mech. Phys. Solids* **27**, 179–212 (1979)
- Hoger, A.: On the residual stress possible in an elastic body with material symmetry. *Arch. Rational Mech. Anal.* **88**, 271–290 (1985)
- Hoger, A.: The constitutive equation for finite deformations of a transversely isotropic hyperelastic material with residual stress. *J. Elast.* **33**, 107–118 (1993)
- Holzapfel, G.A.: *Nonlinear Solid Mechanics. A Continuum Approach for Engineering*. Wiley, Chichester (2000)
- Holzapfel, G.A., Gasser, T.C.: A viscoelastic model for fiber-reinforced materials at finite strains: continuum basis, computational aspects and applications. *Comput. Meth. Appl. Mech. Eng.* **190**, 4379–4403 (2001)
- Holzapfel, G.A., Ogden, R.W. (eds.): *Biomechanics of Soft Tissue in Cardiovascular Systems. CISM Courses and Lectures*, vol. 441. Springer, Wien (2003)
- Holzapfel, G.A., Ogden, R.W. (eds.): *Proceedings of the IUTAM Symposium on Mechanics of Biological Tissue*, Graz 2004. Springer, Heidelberg (2006)
- Holzapfel, G.A., Ogden, R.W.: Constitutive modelling of passive myocardium. A structurally-based framework for material characterization. *Philos. Trans. R. Soc. Lond. A* **367**, 3445–3475 (2009a)
- Holzapfel, G.A., Ogden, R.W. (eds.): *Biomechanical Modelling at the Molecular, Cellular and Tissue Levels. CISM Courses and Lectures*, vol. 508. Springer, Wien (2009b)
- Holzapfel, G.A., Ogden, R.W.: On planar biaxial tests for anisotropic nonlinearly elastic solids. A continuum mechanical framework. *Math. Mech. Solids* **14**, 474–489 (2009c)
- Holzapfel, G.A., Ogden, R.W.: Constitutive modelling of arteries. *Proc. R. Soc. Lond. A* **466**, 1551–1596 (2010)
- Holzapfel, G.A., Ogden, R.W.: On the tension-compression switch in soft fibrous solids. *Eur. J. Mech. A/Solids* **49**, 561–569 (2015)
- Holzapfel, G.A., Gasser, T.C., Ogden, R.W.: A new constitutive framework for arterial wall mechanics and a comparative study of material models. *J. Elast.* **61**, 1–48 (2000)
- Holzapfel, G.A., Sommer, G., Gasser, T.C., Regitnig, P.: Determination of the layer-specific mechanical properties of human coronary arteries with non-atherosclerotic intimal thickening, and related constitutive modelling. *Am. J. Physiol. Heart Circ. Physiol.* **289**, H2048–H2058 (2005)

- Holzapfel, G.A., Niestrawska, J., Ogden, R.W., Reinisch, A.J., Schriefl, A.J.: Modelling non-symmetric collagen fibre dispersion in arterial walls. *J. R. Soc. Interface* **12**, 0188 (2015)
- Humphrey, J.D.: Mechanics of the arterial wall: review and directions. *Crit. Rev. Biomed. Eng.* **23**, 1–162 (1995)
- Humphrey, J.D.: *Cardiovascular Solid Mechanics. Cells, Tissues, and Organs*. Springer, New York (2002)
- Lanir, Y.: Constitutive equations for fibrous connective tissues. *J. Biomech.* **16**, 1–12 (1983)
- Liu, I.-S.: On representations of anisotropic invariants. *Int. J. Eng. Sci.* **20**, 1099–1109 (1982)
- Melnik, A.V., Borja Da Rocha, H., Goriely, A.: On the modeling of fiber dispersion in fiber-reinforced elastic materials. *Int. J. Non-Linear Mech.* **75**, 92–106 (2015)
- Merodio, J., Ogden, R.W.: Material instabilities in fiber-reinforced nonlinearly elastic solids under plane deformation. *Arch. Mech.* **54**, 525–552 (2002)
- Merodio, J., Ogden, R.W.: Instabilities and loss of ellipticity in fiber-reinforced compressible nonlinearly elastic solids under plane deformation. *Int. J. Solids Struct.* **40**, 4707–4727 (2003)
- Merodio, J., Ogden, R.W.: The influence of the invariant I_8 on the stress-deformation and ellipticity characteristics of doubly fiber-reinforced nonlinearly elastic solids. *Int. J. Non-Linear Mech.* **41**, 556–563 (2006)
- Merodio, J., Ogden, R.W., Rodríguez, J.: The influence of residual stress on finite deformation elastic response. *Int. J. Non-Linear Mech.* **56**, 43–49 (2013)
- Ogden, R.W.: *Non-linear Elastic Deformations*. Dover, New York (1997)
- Ogden, R.W.: *Nonlinear Elasticity with Application to Material Modelling*. Centre of Excellence for Advanced Materials and Structures. Lecture Notes, vol. 6. IPPT, PAN, Warsaw (2003a)
- Ogden, R.W.: Nonlinear elasticity, anisotropy and residual stresses in soft tissue. In: Holzapfel, G.A., Ogden, R.W. (eds.) *Biomechanics of Soft Tissue in Cardiovascular Systems*. CISM Courses and Lectures Series, vol. 441, pp. 65–108. Springer, Wien (2003b)
- Ogden, R.W.: Anisotropy and nonlinear elasticity in arterial wall mechanics. In: Holzapfel, G.A., Ogden, R.W. (eds.) *Biomechanical Modelling at the Molecular, Cellular and Tissue Levels*. CISM Courses and Lectures Series, vol. 508, pp. 179–258. Springer, Wien (2009)
- Ogden, R.W.: Nonlinear elasticity with application to soft fibre-reinforced materials. In: Dorfmann, L., Ogden, R.W. (eds.) *Nonlinear Mechanics of Soft Fibrous Materials*. CISM Courses and Lectures Series, vol. 559, pp. 1–48. Springer, Wien (2015)
- Ogden, R.W., Schulze-Bauer, C.A.J.: Phenomenological and structural aspects of the mechanical response of arteries. In: Casey, J., Bao, G. (eds.) *Mechanics in Biology*. AMD-Vol. 242/BED-Vol. 46. ASME, New York (2000)
- Ogden, R.W., Singh, B.: Propagation of waves in an incompressible transversely isotropic elastic solid with initial stress: Biot revisited. *J. Mech. Mater. Struct.* **6**, 453–477 (2011)
- Schriefl, A.J., Zeindlinger, G., Pierce, D.M., Regitnig, P., Holzapfel, G.A.: Determination of the layer-specific distributed collagen fiber orientations in human thoracic and abdominal aortas and common iliac arteries. *J. R. Soc. Interface* **9**, 1275–1286 (2012)
- Shams, M., Destrade, M., Ogden, R.W.: Initial stresses in elastic solids: constitutive laws and acoustoelasticity. *Wave Motion* **48**, 552–567 (2011)
- Spencer, A.J.M.: Theory of invariants. In: Eringen, A.C. (ed.) *Continuum Physics*, vol. 1. Academic Press, New York (1971)
- Spencer, A.J.M.: *Deformations of Fibre-Reinforced Materials*. Oxford University Press, Oxford (1972)
- Spencer, A.J.M.: Constitutive theory for strongly anisotropic solids. In: Spencer, A.J.M. (ed.) *Continuum Theory of the Mechanics of Fibre-Reinforced Composites*. CISM Courses and Lectures Series, vol. 282, pp. 1–32. Springer, Wien (1984)
- Vaishnav, R.N., Vossoughi, J.: Estimation of residual strains in aortic segments. In: Hall, C.W. (ed.) *Biomedical Engineering II: Recent Developments*, pp. 330–333. Pergamon Press, New York (1983)